

SYNTHESIS AND CHARACTERIZATION OF NOVEL ANION EXCHANGE RESIN  
COATED SINGLE-WALLED CARBON NANOTUBES FOR USE IN WATER  
PURIFICATION

by

Billy Ray Johnson

A thesis submitted to the faculty of  
The University of North Carolina at Charlotte  
in partial fulfillment of the requirements  
for the degree of Master of Science in  
Chemistry

Charlotte

2016

Approved by:

---

Dr. Jordan C. Poler

---

Dr. James E. Amburgey

---

Dr. Craig A. Ogle

---

Dr. Thomas A. Schmedake

©2016  
Billy Ray Johnson  
ALL RIGHTS RESERVED

## ABSTRACT

BILLY RAY JOHNSON. Synthesis and characterization of novel anion exchange resin coated single-walled carbon nanotubes for use in water purification. (Under the direction of DR. JORDAN C. POLER)

As human health concerns over disinfection byproducts (DBPs) in drinking water increase, so does the need to development new materials that remove them rapidly and at high-efficiency. Ion exchange (IEX) is an effective method for the removal of natural organic matter (NOM), especially anion exchange resins (AERs) with quaternary ammonium functional groups. However, capacity is limited in existing commercial resin materials because adsorbates can only interact with the outermost surface area, which makes these products inefficient on a mass basis. We have synthesized a novel “NanoResin” exploiting the enhanced NOM removal of the quaternary ammonium resin while utilizing the immense surface area of single-walled carbon nanotubes (SWCNTs), which act as scaffolding for the resin. Our nanomaterials show increased adsorption capacity per gram compared to commercially available adsorbents and reach equilibrium in a fraction of the time. This NanoResin requires only about 10 seconds to reach ion-exchange equilibrium versus more than 30 minutes for commercial resins because kinetics are only limited by diffusion. Using NanoResin as a thin film membrane filter, a NOM surrogate was removed to below its detection limit within 10 seconds of contact. Comparatively, commercial AERs only achieved partial removal after more than 15 minutes. High-capacity adsorption of a low molecular weight (MW) surrogate has been measured. NOM removal was demonstrated in solutions of both low and high specific UV absorbance (SUVA; the absorbance at 254 nm divided by dissolved organic carbon

concentration) composition with these nanomaterials. Additionally, the NanoResin showed increased removal over commercial resins with a NOM concentrate sample taken from Myrtle Beach, SC, demonstrating NanoResin is an effective method of removal for refractory NOM in a natural aqueous environment. Synthesis and characterization of the polymers and nanomaterials are presented in the following thesis, along with a thorough description of the atom transfer radical polymerization (ATRP) mechanism. We measured and characterized the adsorption capacity, adsorption kinetics, and the regeneration and reusability of these new materials for surrogate and natural NOM. The open matrix microstructure of this NanoResin precludes any intraparticle diffusion of adsorbates. Therefore the rate of adsorption is limited only by solvent diffusion to the NanoResin surface. Thus, these nanomaterials act as a “contact resin.”

## DEDICATION

I dedicate this thesis to my incredible parents who have made many sacrifices so that I could succeed. I could not have done this without their love and support.

## ACKNOWLEDGEMENTS

Firstly, I would like to acknowledge my advisor, Dr. Jordan Poler. Through his mentoring, I have grown immensely as a scientist and the valuable lessons he taught me about life and science will serve me well throughout my career. He always goes above and beyond the call of duty to support his students and we are all very thankful for his commitment.

I would also like to acknowledge the members of my thesis committee. I am very appreciative for the input provided by each member and thankful for their willingness to help. The expertise provided by each member was pivotal in solving research problems and for the overall success of the project. Also, I would like to thank my committee for writing letters of recommendation and for their advice when I was deciding between continuing my education or entering the workforce.

I thank fellow members of Poler research group, past and present, for their contributions to my education. Becky, Emily, Megan, and Tim each provided valuable assistance on the NanoResin project and each have played a critical role in the development of the project. Chauncey, Dave, and James collaborated on a separate project, but made working in the Poler research group much more entertaining and it was truly a pleasure to work alongside them. It has been a great honor to serve as a mentor to many of the undergraduate students that have been a part of the group, and I am very appreciative of all members who helped me indirectly through their questions and conversations. I am very proud to call all members of the Poler research group true friends and I look forward to hearing about each member's future successes.

I am very thankful for the rapport I have established with many faculty members during my time as an undergraduate and graduate student at UNC Charlotte. Specifically related to this work, I would like to thank Dr. Murphy for his assistance with various NMR techniques.

In my last year of the program, I was awarded the Thomas D. Walsh Graduate Research Fellowship. I am extremely grateful for the fellowship provided by Dr. Walsh. His contributions to my education are far-reaching and I cannot thank him enough for the confidence he has instilled in me through this fellowship.

Lastly, I would like to acknowledge the support of the Department of Chemistry at UNC Charlotte, UNC Charlotte Faculty research grant, and the NSF Innovation Corps.

## TABLE OF CONTENTS

LIST OF FIGURES	xi
LIST OF TABLES	xiii
LIST OF ABBREVIATIONS	xiv
CHAPTER 1: OVERVIEW	1
CHAPTER 2: ATOM TRANSFER RADICAL POLYMERIZATION	6
2.1. Components and Reaction Conditions of ATRP	14
2.1.1. Monomer	14
2.1.2. Initiator	15
2.1.3. Catalyst	17
2.1.4. Solvent	22
2.1.5. Reaction Conditions	23
2.2. Activators Regenerated by Electron Transfer ATRP	26
2.3. ATRP Conclusions	29
CHAPTER 3: CURRENT NOM REMOVAL TECHNIQUES	30
3.1. Coagulation	31
3.2. Membrane Filtration	33
3.2. Adsorption to Activated Carbon	34
3.3. Ion Exchange	36
CHAPTER 4: SYNTHESIS AND CHARACTERIZATION OF NANORESIN	37
4.1. Chemicals	37
4.2. Making a SWCNT Dispersion	38
4.2.1. Pristine HiPCO SWCNT Dispersion (Centrifugation)	38
4.2.2. Pristine HiPCO SWCNT Dispersion (Glass Wool Method)	39

4.3.	Synthesis of NanoResin	39
4.3.1.	Traditional ATRP in DMF	43
4.3.2.	ARGET ATRP in DMF	44
4.3.3.	ARGET ATRP in Water	44
4.4.	NanoResin Purification	46
4.5.	Characterization of NanoResin	51
4.5.1.	Fourier-Transform Infrared Spectroscopy	51
4.5.2.	Raman Spectroscopy	53
4.5.3.	Dynamic Light Scattering and Zeta Potential Measurements	55
4.5.4.	Scanning Electron Microscopy	60
4.5.5.	UV-VIS-NIR Spectroscopy	60
4.5.6.	Nuclear Magnetic Resonance Spectroscopy for Polymer Characterization	62
CHAPTER 5: COMPARISON OF SELECTED AER TO NANORESIN		67
5.1.	Adsorption Experiments	71
5.1.1.	NOM Removal via Adsorbent Incubation	71
5.1.2.	Surrogate Adsorption via “Fast Filtration”	71
5.1.3.	Surrogate Adsorption via Film Incubation	71
5.1.4.	DOC Removal from Myrtle Beach, SC NOM Concentrate	73
5.1.5.	Regeneration and Reuse of NanoResin	73
5.2.	Results and Discussion	73
5.2.1.	Adsorption Kinetics of a Low MW Surrogate	73
5.2.2.	Adsorption of a Low MW NOM Surrogate	80
5.2.3.	Adsorption of Low and High SUVA Surrogates	83
5.2.4.	Adsorption of Myrtle Beach, SC NOM Concentrate	89
5.2.5.	Regeneration and Reuse of NanoResin	95

CHAPTER 6: CONCLUSIONS AND FUTURE WORK	96
REFERENCES	98
APPENDIX A: AQUEOUS NANORESIN SYNTHESIS	106
A.1. JCP-46D-88	107
A.2. JCP-46D-96	107
A.3. JCP-46D-109	108
A.4. JCP-49D-26	108
A.5. JCP-46D-111	109

## LIST OF FIGURES

FIGURE 1.1:	Size comparison of selected AERs	4
FIGURE 2.1:	Stepwise reaction mechanism for ATRP	8
FIGURE 2.2:	General reaction mechanism of ATRP	10
FIGURE 2.3:	Simplified ATRP reaction mechanism	11
FIGURE 2.4:	ATRP monomer conversion as a function of time	13
FIGURE 2.5:	ATRP equilibrium constants for commonly used ATRP initiators	16
FIGURE 2.6:	ATRP equilibrium constants for commonly used ATRP ligands	19
FIGURE 2.7:	ATRP ligands as a function of redox potential	21
FIGURE 2.8:	Effect of solvent polarity on $K_{\text{ATRP}}$	24
FIGURE 2.9:	Effect of temperature on the rate of activation	25
FIGURE 2.10:	Simplified ARGET ATRP mechanism	27
FIGURE 2.11:	General ARGET ATRP mechanism	27
FIGURE 4.1:	Scheme for ARGET ATRP synthesis of NanoResin	40
FIGURE 4.2:	Scheme for ARGET ATRP of vbTMAC in DMF	41
FIGURE 4.3:	Copper/TPMA catalyst system used in ARGET ATRP	42
FIGURE 4.4:	Scheme for ARGET ATRP of vbTMAC in water	45
FIGURE 4.5:	Reaction apparatus for aqueous NanoResin synthesis	47
FIGURE 4.6:	Washing of excess polymer during NanoResin purification	48
FIGURE 4.7:	Rinsing of residual DMF during NanoResin purification	50
FIGURE 4.8:	FTIR overlay of monomer, pristine SWCNTs, and NanoResin	52
FIGURE 4.9:	Raman overlay of pristine SWCNTs and NanoResin	54

FIGURE 4.10: Molecular dynamics anneal simulation of poly(vbTMAC) on a SWCNT	56
FIGURE 4.11: RBM overlay of pristine SWCNTs and NanoResin	57
FIGURE 4.12: Electrical double layer representation of NanoResin	59
FIGURE 4.13: Electron micrographs of pristine SWCNTs and NanoResin	61
FIGURE 4.14: NMR spectrum of aqueous ARGET ATRP reaction (initial)	64
FIGURE 4.15: NMR spectrum of aqueous ARGET ATRP reaction (after 150 mins)	65
FIGURE 4.16: Monomer conversion as a function of time and Kinetics Plot of aqueous NanoResin synthesis	66
FIGURE 5.1: Sodium fluorescein as a low MW NOM surrogate	68
FIGURE 5.2: MW profile of instant coffee mix used as low SUVA NOM surrogate	70
FIGURE 5.3: NanoResin adsorption experiment using “fast filtration”	72
FIGURE 5.4: NanoResin regeneration experiment	74
FIGURE 5.5: Kinetic removal of low MW NOM surrogate	76
FIGURE 5.6: Gel and macroreticular resin structures compared to open NanoResin structure	77
FIGURE 5.7: 10-second adsorption comparison of NanoResin to MIEX <sup>®</sup> and DOWEX <sup>®</sup>	78
FIGURE 5.8: Adsorption isotherm comparison of commercially available adsorbents to NanoResin	82
FIGURE 5.9: Adsorption isotherm comparison of commercially available adsorbents to NanoResin plotted as a log-log graph	85
FIGURE 5.10: NaFL removal by NanoResin, MIEX <sup>®</sup> , and DOWEX <sup>®</sup>	86
FIGURE 5.11: 15-minute adsorption of low and high SUVA surrogate NOM by NanoResin.	91
FIGURE 5.12: NanoResin regeneration through fifteen cycles	94

## LIST OF TABLES

TABLE 5.1:	Coagulation data for low MW NOM surrogate, sodium fluorescein	69
TABLE 5.2:	Raw data from Figure 5.7, low MW surrogate after 10 second incubation	79
TABLE 5.3:	Raw data from Figure 5.8, low molecular weight surrogate (sodium fluorescein) adsorption isotherm	84
TABLE 5.4A:	Raw data from 15-minute, low SUVA surrogate adsorption experiments	88
TABLE 5.4B:	Raw data from 15-minute, low SUVA surrogate adsorption experiments	88
TABLE 5.5:	Raw data from 15-minute, high SUVA surrogate adsorption experiments	90
TABLE 5.6A:	Raw data from 5-minute, low SUVA surrogate adsorption experiments	92
TABLE 5.6B:	Raw data from 5-minute, low SUVA surrogate adsorption experiments	92
TABLE 5.7A:	Raw UV254 data from Section 5.2.4, adsorption of NOM concentrate	93
TABLE 5.7B:	Raw TOC data from Section 5.2.4, adsorption of NOM concentrate	93
TABLE A.1:	Summary of aqueous NanoResin synthesis results	110

## LIST OF ABBREVIATIONS

AA	L-ascorbic acid
AER	anion exchange resin
ARGET	activators regenerated by electron transfer
ATR	attenuated total reflectance
ATRA	atom transfer radical addition
ATRP	atom transfer radical polymerization
BB	benzyl bromide
BDE	bond dissociation energy
bipy	2,2'-bipyridine
CRP	controlled radical polymerization
DBP	disinfection byproduct
DLS	dynamic light scattering
DMF	N,N-dimethylformamide
DOC	dissolved organic carbon
DP	degree of polymerization
EPM	electrophoretic mobility
FTIR	Fourier transform infrared spectroscopy
GAC	granular activated carbon
HAA	haloacetic acid
HEBiB	2-hydroxyethyl 2-bromoisobutyrate
HiPCO	high pressure carbon monoxide

IEX	ion exchange
mg-C/L	milligrams of carbon per liter of solution
MIEX <sup>®</sup>	magnetic ion exchange
MS	mass spectrometry
MW	molecular weight
MWCNT	multi-walled carbon nanotube
NaFL	sodium fluorescein
NMR	nuclear magnetic resonance
NOM	natural organic matter
PAC	powdered activated carbon
RBM	radial breathing modes
SBA	strong base anion exchange resin
SEM	scanning electron microscopy
SSA	specific surface area
SUVA	specific UV absorbance
SWCNT	single-walled carbon nanotube
THM	trihalomethane
TOC	total organic carbon
TPMA	tris(2-pyridylmethyl)amine
USEPA	United States Environmental Protection Agency
vbTMAC	vinylbenzyl trimethylammonium chloride
WBA	weak base anion exchange resin

## CHAPTER 1: OVERVIEW

Natural organic matter exists in all active water resources. However when their levels are too high, due to natural or the continued rise of anthropogenic causes, they must be reduced. These compounds, specifically humic and fulvic acids, are a source of a potential health hazard. Modern water treatment methods rely on the use of chlorine to destroy microbial pathogens. However, chlorine reacts with NOM to form disinfection byproducts with deleterious human health risks. The two most common regulatory problems stem from trihalomethanes (THMs) and haloacetic acids (HAAs), and subsequent interest has been placed on efficient removal of their precursors.<sup>1-2</sup> It is becoming increasingly difficult for water treatment facilities to mitigate the formation of these DBPs at the limits set by the USEPA; 80 ppb for THM and 60 ppb for HAA. Possible health risks from prolonged exposure include kidney, liver, and central nervous system issues, as well as cancer.<sup>3-4</sup> Better treatment technologies are necessary to continue to improve water quality and reduce the precursors which lead to the formation of these carcinogens in drinking water. Removal of NOM is a primary concern for many drinking water utilities, and the extent of its removal depends on the efficiency of the treatment methods employed. Mismanagement of water treatment facilities and poor public policy, acutely punctuated by recent events in Flint MI, exemplify a potential systemic risk to our society.<sup>5</sup> Even with the practice of “enhanced coagulation” as prescribed by the USEPA, a source water with 2 mg/L of dissolved organic carbon

(DOC) and a moderate alkalinity of 60-120 mg/L would only be required to remove 25 % of the total organic carbon present in the water.<sup>6</sup> Many water utilities rely solely on coagulation as the means of lowering levels of DOC; however, this is not an efficient method for low molecular weight (MW) and hydrophilic varieties of NOM, as these smaller molecules are more readily removed by an adsorbent material.<sup>7-10</sup> Activated carbon is the most widely used of all adsorbent materials, but comes with a high operating cost, and with increasing concentrations of NOM being observed in drinking water sources worldwide, there has been a significant increase in demand for more efficient removal.<sup>11-12</sup>

Natural organic matter comprises decomposed plant and animal residues, encompassing an extensive variety of organic compounds, with an extremely wide range of molecular weights.<sup>13-14</sup> The majority of these compounds are weak electrolytes, leaving them as anionic species in water, thus making anion exchange resins an effective method for removal.<sup>15-16</sup> Unfortunately, commercially-available anion exchange resins (AERs) are limited in their ability to remove positively charged or neutral NOM; conversely, styrenic polymer resins have demonstrated an increased ability to adsorb these types of NOM due to dispersive interactions with the styrene backbone.<sup>7, 14</sup> Most commercially-available anion exchange resins employ a quaternary ammonium functional group in the chloride form.<sup>17</sup> These strong base AERs are being investigated as a method of water treatment because of their relatively fast equilibrium times,<sup>7</sup> and an inherent ability to remove specific DBP precursors that current treatment methods cannot.<sup>18-20</sup> These types of ion exchange resins have been proven to be more effective than coagulation and activated carbon treatment methods.<sup>17, 20-21</sup> However, due to low

specific surface area (SSA), accessible ion-exchange surface area is limited. While small molecules can effuse into the near-surface region of the material given sufficient time, high molecular weight NOM cannot due to its size. This slows the sorption kinetics and also lowers the overall capacity of the resin because these large molecules restrict transport of smaller molecules to the active adsorption sites. Increasing external IEX surface area lowers the diffusion path of adsorbates and minimizes these issues.<sup>22</sup>

To enhance NOM removal even further, we have synthesized novel nanomaterials by functionalizing the surface of single-walled carbon nanotubes (SWCNTs) with a strong base anion exchange resin to exploit the large SSA of SWCNTs.<sup>23</sup> This allows NOM of all sizes to readily adsorb to the increased number of active ion exchange sites on the surface, and for a greater percentage of active sites to be utilized. As described by Bolto et al. (2001), water content was found to be the most important parameter of IEX efficiency for removing charged aqueous NOM of both hydrophilic and hydrophobic varieties.<sup>7</sup> NanoResin has a completely open resin matrix, with 0% crosslinking, thus 100% water content (ion exchange polymer is completely water soluble). This allows for all ion exchange sites to be on the surface of the particle, making the resin essentially a contact resin with kinetics limited only by solvent diffusion as opposed to intraparticle diffusion. This property differentiates this NanoResin from other resin matrices. The width of our NanoResin is  $w \sim 10$  nm. This is more than three orders of magnitude thinner than MIEX<sup>®</sup> resin beads,<sup>24</sup> ( $\sim 180$   $\mu\text{m}$ ) or DOWEX<sup>®</sup> 21K ( $\sim 1$  mm) as illustrated in figure 1.1. Hence, the SSA for adsorption is significantly higher for the nanomaterials we describe below. The higher effective porosity of NanoResin relative to MIEX<sup>®</sup>

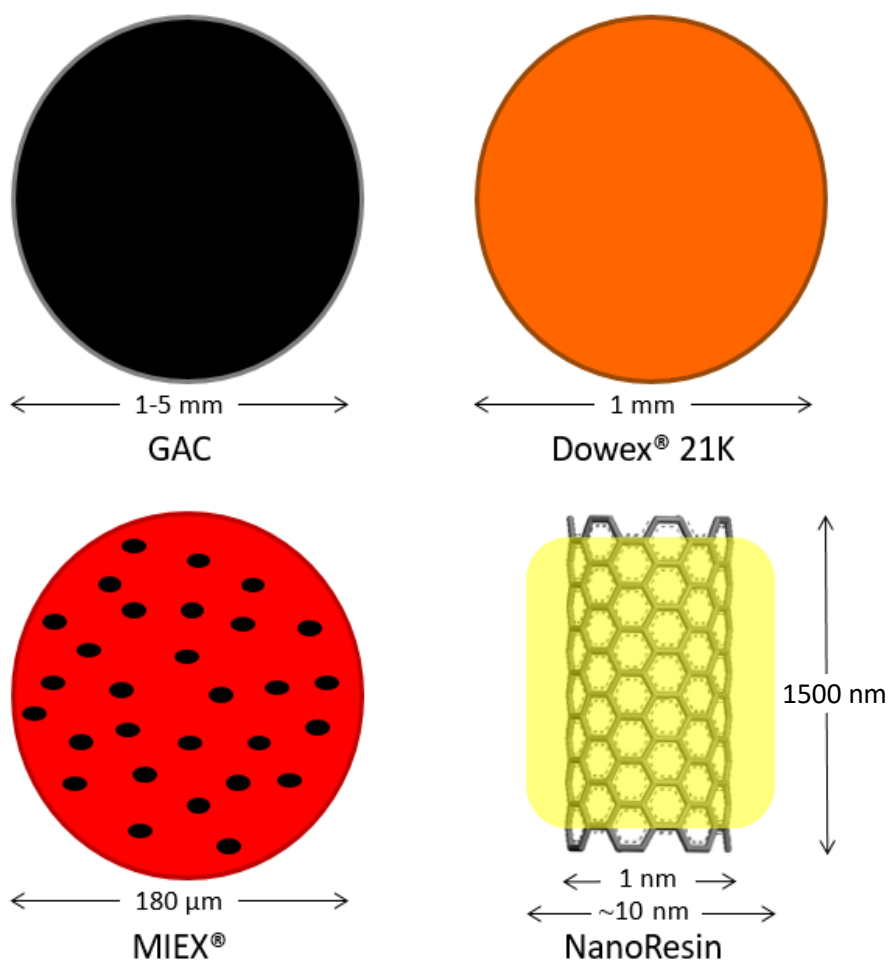


FIGURE 1.1: Size Comparison of Selected AERs. NanoResin has more than  $10^6$  times the specific surface area compared to commercial resins

particles thereby reduces the time (and reactor size) required for efficient removal of dissolved organic contaminants from source waters. Our nanomaterials form stable dispersions in water, and show adsorption capabilities far greater than current removal technologies at a faster rate. Moreover, the ability to quickly regenerate this high-capacity NanoResin could make our novel nanoscale anion exchange resin a cost-effective alternative to current water treatment methods.

## CHAPTER 2: ATOM TRANSFER RADICAL POLYMERIZATION

Developed in 1995, by Krzysztof Matyjaszewski at Carnegie Mellon University, Atom Transfer Radical Polymerization (ATRP) is a robust polymerization mechanism used to polymerize vinyl monomers with a great degree of tunability.<sup>25</sup> ATRP is a form of Controlled Radical Polymerization (CRP) and was derived from a common organic chemistry mechanism for carbon-carbon bond formation known as Atom Transfer Radical Addition (ATRA). Both mechanisms require an initiating alkyl halide, a vinylic molecule/monomer, and a catalyst composed of a transition metal complexed with a ligand.

In ATRA, a halogen atom is abstracted from an alkyl halide,  $R-X$ , by a transition metal species,  $M_t^z$ , forming an active radical,  $R\bullet$ , and an oxidized transition metal species,  $M_n^{z+1}-X$ . The radical then reacts with an unsaturated molecule,  $Y$ , forming a new carbon-carbon bond, and an intermediate radical,  $R-Y\bullet$ . This is followed by a deactivating back-transfer of the halogen atom from the transition metal species to the newly formed organic radical adduct, producing the desired product,  $R-Y-X$ , while reducing and regenerating the transition metal species,  $M_t^z$ . The process can then be repeated until all of the alkyl halide has been reacted.<sup>26</sup>

The difference between ATRA and ATRP occurs when the deactivated product from ATRA,  $R-Y-X$ , is reactivated by oxidizing the transition metal species by re-abstracting the halogen. This allows for repeated addition of the unsaturated compound

(monomer in ATRP) through reaction with the intermittently formed radical, leading to controlled chain-growth polymerization. Controlled polymerization is simply achieving the desired degree of polymerization, DP, with low polydispersity. This requires that the radical species be stable before and after activation/deactivation, allowing the cycle to repeat until all of the monomer is converted. A stepwise scheme for ATRP, shown in Figure 2.1, includes three basic steps: initiation, propagation, and termination.

ATRP initiation occurs when the catalyst complex, consisting of a transition metal complexed with a ligand,  $M_t^z/L_n$ , abstracts a halogen atom from the alkyl halide initiator,  $R-X$ , creating an active radical species,  $R\bullet$ , and an oxidized catalyst complex,  $X-M_t^{z+1}/L_n$ . This is a reversible step with a forward rate constant of  $k'_{act}$ , and a reverse rate constant of  $k'_{deact}$ . The radical species then reacts with the double bond of the vinyl monomer,  $M$ , to irreversibly form the first active polymer adduct,  $R-M\bullet$ , with a rate constant of  $k_i$ . The chain is then reversibly deactivated through the back-transfer of the halogen atom from the catalyst complex; leaving a dormant chain,  $R-M-X$ , and the reduced catalyst,  $M_t^z/L_n$ . This back transfer completes the redox cycle of the catalyst complex, allowing it to complete the process again.

After initiation, propagation proceeds to grow polymer chains to the desired length. During propagation, the catalyst species begins in the lower oxidation state,  $M_t^z/L_n$ , where it can re-abstract and activate the polymer chain, with a rate constant of  $k_{act}$ . This leaves the catalyst complex in a higher oxidation state,  $X-M_t^{z+1}/L_n$ , and an active radical chain,  $R-M\bullet$ . The active chain can then propagate through the addition of another unsaturated monomer unit, with rate constant of  $k_p$ . Deactivation follows once again by back-transfer of the halogen atom from the catalyst to the active chain, with a



rate constant of  $k_p$ , leaving the catalyst in the deactivated state,  $M_t^z/L_n$ , and a dormant polymer chain,  $R-M_n-X$ .

Throughout the propagation process, termination reactions ( $k_t$ ) inevitably occur, but in a well-controlled ATRP reaction, only a small percentage of polymer chains terminate. These reactions are primarily the result of bimolecular termination or catalyst disproportionation. Bimolecular termination occurs when two active chains combine (ex:  $R-M_n\bullet$  and  $R-M_m\bullet$ ) to give an irreversibly dormant chain,  $R-M_n-M_m-R$ . This termination results in a buildup of the oxidized catalyst species,  $X-M_t^{z+1}/L_n$ , which slows the overall rate of the reaction.<sup>27</sup> Disproportionation of the catalyst complex can also result in an increase in  $k_t$ . This happens when the transition metal catalyst complex in its lower/activating oxidation state is simultaneously oxidized and reduced, instead of activating the alkyl halide. For example, using a copper catalyst,  $Cu^I$  should activate, but when undergoing disproportionation,  $Cu^0$  and  $Cu^{II}$  are formed. All three steps have been combined in figure 2.2, and further simplified in figure 2.3.<sup>27</sup> Since copper catalysts are most commonly used for ATRP, all further examples and figures will be based on a copper catalyst.

If initiation is fast and termination is negligible, in the absence of  $O_2$ , then well-defined polymers with narrow molecular weight ranges can be formed.<sup>28</sup> Equilibrium exists between active (radical) chains and dormant (halide-capped) chains, as

$$K_{ATRP} = \frac{k_{act}}{k_{deact}}. \quad (2.1)$$

To limit bimolecular termination, the concentration of active radicals must be kept low, therefore the majority of the chains are dormant at any given time, and the equilibrium is

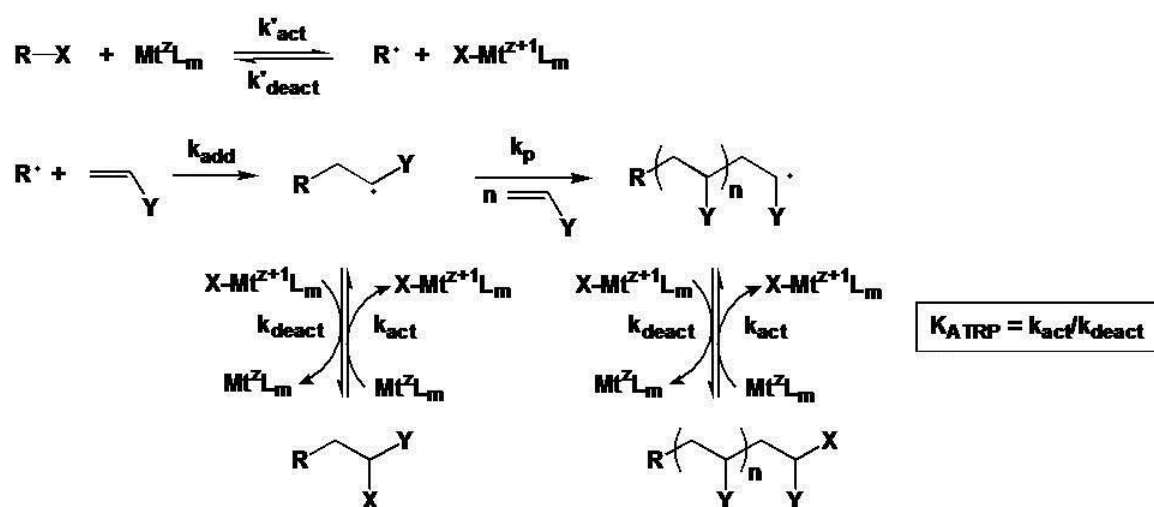


FIGURE 2.2: General reaction mechanism of ATRP showing all activation and deactivation steps (Matyjaszewski et. al., 2001).

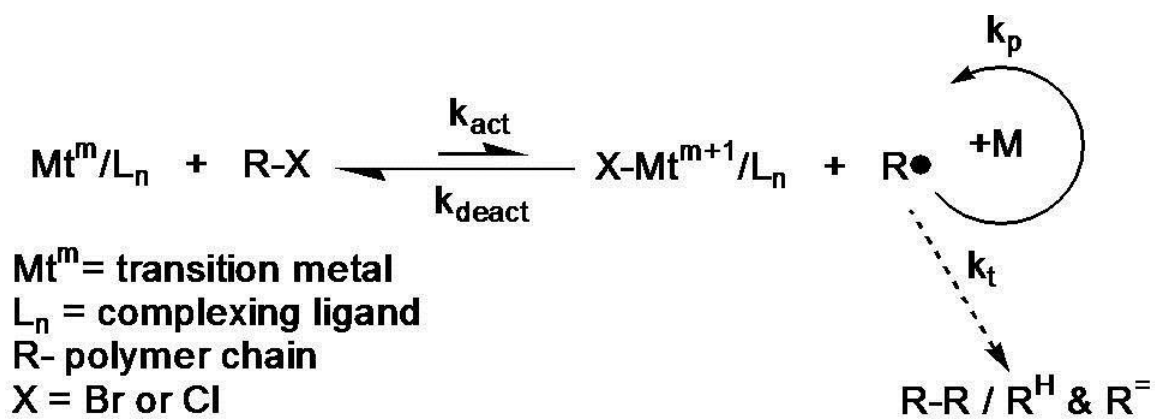


FIGURE 2.3: Simplified ATRP reaction mechanism. As displayed,  $k_{\text{deact}} \gg k_{\text{act}}$ . If concentration of active chains is not kept at a low enough concentration, termination reactions will increase (Matyjaszewski et. al., 2001).

shifted to the left ( $k_{\text{deact}} \gg k_{\text{act}}$ ).<sup>29</sup> This means that a low concentration of radicals would be required to propagate a large number of polymer chains. To ensure that all polymer chains have the same probability of adding a monomer unit,  $k_{\text{deact}}$  must be significantly higher than the rate constant for propagation; if this is true, greater control and a much more narrow range of molecular weights can be achieved.<sup>30</sup> The rate law of ATRP,  $R_p$ , relates directly to the equilibrium constant and can be defined as:

$$R_p = k_{\text{app}}[M]M = k_p[M][R-X] \frac{k_{\text{act}}[\text{Cu}^{\text{I}}\text{X}/\text{L}]}{k_{\text{deact}}[\text{Cu}^{\text{II}}\text{X}_2/\text{L}]}, \quad (2.2)$$

where  $k_{\text{app}}$  is the apparent rate constant (from  $\ln([M_0]/[M])$  vs time),  $[M]$  is the monomer concentration,  $[R-X]$  is the concentration of dormant chains (X is the initiator halide),  $[\text{Cu}^{\text{I}}\text{X}/\text{L}]$  is the concentration of the activating catalyst species (L is the catalyst ligand), and  $[\text{Cu}^{\text{II}}\text{X}_2/\text{L}]$  is the concentration of the deactivating catalyst species in the system.

Since the majority of chains in a well-controlled ATRP system are dormant,  $[R-X]$  can be approximated based on the initiator concentration.<sup>31</sup> The rate of polymerization will slow as monomer concentration decreases (and is converted into polymer), as shown in figure 2.4 where conversion vs time is logarithmic.<sup>27</sup> ATRP is a first-order kinetic process with respect to monomer concentration, as long as termination is minimal, and a constant concentration of the active catalyst species is maintained.<sup>27</sup> Based on equation 2.2, the most controllable aspect of the rate of polymerization is via  $K_{\text{ATRP}}$  ( $k_{\text{act}}/k_{\text{deact}}$ ).

Aside from the ratio of active to dormant chains, equilibrium is controlled by five critical parameters: initiator structure/leaving atom, catalyst (transition metal and ligand), solvent, temperature, and pressure. These variables are discussed further in section 2.1.

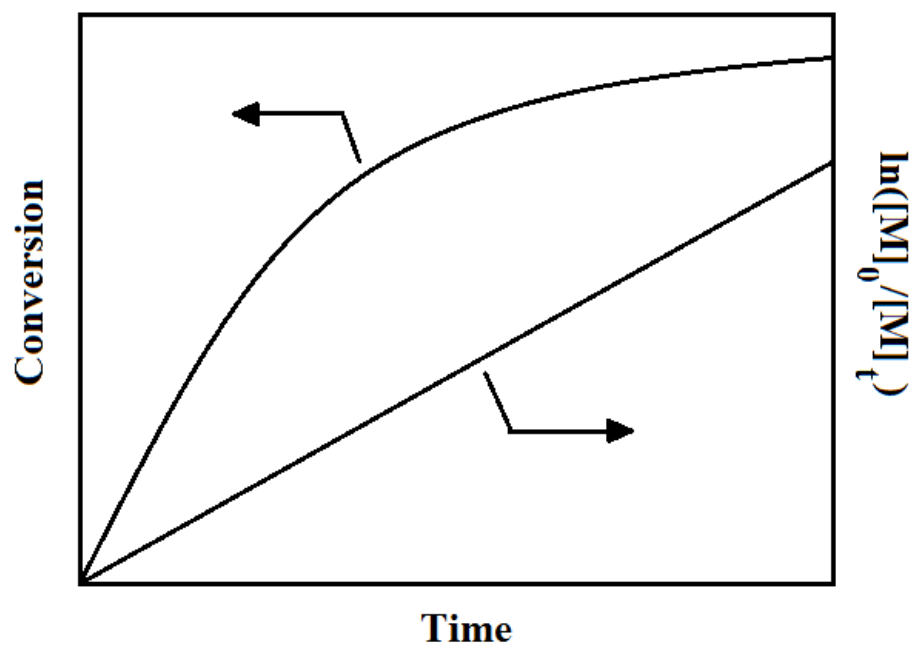


FIGURE 2.4: ATRP monomer conversion as a function of time. Semi-logarithmic plot shows first order kinetics with respect to monomer concentration (Matyjaszewski et. al., 2001).

## 2.1. Components and Reaction Conditions of ATRP

ATRP is a robust polymerization mechanism that allows most monomer types to be polymerized using a wide variety of ATRP reagents. No two ATRP systems have the same equilibrium constants, propagation rates, or polydispersity. ATRP is a multicomponent system, where each component must be optimized based on the monomer being used, desired polymer structure, polymer length, and polymerization control. If the equilibrium constant is too low, polymerization will not occur, but if  $K_{\text{ATRP}}$  is too high the radical concentration will be too great and bimolecular termination will increase resulting in a wide range of MWs. From experimental data, relatively low values of  $K_{\text{ATRP}}$  ( $\sim 10^{-9}$  to  $\sim 10^{-4}$ ) are desirable to keep radical concentrations low and minimize bimolecular termination.<sup>25, 27</sup> Through careful selection of initiator and catalyst, as well as appropriate reaction conditions in a suitable solvent, well controlled ATRP of numerous monomers can be achieved.

### 2.1.1. Monomer

All ATRP monomers have one thing in common: an accessible, terminal, (vinyl) double bond. Types of vinylic monomers used in ATRP synthesis include, acrylamides, acrylates, acrylonitrile, dienes, methacrylamides, methacrylates, and styrenes as well as their derivatives.<sup>28</sup> Each monomer has an intrinsic ATRP equilibrium constant based on the system's activating and deactivating species that requires optimization to maintain polymerization control.<sup>27</sup> A monomer's ability to stabilize radicals through resonance and inductive effects, increases its equilibrium constant.<sup>32</sup> However, since a monomer is typically chosen based on structure or functional groups, it is necessary to change other components of the system to maintain control.

### 2.1.2. Initiator

The primary purpose of the initiator is to dictate the number of polymer chains in an ATRP system based on the initial ratio of monomer to initiator ( $[M]_0:[R-X]_0$ ).<sup>25</sup> From this ratio, the theoretical molecular weight or degree of polymerization (DP) can be determined from

$$DP = \frac{[M]_0}{[R-X]_0} \times (\text{conversion}), \quad (2.3)$$

where molecular weights increase linearly with conversion. To maintain control over polymerization and maintain a narrow range of molecular weights, initiation must be fast to ensure consistency in the number of propagating chains.<sup>27</sup>

Initiators have a direct effect on the ATRP equilibrium constant,  $K_{\text{ATRP}}$ , based mostly on the leaving atom (halide) and initiator structure. The initiator effect on  $K_{\text{ATRP}}$  is largely defined by the product of the equilibrium constants for homolytic bond dissociation of the initiator and the formation of the deactivating catalyst species (halidophilicity).  $K_{\text{ATRP}}$  is inversely proportional to the bond dissociation energy (BDE) of the carbon-halogen bond of the initiator, with lower BDEs resulting in greater  $K_{\text{ATRP}}$ .<sup>33</sup> As atomic radii increase moving down the periodic table, BDEs decrease. This trend is reflected in figure 2.5 where the “activity” (greater  $K_{\text{ATRP}}$ ) of commonly used initiators and their activities are displayed.<sup>33</sup> Therefore, bromide initiators are significantly more active than the corresponding chloride. For example, allyl chloride (AllCl) and allyl bromide (AllBr) have equilibrium constants of  $2.3 \times 10^{-6}$  and  $1.7 \times 10^{-5}$ , respectively. This trend predicts, in terms of activity, that  $F < Cl < Br < I$ ; however, almost all ATRP initiators are of the chloride and bromide variety. Alkyl fluorides have not been used as ATRP initiators, as the C-F bond is simply too strong for the fluorine atom to be facily

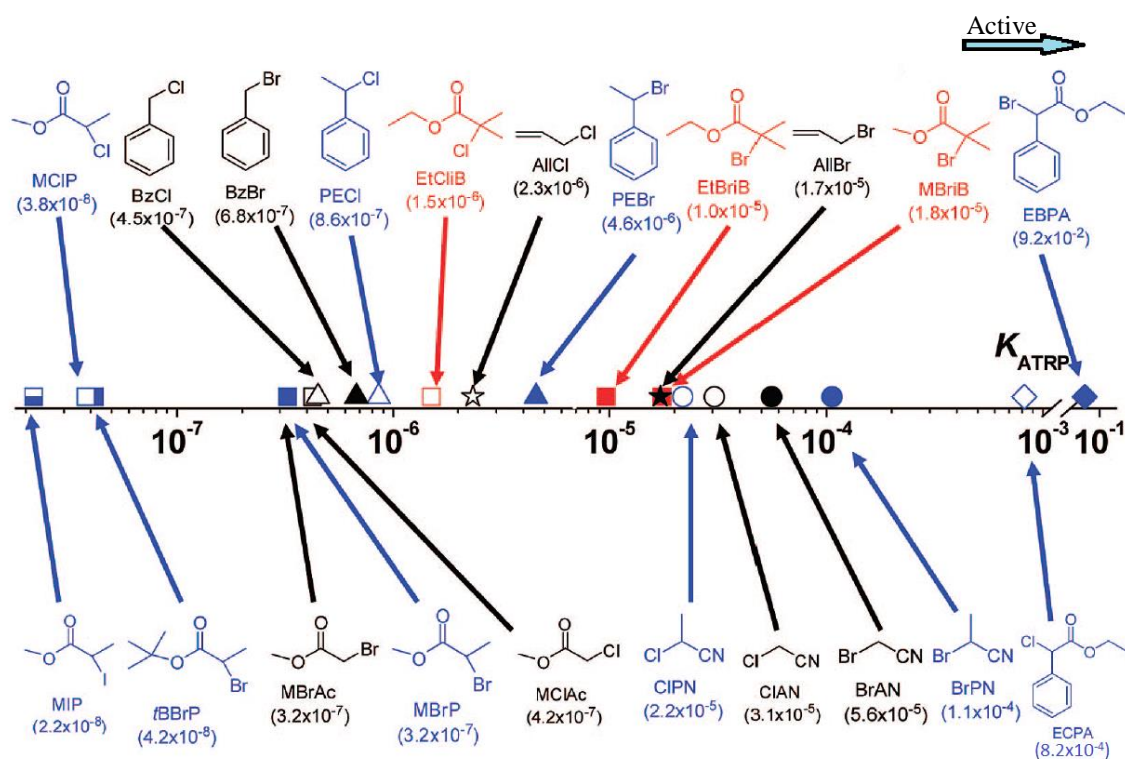


FIGURE 2.5: ATRP equilibrium constants for commonly used ATRP initiators under same reaction conditions (Cu/TPMA in acetonitrile at 22 °C). Color key based on halogen substitution: Red (tertiary), Blue (secondary), black (primary) (Tang, *et al.*, 2008).

abstracted to initiate ATRP. Iodine has been used in ATRP, but with limited success due to the limited stability of the  $\text{Cu}^{\text{II}}-\text{I}$  bond.<sup>33</sup>

The initiator structure also plays a small role in activity in that  $K_{\text{ATRP}}$  increases based on substitution (primary < secondary < tertiary). This is shown in figure 2.5, and exemplified by comparing benzyl chloride (BzCl) to phenylethyl chloride (PeCl) with equilibrium constants of  $4.5 \times 10^{-7}$  and  $8.6 \times 10^{-7}$ , respectively. Of the commonly used initiators and their equilibrium constants listed in figure 2.5, activity spans six orders of magnitude; this illustrates the tunability of ATRP just by altering the initiator. Again, it should be remembered that the more “active” the system, the higher the radical concentration, which leads to increased termination and loss of polymerization control; a balance must be achieved between the rate of polymerization and the concentration of active radicals to maintain a well-controlled system.

### 2.1.3. Catalyst

The most critical component in an ATRP system is the catalyst system, which can be thought of simply as a halogen transfer vehicle. Without this transition metal catalyst, radicals would not be formed, and controlled radical polymerization could not be achieved. While the rate of polymerization,  $R_p$ , is directly proportional to the concentration of the catalyst, according to equation 2.2, there is no effect on the polymer's molecular weight.<sup>30</sup> The catalyst controls activation and deactivation of growing polymer chains, therefore the ATRP equilibrium is directly linked to catalyst system employed. Again,  $K_{\text{ATRP}}$  must be optimized. Equilibrium constants too low can slow or stop polymerization, and too high leads to increased polydispersity and a poorly controlled polymerization. ATRP catalysts are composed of a transition metal center complexed with a stabilizing ligand. An effective catalyst must satisfy several criteria:

1) the transition metal center must be capable of a one-electron redox couple to allow for atom transfer, 2) upon oxidation, the coordination sphere of the metal center must be able to accommodate the inclusion of the abstracted halogen atom, 3) the metal center must have an affinity for halogens, and 4) the catalyst cannot lead to significant side reactions that would alter the function of the catalyst, it should promote radical formation and propagation.<sup>27-28, 30</sup>

A variety of transition metals have been successfully used for ATRP, such as nickel, ruthenium, aluminum, iron. However, copper is the most widely used in ATRP catalyst systems and will be the focus of this thesis. The two oxidation states of the copper catalyst serve complimentary purposes; the copper (I) complex creates active polymer chains through abstraction of the halogen atom from the dormant species and allowing propagation, subsequently the copper (II) complex deactivates polymer chains through back-transfer of a halogen atom after the addition of a small number of monomer units promoting a well-controlled polymerization. This dynamic relationship between active and dormant chains intrinsic to the catalyst system being used and must be optimized to maintain polymerization control.

Choosing the correct ligand is essential to achieve the desired ATRP equilibrium constant.<sup>25</sup> While the monomer and initiator both have significant effects on  $K_{\text{ATRP}}$ , they are typically predetermined based on desired polymer structure. However, the ligand can be adjusted to obtain an optimal equilibrium constant.<sup>30</sup> The ligand in an ATRP catalyst complex serves to solubilize transition metal salts, to increase the reactivity of the metal center through electron donation, and to stabilize the catalyst complex.<sup>27</sup> Nitrogen-based polydentate ligands have proven to be the most activating ligands for copper-based

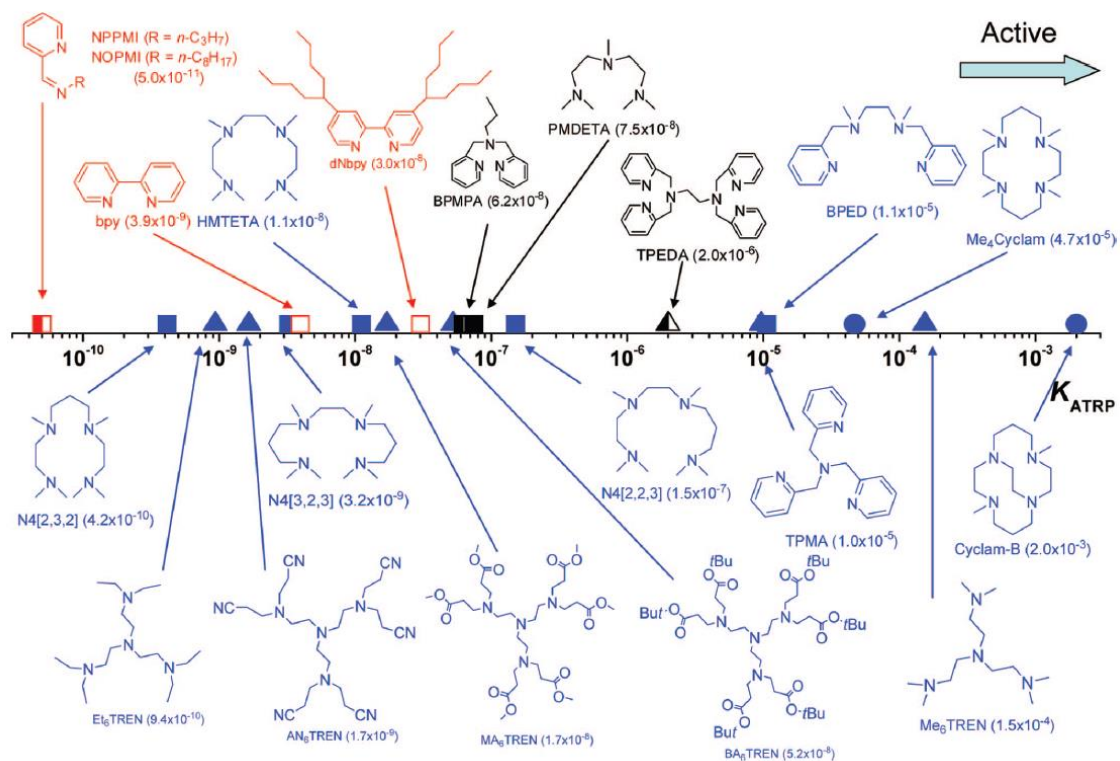


FIGURE 2.6: ATRP equilibrium constants for commonly used ATRP ligands under same reaction conditions (Initiator: EtBriB, Catalyst salt: CuBr in acetonitrile at 22 °C). Color key based on the number of nitrogen atoms: Red (2), Blue (3 or 6), black (4) (Tang, *et al.*, 2008).

ATRP, and they control the equilibrium position through both electronic and steric mechanisms. The steric effect comes by reducing the rate of activation of the catalyst system, by making it more difficult for the halogen atom to interact with the metal center. The more prominent factor affecting catalyst activity comes from stabilization of the deactivating ( $\text{Cu}^{\text{II}}$ ) catalyst species through electron donation by the ligand.<sup>34-35</sup>

In figure 2.6, a series of commonly used ligands are displayed as a function of activity, demonstrating the effect of ligand choice on equilibrium position.<sup>33</sup> A general trend of increasing activity based on an increasing number of nitrogen atoms can be observed; however, this is not always true as seen with the N4 ligands in figure 2.6. Activity depends mostly on how the ligand attachment distorts the desired geometry of the catalyst structure and the effect on redox potential of the metal center. In the most simplistic generalization, ligand activity correlates most directly to electron donating groups on the ligand which can increase the reductive potential of the catalyst. This is plotted in figure 2.7, where ATRP equilibrium is plotted as a function of redox potential.<sup>33</sup> The ideal ATRP catalyst should have a large equilibrium constant so that it can be used at lower concentrations but still maintain control and a narrow range of molecular weights.<sup>35-36</sup>

Another important factor relating to the catalyst is the choice of the starting halide salt; this factor is based on the relative bond strength of the carbon-halogen and copper-halogen bonds that are repeatedly formed and broken during ATRP. C/Cu–X bonds are typically weaker in bromine ATRP, allowing for a more efficient polymerization that can be conducted at lower temperatures.<sup>28</sup>

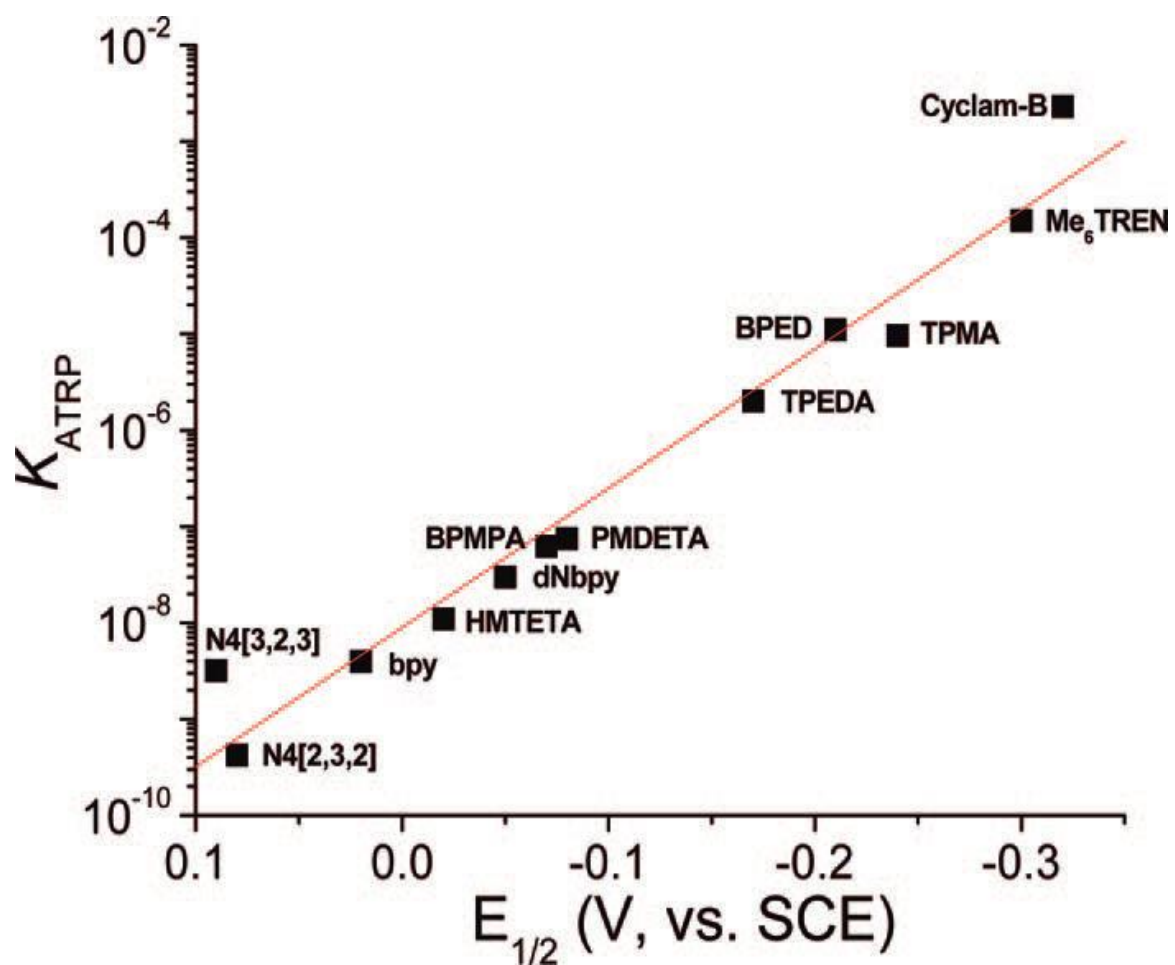


FIGURE 2.7: ATRP ligands as a function of redox potential (refer to figure 8 for ligand structure). Greater electron donation by a ligand to the transition metal center correlates directly to an increase in  $K_{\text{ATRP}}$  and a lower redox potential (Tang, *et al.*, 2008).

Choosing the proper catalyst/ligand is the most important part of a well-controlled ATRP synthesis. The most active catalyst isn't always the best option, as a sufficient rate constant of deactivation must be maintained to keep polydispersity low. Catalyst solubility and stability must also be considered based on solvent choices due to potential side reactions, catalyst dissociation, and/or catalyst precipitation that would effectively lower  $K_{\text{ATRP}}$ .<sup>37</sup>

#### 2.1.4. Solvent

ATRP can be conducted on neat monomer or within a solvent. Solvents may become necessary due to solubility issues; either the polymer is not soluble in its monomer, or the monomer being polymerized is a solid at reaction temperatures. Aprotic solvents, solvents that do not contain O–H or N–H groups that would allow hydrogen bonding, are primarily used for ATRP. More recently, aqueous/protic solvent systems have been of great interest to synthesize water soluble polymers, or to move away from traditional ATRP solvents that can be volatile or hazardous. Water is safe, inexpensive, and environmentally benign. However, a litany of side-reactions has led to very poor polymerization control and low molecular weight polymers.<sup>38</sup>

Solvents must be chosen carefully based on interactions with the catalyst. Several factors must be considered such as chain transfer, catalyst interactions, and polymer endgroup interactions. Chain transfer typically limits total conversion as the solvent can potentially act as a chain transfer agent resulting in low molecular weight chains. Catalyst interactions can be detrimental to polymerization due to solvolysis of the copper-halogen bond, and/or displacement of certain ligands. Lastly, the carbon-halogen bond of the initiator or dormant polymer chain can undergo solvolysis such that endgroup functionality would be lost thereby limiting conversion.<sup>28</sup>

Moreover, solvent choice has an inherent effect on the equilibrium constant,  $K_{\text{ATRP}}$ . This increase in activity directly corresponds to the polarity of the solvent as shown in figure 2.8.<sup>39</sup> Polar solvents accelerate the reaction, while stabilizing the deactivating  $\text{Cu}^{\text{II}}$  species and allowing the desired DP to be achieved with a narrow range of molecular weights.<sup>40</sup>

#### 2.1.5. Reaction Conditions

ATRP equilibrium and polymerization control can also be significantly altered by adjusting temperature and pressure as well as overall reaction time. This idea is more far-reaching than simply increasing the number of collisions between molecules with an increase in temperature as Collision Theory suggests.<sup>41</sup> While it is true that polymerization occurs faster at increased temperatures (Figure 2.9), better polymerization control is also achieved.<sup>42</sup> This happens because the energy of activation is markedly higher for termination or disproportionation compared to that of propagation.<sup>28</sup> From equation 2.2, the rate of polymerization slows with conversion as it is directly proportional to monomer concentration. Therefore, at high monomer conversion it is deleterious to allow the polymerization to proceed as the rate of most side reactions is independent of monomer concentration. Failure to consider this can result in significant loss of endgroup functionality.<sup>30</sup> Increasing the pressure inside of the ATRP reaction vessel has also been shown to significantly increase polymerization control and rate much, like temperature. This is done by increasing both the equilibrium constant as well as the rate constant for propagation. Increasing pressure results in an increase in propagation while suppressing termination. Termination suppression is thought to be directly associated with the increase in viscosity.<sup>43-44</sup>

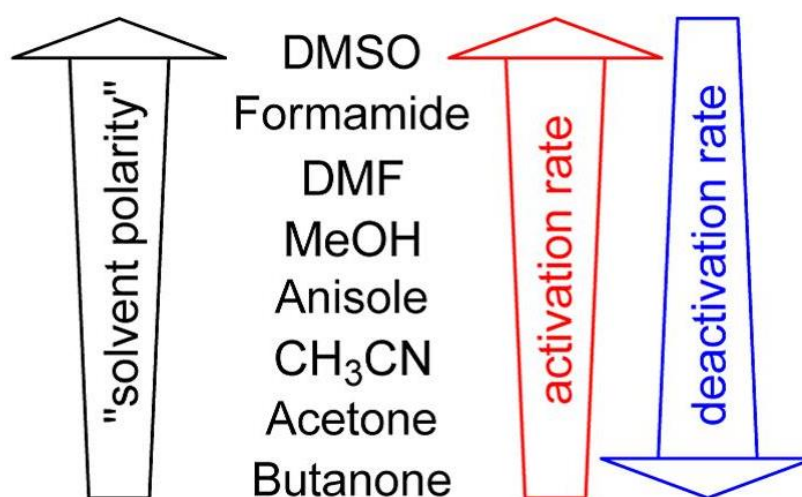


FIGURE 2.8: Effect of solvent polarity on  $K_{\text{ATRP}}$ . The ATRP equilibrium constant increases proportionally to solvent polarity. Depending on the polarity of the solvent, this could be used to speed up, or slow down, an ATRP system (Horn, *et al.*, 2013).

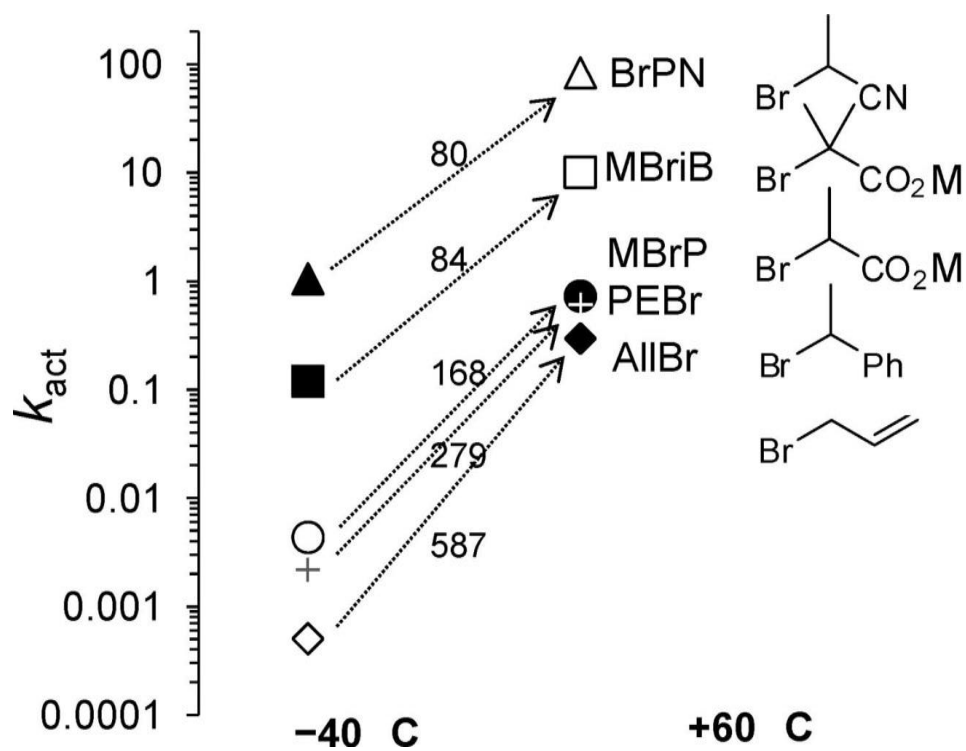


FIGURE 2.9: Effect of temperature on the rate of activation. The activation rate constant  $k_{act}$  plotted as a function of increasing temperature, showing  $k_{act}$  increases with temperature (Seeliger, *et al.*, 2009).

## 2.2. Activators Regenerated by Electron Transfer ATRP

To reduce copper concentrations in ATRP, Matyjaszewski et al. developed a modified version of traditional ATRP known as activators regenerated by electron transfer (ARGET). ARGET ATRP relies on the same basic mechanism as traditional ATRP, but allows copper concentrations to be lowered to the parts per million level through the use of an environmentally benign reducing agent as depicted in figure 2.10.<sup>45-</sup><sup>46</sup> In traditional ATRP, bimolecular termination reactions ( $k_t$ ) cannot be avoided, and eventually leads to a buildup of “deactivators” ( $\text{Cu}^{\text{II}}$  species) requiring an excess of catalyst to be added to the system in the beginning to account for termination. ARGET ATRP employs a reducing agent to continuously produce “activators” ( $\text{Cu}^{\text{I}}$  from  $\text{Cu}^{\text{II}}$ ), and as shown in figure 2.11.<sup>47</sup> Not only does ARGET lower the catalyst concentration to part per million levels (with respect to monomer), but it also practically eliminates the need for catalyst removal upon reaction completion.<sup>35</sup> The rate of polymerization was defined in equation 2.2, also governs ARGET ATRP as the rate depends on the *ratio* of  $[\text{Cu}^{\text{I}}]$  to  $[\text{Cu}^{\text{II}}]$  and not the actual concentrations of each.<sup>31</sup> While the rate of the reaction maintains the same in comparison to traditional ATRP, greater control can be achieved as many of the side reactions that limit MW are inherently minimized with the lower catalyst concentration.<sup>35</sup>

This “green” method begins with using the oxidatively stable copper (II) species, but the reaction will not start until the reducing agent is introduced to the system. Commonly used and FDA approved reducing agents are ascorbic acid, glucose, and tin (II) 2-ethylhexanoate.<sup>48</sup> To maintain polymerization control, strong reducing agents (such as ascorbic acid) should not be used since reduction from  $\text{Cu}^{\text{II}}$  to  $\text{Cu}^{\text{I}}$  happens too

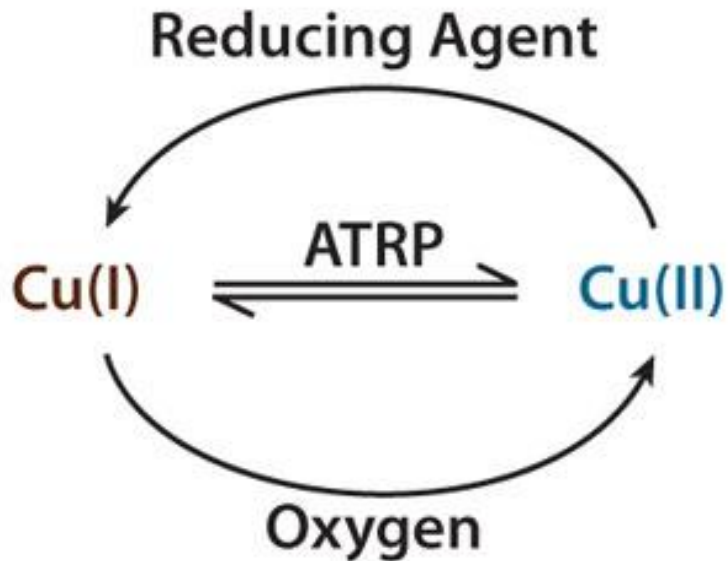


FIGURE 2.10: Simplified ARGET ATRP mechanism shows the use of a reducing agent to steadily produce the activating  $\text{Cu}^{\text{I}}$  species by reducing the deactivator. (Matyjaszewski, *et al.*)

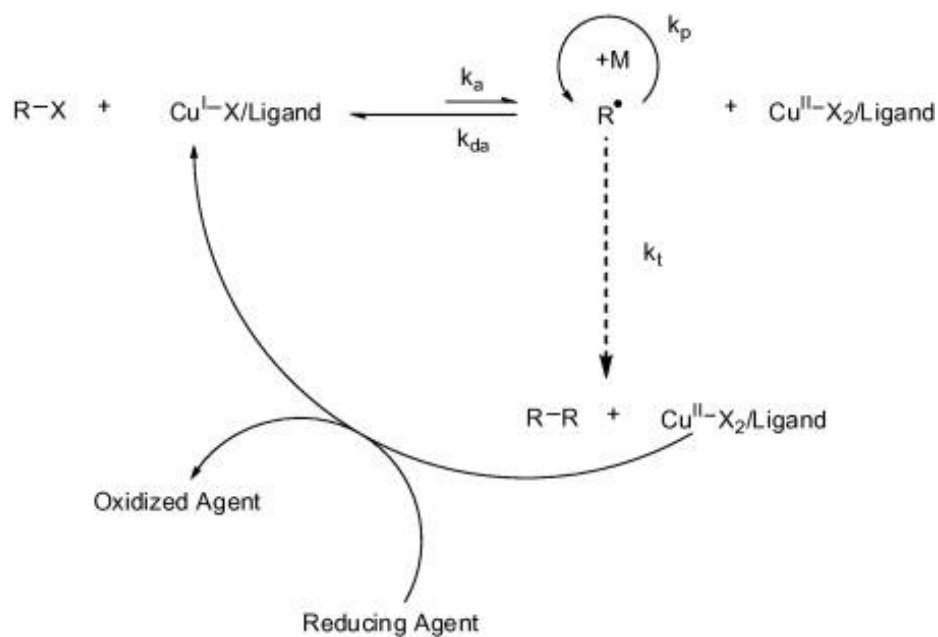


FIGURE 2.11: General ARGET ATRP mechanism. This method utilizes trace amounts of catalyst without lowering the rate of polymerization (Jakubowski, *et al.*, 2006).

quickly, increasing the radical concentration and leading to a wide range of molecular weights. Stronger reducing agents should only be used when limited solubility controls concentration. To circumvent this issue when using strong reducing agents, slowly feeding the regenerant into the ATRP solution can control the rate of reduction and radical concentration.<sup>38</sup> Concentration of reducing agent also plays a role in polymerization rates, but at the cost of polymerization control so optimization and expectations must be considered. Reduction should be slow, but efficient to maintain polymerization control.<sup>48</sup>

Like traditional ATRP, a variety of solvents can be used for ARGET ATRP, but the activity increases with solvent polarity. Aprotic solvents are primarily used for ARGET ATRP synthesis. The same side reactions exist for protic solvents (like water), but hydrolysis/solvolytic of copper-halogen and carbon-halogen bonds is much more problematic. Aqueous systems are of the most interest for ATRP. Due to water's relatively high dipole moment (1.85 D),  $K_{\text{ATRP}}$  is very large in aqueous systems; in some cases four orders of magnitude higher in water than in organic solvents.<sup>49</sup> As stated previously, higher equilibrium constants lead to high concentrations of radicals and eventually an increased rate of termination. Choosing a less activating ligand can be beneficial by lowering  $K_{\text{ATRP}}$  to an optimal range for that particular system. This was proven experimentally when tris(2-pyridylmethyl)amine (TPMA) was found to be the most versatile ligand for aqueous ARGET ATRP synthesis based on  $K_{\text{ATRP}}$  and halidophilicity (stabilization of deactivator) despite being less activating than ligands such as Me<sub>6</sub>TREN or Me<sub>4</sub>Cyclam.<sup>50</sup> Contrarily to lowering  $K_{\text{ATRP}}$ , decreasing the

catalyst concentration can minimize the concentration of active radicals with respect to monomer concentration and lessen the number of chains terminating.

### 2.3. ATRP Conclusions

Atom transfer radical polymerization is a versatile and well-known polymerization mechanism that allows a great degree of tunability depending on the system being used. Care must be taken to optimize the parameters according to the desired degree of polymerization and reaction time while maintaining control of polymerization. ARGET ATRP provided a significant improvement over traditional ATRP by drastically lowering the catalyst concentration without altering polymerization rates or sacrificing control. This advancement makes ATRP a much more environmentally friendly process that can also be conducted in the presence of limited amounts of O<sub>2</sub> also making it a viable industry technique.<sup>47</sup>

ATRP was the chosen method for NanoResin synthesis due to the versatility and adaptability of the method. Very little literature exists for ATRP of ionic monomers, like vbTMAC, in aqueous systems. However, by optimizing the reagents discussed above, a direct and efficient pathway was developed. Once the polymer synthesis was complete, the same mechanism for propagation was used for covalently attaching the polymer to SWCNTs. Again, the adaptability of this method allowed for a simple, one-pot synthesis, of our NanoResin.

## CHAPTER 3: CURRENT NOM REMOVAL TECHNIQUES

Clean water is essential to life. Water disinfection is one of the most important preventative health measures ever established and has led to significant decreases in waterborne illnesses such as cholera, typhoid fever, and amoebic dysentery.<sup>51</sup> While disinfection processes like chlorination, chloramination, and ozonation are very effective at killing dangerous microorganisms, they are also strong oxidizing agents. This highly oxidative environment gave way to an unintended rise in hazardous compounds known as disinfection byproducts.<sup>52</sup> DBPs are formed when natural organic matter is oxidized in the presence of chlorine or bromine.<sup>53</sup> Currently, there are three major classes of regulated DBPs: trihalomethanes, haloacetic acids, and oxyhalides (bromates and chlorites). Of these three classes, 11 compounds are actively regulated by the USEPA, and more than 600 are compounds that have been listed as DBPs.<sup>54-55</sup> Many water utilities have now adopted the practice of attempting to remove DBP precursors before disinfection in effort to thwart the formation of these potentially hazardous compounds.<sup>52</sup>

NOM is found in all water sources and must be removed from water before disinfection to prevent the formation of DBPs. An overall increase in NOM levels has been observed over the past 20 years, significantly altering how drinking water must be treated.<sup>55</sup> This increase in NOM serves as an energy source for microorganisms, which in turn requires water utilities to increase disinfection, consequently increasing DBP formation.<sup>13, 56</sup> NOM consists of an assortment of organic compounds both aromatic and

aliphatic, with a variety of functional groups that leave the majority of NOM negatively charged at neutral pH.<sup>55</sup> Currently, most modern treatment utilities use a combination of coagulation and filtration to remove NOM. However, as populations continue to grow, less than ideal water sources with higher levels of NOM will have to be treated, and new methods are needed to do so.<sup>57</sup> Current treatment methods have limited effectiveness at removing smaller, more hydrophilic molecules; particularly low MW and low SUVA compounds. It's these refractory DBP precursors that have created interest in new materials for the removal of natural organic matter. The NOM composition varies significantly from region to region based on a multitude of environmental and anthropogenic factors that can vary seasonally. This means that water utilities must be equipped with the means to remove even the most recalcitrant NOM varieties at all time to keep DBP formation to a minimum.<sup>13</sup> Three major removal techniques currently exist in water treatment: coagulation through chemical addition, membrane filtration (mostly based on size exclusion), and physical adsorption of NOM using activated carbon, but ion-exchange will also be discussed below as an underutilized alternative with great potential.

### 3.1. Coagulation

Current water treatment practice in the United States relies primarily on conditioning of the water by coagulation and flocculation, followed by sedimentation/filtration.<sup>22</sup> Coagulation is the chemical addition of a coagulant, whereas flocculation is the aggregation of particles into larger particles known as flocculant particles. Coagulation works by collapsing the electrical double layer of the NOM and particulates in the water. This destabilization reduces the repulsive forces between the particles, and they begin to aggregate and form larger structures (flocs).<sup>22</sup> The two

primary coagulants are aluminum ( $\text{Al}^{3+}$ ) and iron ( $\text{Fe}^{3+}$ ) salts that are cationic when dissociated in water and function by attracting the negatively charged NOM. This neutralizes the charges and creates insoluble aggregates that eventually settle out during sedimentation. Alum, or aluminum sulfate ( $\text{Al}_2(\text{SO}_4)_3$ ), along with ferric chloride ( $\text{FeCl}_3$ ) are the primary coagulants used in water treatment with the iron chloride being more effective at removing NOM.<sup>13</sup> The effectiveness of coagulation depends on the coagulant used, mixing conditions, pH, temperature, and NOM properties (MW, functional groups, SUVA, and charge).<sup>55</sup> If conditions are not optimized, NOM removal is significantly reduced.

Traditionally, coagulation was used only to remove turbidity and color from water, and this is typically an easily achievable goal for coagulation. However, since it also must function to remove NOM, which is much more difficult, a process known as “enhanced coagulation” has been adopted to ensure that the total organic carbon (TOC) content has been reduced to safe levels before chlorination. Enhanced coagulation requires optimization of pH along with an excessive coagulant dose, or an alternative coagulant, to lower TOC.<sup>55</sup>

Coagulation has been the primary means of NOM removal for decades, but its viability moving forward is being questioned, and new means of NOM removal are being investigated. One of the more recent concerns about coagulation is based on potential adverse health effect stemming from the use of aluminum salts as there is growing evidence of a link between aluminum exposure from drinking water and Alzheimer’s disease, dementia, and overall cognitive decline.<sup>58</sup> As for the effectiveness of coagulation as an NOM removal agent, it is best suited to remove large, high MW,

compounds like humic acid.<sup>13</sup> However, coagulation cannot effectively remove low MW or low SUVA compounds, even in optimal conditions.<sup>56</sup>

The recent events in Flint, MI highlight the need to seek alternative methods for water treatment, as the EPA's prescribed method of treatment played a significant role in the unfortunate catastrophe. The issue began when Flint switched from buying treated water from Detroit, to treating water from the Flint River as a cost-saving measure. The Flint River has an inherently high chloride concentration, making the water slightly corrosive in nature. After disinfection with chlorine, unsafe levels of DBPs were generated, meaning there was too much NOM in the water and it had to be removed. Using the prescribed EPA treatment of enhanced coagulation, an excess of ferric chloride was added to lower NOM levels. The  $\text{Fe}^{3+}$  cation effectively removed the NOM, but left behind extremely high levels of chloride ions. Between the chlorine from disinfection, the chloride ions from coagulation, and the naturally corrosive nature of the Flint River, the protective phosphate/mineral layer on the distribution pipes was dissolved. Iron and lead were then leached from the distribution pipes directly into the drinking water of Flint's residents.<sup>5, 59</sup>

### 3.2. Membrane Filtration

Membrane filtration is an attractive water treatment option because it does not rely on chemical addition to remove NOM, and its demand has increased as stricter regulations on water quality are being promulgated.<sup>60</sup> Both physical and chemical means of separation are employed in membrane filtration as water must pass through a semipermeable membrane, where the clean water is separated from the impermeable contaminants. There are four types of membrane filters currently being used in water treatment: 1) microfiltration (~0.1  $\mu\text{m}$  pores), 2) ultrafiltration (~10 nm pores), 3)

nanofiltration (~1 nm pores), and 4) reverse osmosis.<sup>22</sup> Filtration relies on a size exclusion mechanism to remove dispersed solids, and even individual ions, from water, and reverse osmosis utilizes a concentration gradient and extreme pressure to overcome the osmotic pressure of the solution and allow clean water to pass through a membrane via active transport. Depending on the membrane, a certain pressure requirement must be met to push the feed stream through the semipermeable membranes to remove the impermeable components.

Membrane filtration is growing in popularity in water treatment as low-pressure membranes are being investigated as potential replacements for coagulation, which would also serve as a cost-cutting measure.<sup>60-61</sup> However, fouling is a serious issue with membrane filtration, so high MW NOM would ideally be removed before filtration, otherwise performance will decline and hydraulic resistance will increase significantly.<sup>61</sup> Pre-treating the influent with coagulation or ion-exchange beforehand could possibly reduce the problem.<sup>4, 10, 56, 60</sup> Conversely, membrane filtration has also been considered as a method of pretreatment before treatment with activated carbon.<sup>22</sup>

### 3.2. Adsorption to Activated Carbon

Adsorption can be either a physical or chemical means of removing certain adsorbates from water by the use of an adsorbent material. Physical adsorption requires the adsorbate to physically come into contact with the adsorbent with some sort of van der Waals interaction to retain the adsorbate after contact. The most commonly used adsorbent media in water treatment is activated carbon. Chemical adsorption requires exchange of electrons in a nonreversible fashion, which is much less common in water treatment.<sup>22</sup>

The type of NOM plays a large role in measuring the effectiveness of activated carbon. NOM charge distribution, SUVA, H-bonding with the substrate, and size all play a role in adsorption.<sup>62-63</sup> There are two types of activated carbon commonly deployed in water treatment; granular activated carbon (GAC) and powdered activated carbon (PAC). Both have their inherent pros and cons, but both can be used to remove NOM.

Granular activated carbon is primarily used for removing DBP precursors, but it can also be used for trace contaminant removal. GAC has an average particle size between 0.5 and 3 mm.<sup>22</sup> As for removal of NOM, GAC cannot remove larger fractions (> 10 kDa) due to size exclusion, and works best with compounds between 500 and 4,000 Da, which fit comfortably within the pores. However, smaller MW fractions are typically more hydrophilic, which makes them far less adsorbable.<sup>62</sup> The idea that larger NOM is effectively removed with GAC makes it a potential candidate to work in tandem with coagulation, which works best with larger MW fractions. Unfortunately, neither method can effectively remove the smallest MW fraction. Currently, GAC is not widely used due to low equilibrium capacities and slow sorption kinetics of NOM.<sup>64</sup> Despite these flaws, GAC is still being investigated as an alternative to other removal methods. Powdered activated carbon is typically employed for seasonal changes in taste or odor. PAC is much more widely used than its granular counterpart, again for taste and odor control, but rarely for NOM removal.<sup>22</sup>

Activated carbons are regenerated by both thermal and chemical methods, but complete restoration is not possible and often leads to attrition and breakdown of the carbon particles. Reactivation is rarely used unless massive quantities of active carbon are consumed.<sup>22, 65</sup>

### 3.3. Ion Exchange

While ion exchange is a physical means of adsorption, it differs in that the electrostatic interactions between the adsorbate and the adsorbent result in a much stronger adsorption mechanism between oppositely charged ions. Depending on the adsorbate, the adsorbent must have the correct functionality to selectively bind. Both cation and anion exchange resins exist with variations of each. Since we are focused on removal of NOM, most of which is negatively charged, only anion exchange resins will be discussed.

There are three main types of anion exchange resins: Type I and II Strong Base Anion (SBA) exchange resins and a Weak Base Anion (WBA) exchange resin. For removal of NOM, Type I SBA exchange resins are primarily employed, with a chloride counterion.<sup>7</sup> Type I SBA exchangers are better at removing NOM because these types of resins are more strongly basic and therefore more readily remove the weakly ionized NOM when compared to Type II resins.<sup>22</sup> Currently, IEX is not widely used in water treatment, but is growing in popularity and being adapted because of the emergence of a new resin known as MIEX<sup>®</sup>. IEX resins have significantly greater capacities and sorption kinetics compared to activated carbon and is able to be fully regenerated in a brine solution. To make IEX more effective, it can be used in conjunction with coagulation to prevent large molecules, easily removed by coagulation, from blocking active sites.<sup>56</sup> Unlike other removal techniques, the only factor affecting removal is the charge of the NOM. Meaning all MW fractions can be removed by IEX. Since most NOM is negatively charged at treatment pH, IEX is an effective method of treatment for prevention of DBPs; because of this, we chose IEX for the development of our nanoscale water purification materials.

## CHAPTER 4: SYNTHESIS AND CHARACTERIZATION OF NANORESIN

New materials are needed to prevent catastrophes such as Flint, Michigan and to ensure that potentially hazardous DBP precursors are removed before chlorination. Type I SBA exchange resins are an ideal choice for removal NOM without increasing the corrosivity of the water, and without further chemical addition. Data show that ion-exchange has proven to be more effective than coagulation and activated carbon in some cases, and significantly higher levels for NOM removal have been seen by combining IEX with coagulation.<sup>17, 66</sup>

For the removal of NOM, a Type I SBA with a quaternary ammonium functional group (poly(vbTMAC)) was synthesized using traditional ATRP and ARGET ATRP in both DMF and water. The AER was then covalently attached to a SWCNT, which acts as a scaffold for the resin. Without scaffolding, the polymer would be free in solution with no way to remove or regenerate the materials for water treatment. The nanotubes were functionalized through the same mechanism used for ATRA/ATRP; however, instead of propagating through addition to an alkene on a vinylic monomer, polymers of a pre-determined length were added when an active polymer chain reacts with a double bond on the carbon nanotube, functionalizing the tube with the polymer chain.

### 4.1. Chemicals

All reagents were used as purchased without further purification. N,N-Dimethylformamide (DMF)(Fisher, Spectranalyzed) was kept dry under a N<sub>2(g)</sub> blanket

such that water contamination was below 1000 ppm. SWCNTs were HiPCO (Grade P CNT from CNI, now Unidym, 0.8–1.2 nm diameter, 100–1000 nm length; Lot: P0276), vinylbenzyl trimethylammonium chloride (vbTMAC)(Fisher, 97%; 60:40 para:meta, Lot: A0311318, A0353947), copper (I) bromide (Acros, 98%, Lot:A0311968), copper (II) bromide (Acros, 99+ %; anhydrous, Lot: A0344238), tris(2-pyridylmethyl)amine (TPMA)(TCI, >98.0 %; Lot : Z8GMO-AD; Aldrich, 98%, Lot: MKBV9365V), 2,2'-bipyridine (bipy)(Merck, 99.5%, Lot: 44169), benzyl bromide (BB)(Acros, 98 %; Lot: A0318979), 2-hydroxyethyl 2-bromoisobutyrate (HEBiB)(Aldrich, 95%, Lot: MKBW2607V), and L-Ascorbic Acid (AA)(Fisher; Lot # 144594). MIEX<sup>®</sup> (5% brine solution; Batch # 06092904) was removed from brine and dried for weighing before adsorption experiments. DOWEX<sup>®</sup> 21K Cl anion-exchange resin (Batch # 01009KE) was rinsed with acetone and water before drying for weighing and subsequent adsorption experiments.

#### 4.2. Making a SWCNT Dispersion

It is necessary to disperse SWCNTs from the powdered form, used during NanoResin synthesis, to maximize the surface area available for functionalization. SWCNT dispersions were prepared by adding powder (0.5 mg) to DMF (30 mL) then tip ultrasonicated without temperature or gas environment regulation for 30 minutes at 10 W RMS using a Fisher Scientific Sonic Dismembrator 100 (1/8" tip ultrasonicator). Once dispersed, two primary methods were employed to remove any non-dispersed tubes and/or impurities; 1) centrifugation and 2) filtration through a glass wool membrane.

##### 4.2.1. Pristine HiPCO SWCNT Dispersion (Centrifugation)

After ultrasonication, dispersions were allowed to cool to room temperature before being ultracentrifuged using a Beckman Optima XL-100K at 20,000 g for 20

minutes. The supernatant was carefully collected and diluted when necessary before use.<sup>67</sup>

#### 4.2.2. Pristine HiPCO SWCNT Dispersion (Glass Wool Method)

After ultrasonication, dispersions were cooled to room temperature before filtration. Meanwhile, a glass wool membrane was prepared by packing glass wool into a stainless steel Luer-Lok, 47 mm, filter holder; packing density determined dispersion concentration. The cooled dispersions were then forced through the membrane using a 100 mL glass syringe. The filtrate was then collected and diluted when necessary before use.

#### 4.3. Synthesis of NanoResin

NanoResin has been synthesized using both traditional ATRP and ARGET ATRP, in DMF and water, and with dispersed and non-dispersed SWCNTs. ATRP was chosen because the mechanism of propagation of the polymer is the same as the mechanism of functionalization of the nanotube. This allows for a predetermined degree of polymerization before adding SWCNTs so as to control polymer length, as well as the ability to complete the entire synthesis in a single reaction flask as shown in figure 4.1.

The first major modification in the NanoResin synthesis was going from traditional ATRP using a benzyl bromide/ $\text{Cu}^{\text{I}}\text{Br}/\text{bpy}$  initiating system to ARGET ATRP shown in figure 4.2 with a benzyl bromide/ $\text{Cu}^{\text{II}}\text{Br}_2/\text{TPMA}$  initiating system with ascorbic acid as a reducing agent. This was done in effort to increase the rate of polymerization/functionalization, but also to reduce the amount of copper being used. ARGET ATRP is a “green” process that uses trace amounts (as low as 2 ppm) of a transition metal catalyst to prepare polymers in a relatively narrow range of molecular

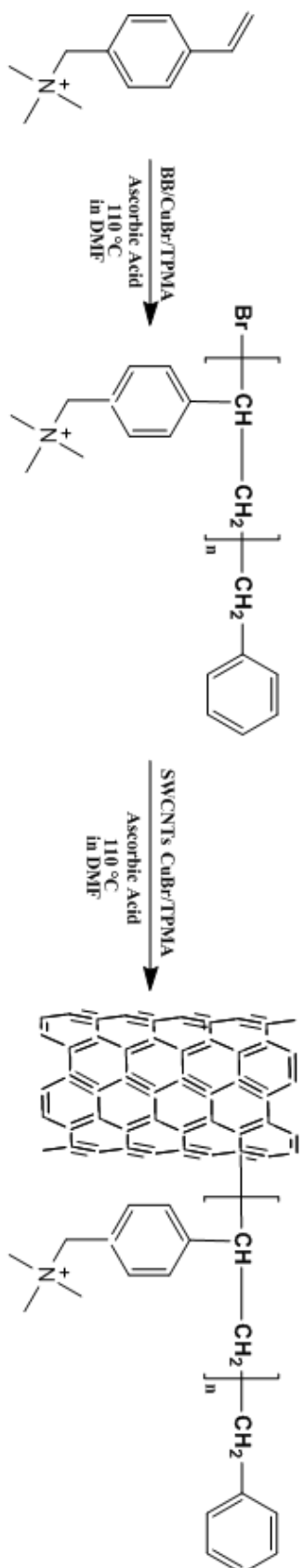


FIGURE 4.1: Scheme for ARGET ATRP synthesis of NanoResin.



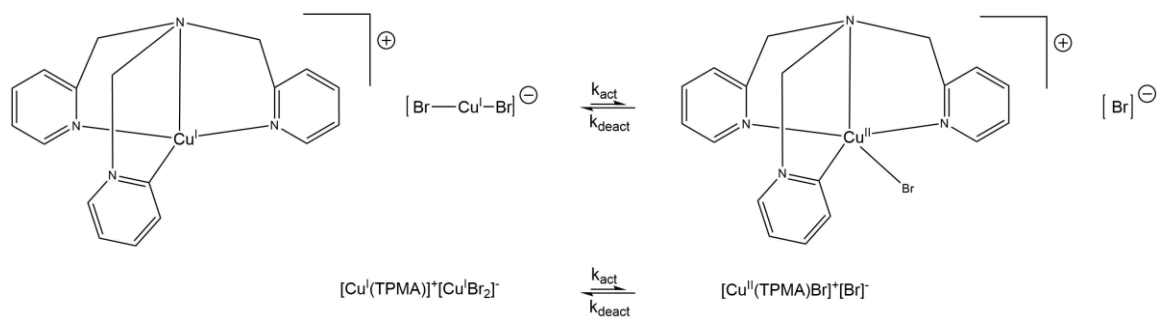


FIGURE 4.3: Copper/TPMA catalyst system used for ARGET ATRP of vbTMAC in both aqueous and DMF syntheses.

weights even in the presence of a small amount of air.<sup>68</sup> Both synthesis pathways were completed in DMF, as it is a much more effective solvent for ATRP conditions as mentioned in section 2.1.5. However, for both environmental as well as experimental reasons, it was decided that DMF was not the best solvent for NanoResin synthesis. An aqueous synthesis would significantly reduce hazardous waste and simplify the arduous NanoResin purification steps. At that point, the synthesis route evolved further from ARGET ATRP in DMF, to an aqueous synthesis. Shown in figure 4.4, aqueous ARGET ATRP employs a HEBiB/CuBr<sub>2</sub>/TPMA initiating system and utilizes ascorbic acid as the reducing agent. All three synthetic pathways are described below.

#### 4.3.1. Traditional ATRP in DMF

Polymerization was performed under ideal ATRP conditions.<sup>27</sup> Degassed vbTMAC (2.229 g, 10.5 mmol) and DMF (40 mL) were added to a dry Schlenk flask, under argon. The resulting mixture was then stirred until fully dissolved. CuBr (31.1 mg, 0.217 mmol) and bpy (102.9 mg, 0.659 mmol) were added to DMF (20 mL) and degassed with argon before adding to the reaction flask. BB (25.8  $\mu$ L, 0.217 mmol) was added to initiate polymerization. The temperature was increased to 110 °C in an oil bath and maintained for fifteen minutes.

Nanotube functionalization was accomplished by adding pristine SWCNT nanotube dispersion (132 mL, 1.87 mg SWCNT) to the reaction flask (still refluxing under argon) under ATRP conditions. Functionalization proceeded for 16-24 hours, at 110 °C, before exposing the reaction flask to air and stopping the reaction.

#### 4.3.2. ARGET ATRP in DMF

Polymerization was performed under ideal ARGET ATRP conditions.<sup>47</sup>

Degassed vbTMAC (1.231 g, 5.81 mmol) and DMF (80 mL) were added to a dry Schlenk flask, under argon. The resulting mixture was stirred until fully dissolved. CuBr<sub>2</sub> (1.16 μmol) and TPMA (11.6 μmol) in DMF (2.8 mL) was added and the mixture stirred for 10 minutes before adding BB (0.116 mmol). AA (11.6 μmol) was added to initiate polymerization. The reaction flask was then placed into a 110 °C oil bath for 20 minutes.

Nanotube functionalization was accomplished by adding 100 mL of DMF to the reaction flask (still refluxing under argon). Next, pristine SWCNT nanotube dispersion (116 mL, 1.13 mg SWCNT) was added, and the catalyst complex recharged in the same ratio as above. Functionalization proceeded for 16-24 hours, at 110 °C, before exposing the reaction flask to air and stopping the reaction.

#### 4.3.3. ARGET ATRP in Water

Polymerization was performed under ideal ARGET ATRP conditions.<sup>47</sup> All solutions were sparged with Ar for fifteen minutes before use. In a dry Schlenk flask, under argon, vbTMAC (1.00 g, 4.72 mmol) was dissolved into water (10.000 mL). The resulting mixture was stirred until fully dissolved. CuBr<sub>2</sub> (0.236 μmol) and TPMA (14.2 μmol) in water (0.942 mL) was added, followed by the addition of HEBiB (6.85 μL, 47.2 μmol). The reaction flask was then placed into a 98 °C oil bath. A 1.6 mM AA solution was then fed into the reaction solution with a syringe pump at a rate of 10 μL/min (16 nmol/min) to initiate polymerization while maintaining a low concentration of active radicals. Polymerization was allowed to proceed for 1208 minutes; the reaction scheme can be shown in figure 4.4.

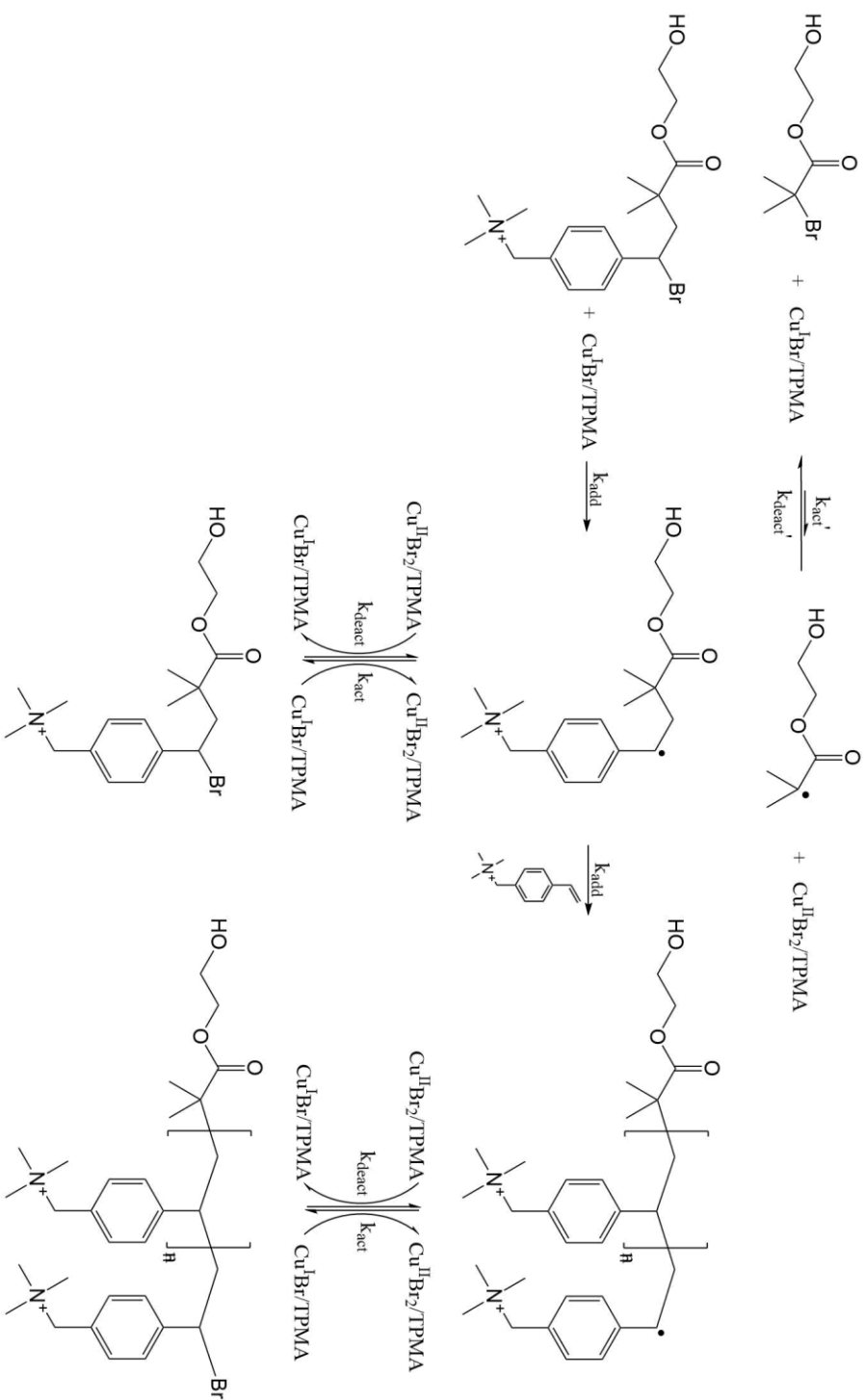


FIGURE 4.4: Scheme for ARGET ATRP of vtTMAC, in water, using HEBiB/CuBr<sub>2</sub>/TPMA as an initiating system. HEBiB was chosen as an initiator for aqueous polymerization due to its solubility in water and high  $K_{\text{ATRP}}$ .  $[\text{M}]:[\text{R-X}]:[\text{Cu}]:[\text{TPMA}] = 100:1:0.005:0.3$ , for 30 minutes at 98 °C under argon. AA was slowly fed in at a rate of 16 mmol/min.

Nanotube functionalization was accomplished by adding 4.50 mg of HiPCO SWCNT powder to 5.00 mL of degassed water, and ultrasonicated at 10 W RMS for 15 minutes before adding to the flask (still refluxing under argon). The catalyst complex and reducing agent was then recharged in the same ratio as polymerization, and the feed rate of AA was increased to 80 nmol/min. A tip ultrasonicator was then fixed in the reaction solution and sealed to prevent aggregation of SWCNTs during functionalization. The sonicator was kept at 5 W (RMS) for three hours and then removed. Functionalization proceeded for a total of 24 hours, at 95 °C, before exposing the reaction flask to air and stopping the reaction. The reaction apparatus is shown in figure 4.5.

#### 4.4. NanoResin Purification

Upon conclusion of NanoResin synthesis (in both DMF and H<sub>2</sub>O), the reaction flask was charged with 50-100 mL of solvent, and tip ultrasonicated at 15 W RMS for ten minutes. The reaction mixture was then filtered through a 0.45 µm polypropylene membrane using a vacuum filtration apparatus and washed with water to remove any excess polymer, unreacted monomer, catalyst, or reducing agent.

Removing all non-covalently attached polymer from the NanoResin is critical since free polymer would increase the apparent adsorption characteristics of the resin. Without addition of SWCNTs (no covalent attachment), the polymer strands are easily filtered and removed from the sample as the polymer is completely soluble in water. Since the polymer remains bound to the NanoResin sample after successive rinses, as determined by the FTIR spectra (Section 4.5.1.), it shows the polymer is strongly attached to the surface of the SWCNTs. Any un-functionalized polymer is easily rinsed away from the NanoResin material. Removal of unbound polymer was quantified using filtration and rinsing with water as shown in figure 4.6. A calibration curve was

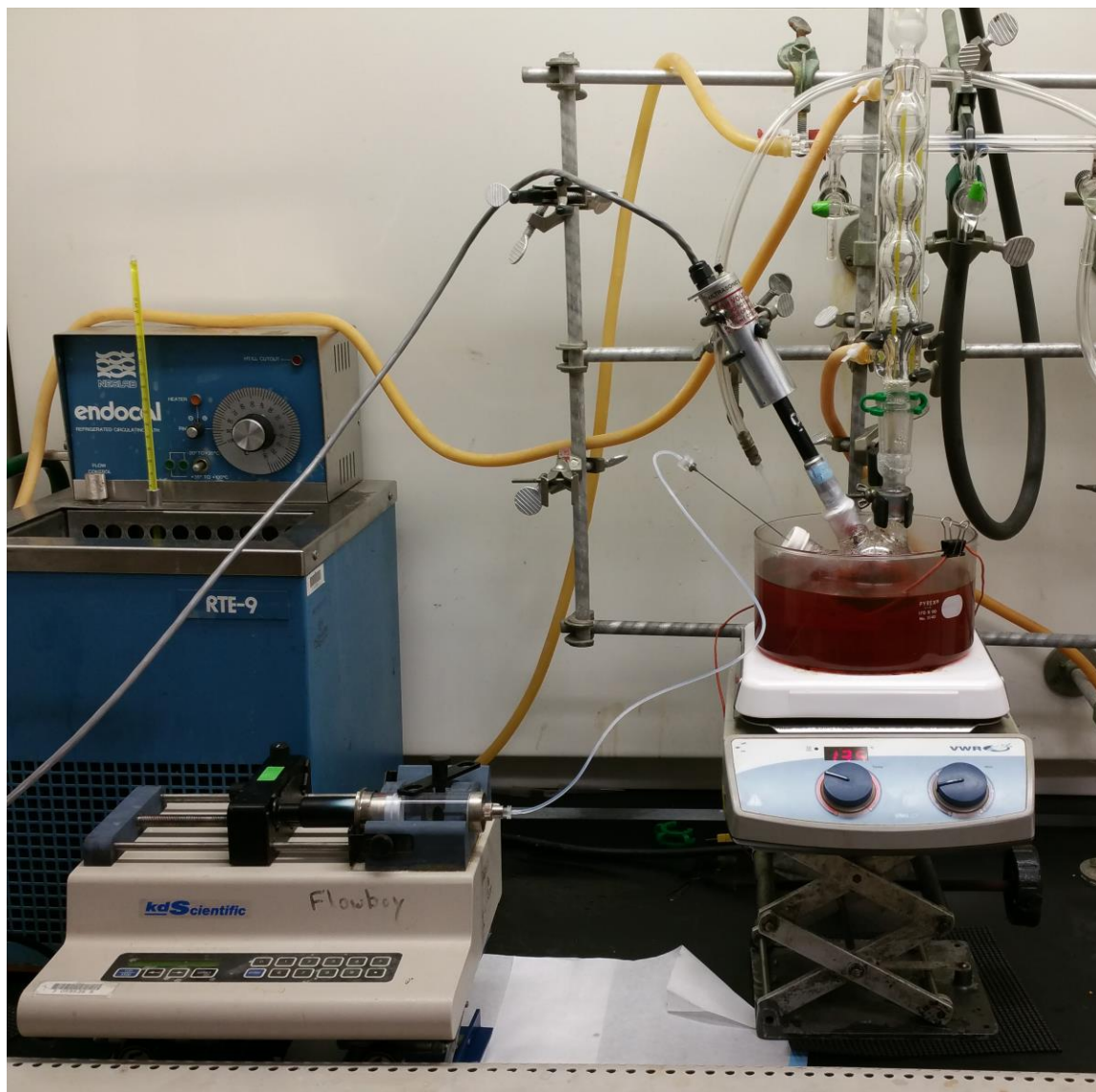


FIGURE 4.5: Reaction apparatus for aqueous NanoResin synthesis. A syringe pump was used to slowly feed in AA (16 nmol/min) to keep the concentration of growing radicals low and ensure a well-controlled polymerization. A tip ultrasonicator was used to keep the SWCNTs from aggregating in water.

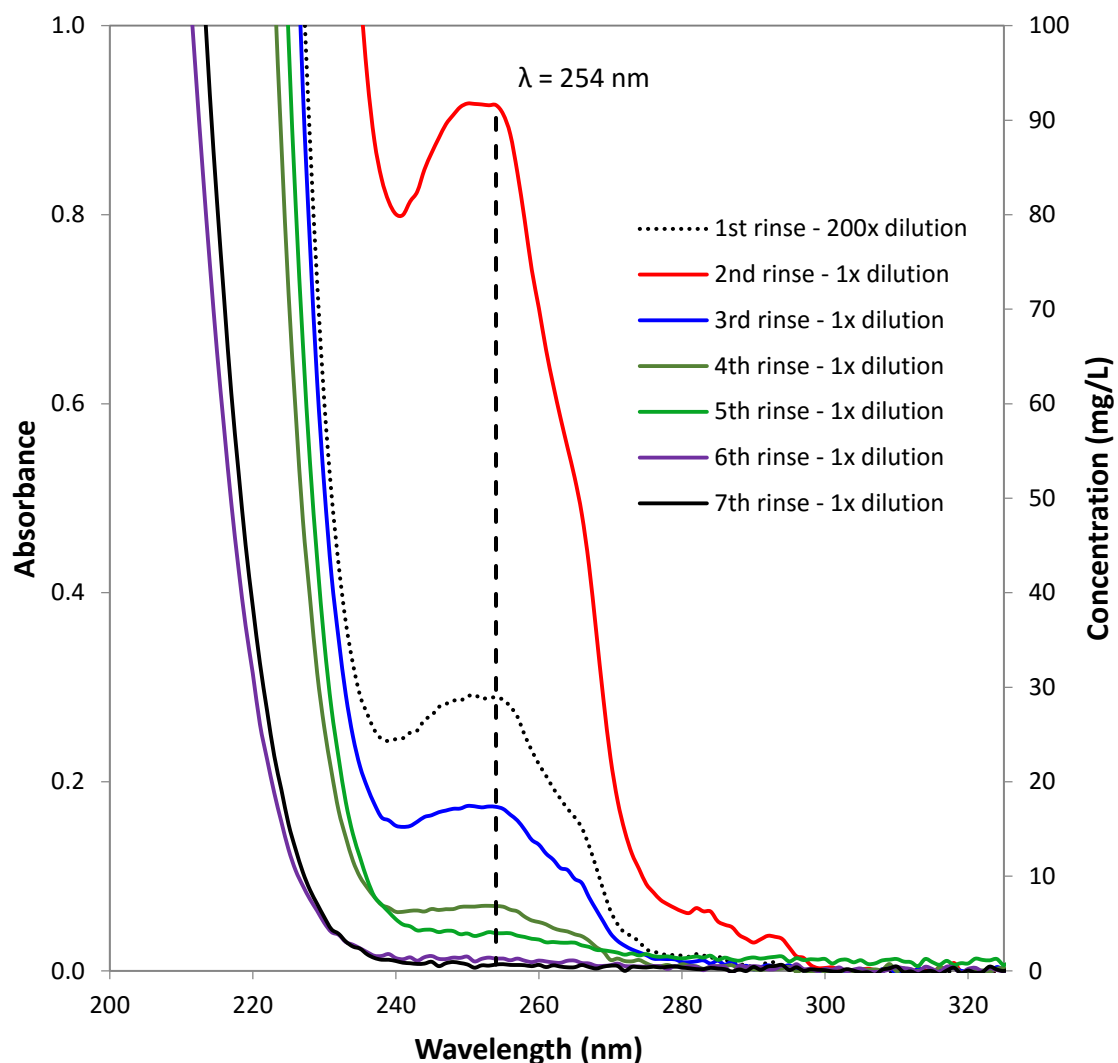


FIGURE 4.6: Washing of excess polymer during NanoResin synthesis. Successive washes with 10 mL aliquots of water shows excess polymer is removed by rinsing with water. Note the spectrum of the first rinse (black dotted line) was taken after we diluted the filtrate 200x to get the absorbance < 1. These spectra show that most of the polymer is removed during the first rinse. After seven rinses, < 1 mg/L of polymer remained ( $\epsilon_{\text{poly-vbTMAC}} = 0.0102 \pm 0.0007 \text{ M}^{-1} \cdot \text{cm}^{-1}$ ). The vertical dashed line is at 254 nm where the polymer concentration is measured and displayed on the right axis. Polymer extinction coefficient measured using poly(vbTMAC) with a MW of  $\sim 8,000 \text{ g/mol}$ . The strong absorbance between 210 and 240 nm is the result of residual DMF from the synthesis. This absorbance is not present in the aqueous synthesis.

developed to determine the extinction coefficient of poly(vbTMAC), where  $\epsilon_{254} = 0.0102 \pm 0.0007 \text{ (mg/L)}^{-1} \cdot \text{cm}^{-1}$ , yielding a minimum detection limit of  $< 0.7 \text{ mg/L}$  after washing with 70 mL. The poly(vbTMAC) functionalized to the SWCNTs cannot be removed by rinsing with water. Even after the NanoResin is redispersed into water by sonication, the polymer cannot be detected by our UV-Vis method.

Removing residual DMF from the NanoResin is challenging. Despite the miscibility of DMF in  $\text{H}_2\text{O}$ , there is a strong ion-dipole interaction between DMF and the polymer and the SWCNTs (does not apply to NanoResin synthesized in water).<sup>67</sup> Any DMF remaining in solution inflates TOC measurements during resin adsorption studies, and renders the tests inaccurate. A calibration curve was measured to determine the extinction coefficient of DMF in water, where  $\epsilon_{230} = 0.00414 \pm 0.00001 \text{ (mg-C/L)}^{-1} \cdot \text{cm}^{-1}$ , with a minimum detection of  $< 0.2 \text{ mg-C/L}$ . After the rinsing procedure, DMF was removed to below detection levels, this rinsing can be shown in figure 4.7. However, DMF still remained bound to the NanoResin, and displaced by NOM during adsorption experiments, which limited the ability to study surrogate removal by TOC, and shifted focus to an aqueous synthetic route for NanoResin.

Once all excess polymer and DMF (if applicable) had been removed, the retentate was added to DI water and tip ultrasonicated at 15 W RMS for 10 minutes. If the hydrophobic nanotubes were successfully coated in the hydrophilic polymer, they disperse into water. Once dispersed in water, the functionalized SWCNT dispersion was then ultracentrifuged at 20,000 g for 20 minutes to sediment any non-functionalized SWCNTs, and the supernatant was carefully collected.

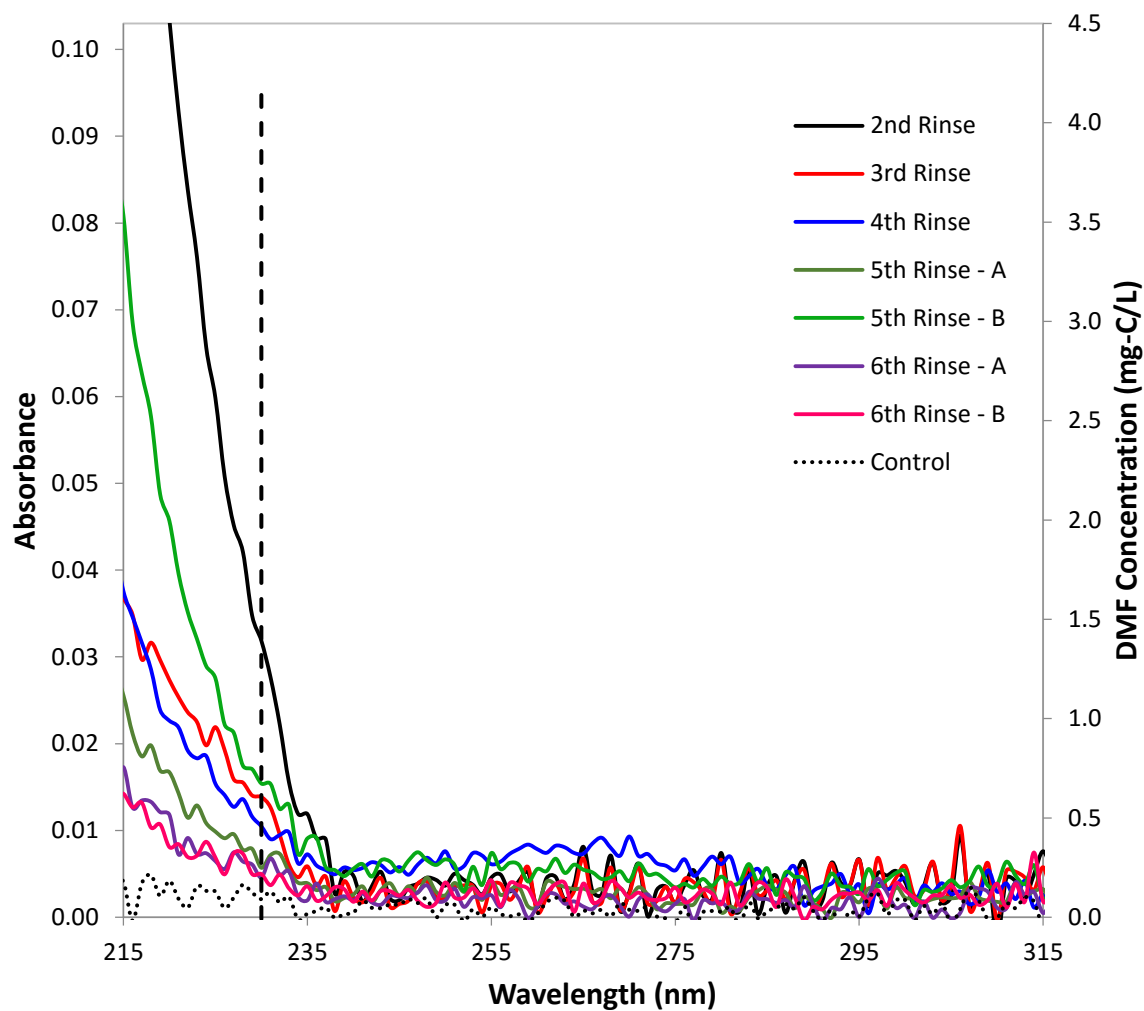


FIGURE 4.7: Rinsing of residual DMF during NanoResin purification. After filtration the NanoResin is re-dispersed into 125 mL of water, then filtered and washed with 25 mL of water. The 25 mL filtrate is analyzed by UV spectroscopy. A calibration curve was measured to determine the extinction coefficient of DMF in water, where  $\epsilon_{230} = 0.00414 \pm 0.00001 \text{ (mg-C/L)}^{-1} \cdot \text{cm}^{-1}$ , with a minimum detection of  $<0.2 \text{ mg-C/L}$ . After rinsing procedure, DMF was removed to below detection levels.

#### 4.5. Characterization of NanoResin

Un-functionalized SWCNTs are not dispersible in water. Our functionalized SWCNTs disperse into water, because the SWCNTs are coated in poly(vinylbenzyl trimethylammonium chloride) (a Type I Strong Base AER). This allows us to easily separate functionalized NanoResin from un-functionalized SWCNTs. Once separated, multiple methods were used for characterization.

Polymerization was confirmed using Perkin-Elmer Spectrum 100 FTIR Spectrometer with ATR using solid samples. Nanotube functionalization was confirmed with a Kaiser Raman Analyzer, dried samples were analyzed using 20 second exposures with three accumulations. SWCNT concentration in DMF was observed using a Cary 5000 UV-Vis-NIR Spectrophotometer at 1025 nm where only the SWCNTs absorb. We use the extinction coefficient  $\epsilon_{1025} = 0.0247 \text{ (mg/L)}^{-1} \cdot \text{cm}^{-1}$  and the volume of dispersion to calculate the mass of SWCNTs before and after polymer functionalization to the SWCNTs. NanoResin concentration was determined by solvent evaporation after purification. Scanning electron microscopy (SEM) data were obtained with a Raith 150 microscope operated at 10 kV; this was used to confirm a conformal polymer coating of the nanotubes.

##### 4.5.1. Fourier-Transform Infrared Spectroscopy

FTIR was used to confirm polymerization based on a shift in energy that could be observed as the monomer was polymerized. Since ATRP adds in a head-to-tail fashion, propagation occurs through the vinylic double bond of the monomer. This leaves an aliphatic bond to link the growing polymer chain which results in a clear shift in stretching frequencies between the monomer and polymer. The carbon–hydrogen stretch of a vinyl alkene (monomer) characteristically absorbs between 3010 and 3095  $\text{cm}^{-1}$ ,

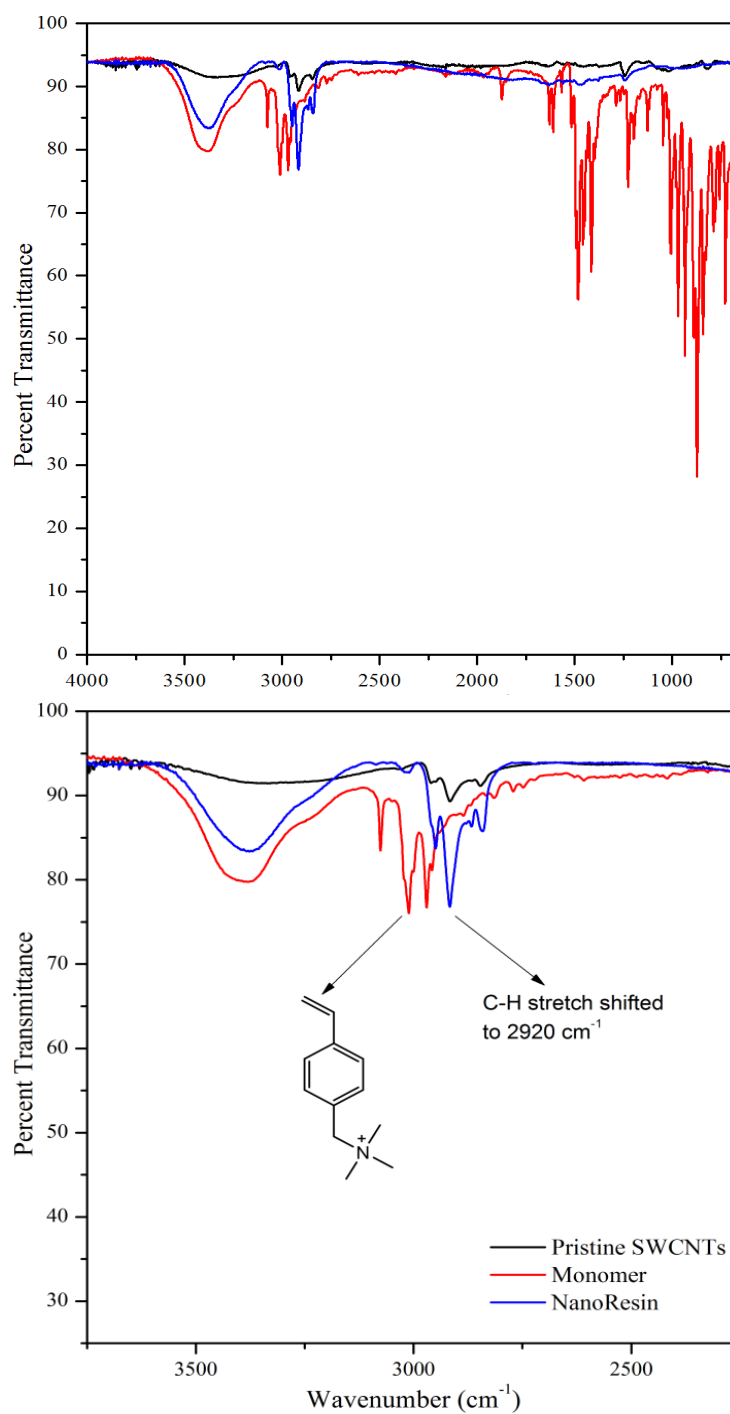


FIGURE 4.8: FTIR overlay of monomer (red trace), pristine SWCNTs (black trace), and NanoResin (blue trace). Successful polymerization is demonstrated when the C-H stretch of the vinyl monomer shifts from 3015 cm<sup>-1</sup> to 2920 cm<sup>-1</sup> for the functionalized SWCNTs.

whereas the C–H stretch of an alkane (polymer) is 2853-2962  $\text{cm}^{-1}$ .<sup>69</sup> Figure 4.8 confirms a successful polymerization as the C–H stretch of the monomer (red trace) shifts from 3015  $\text{cm}^{-1}$  to 2920  $\text{cm}^{-1}$  for the NanoResin sample (blue trace). Measurements were made using a Perkin-Elmer Spectrum 100 FT-IR Spectrometer with an ATR plate; 8 scans with 2.00  $\text{cm}^{-1}$  resolution. The monomer spectrum was obtained using dried vbTMAC powder without baseline correction. The NanoResin and pristine SWCNT (black trace) spectra were obtained by depositing samples onto a polypropylene support membrane and required manual baseline correction.

#### 4.5.2. Raman Spectroscopy

Raman spectroscopy was used to investigate the covalent and permanent attachment between the polymer and SWCNT. The Raman spectrum of SWCNTs consists of three key characteristic absorption bands: radial breathing modes (RBMs) between 100-400  $\text{cm}^{-1}$ , graphitic band (G-band) at 1580  $\text{cm}^{-1}$ , and the defect-induced band (D-band) at 1350  $\text{cm}^{-1}$ , as shown in the baseline-normalized spectra in Figure 4.9(a).<sup>70-71</sup> The G-band results from in-plane vibrations of  $\text{sp}^2$  hybridized carbon atoms and dominates the spectrum as expected. The D-band comes from out-of-plane vibrations resulting from structural defects in the SWCNT; indicative of the presence of  $\text{sp}^3$  hybridized bonds. An increase in the ratio of D:G intensity ( $I_D/I_G$ ) of the SWCNTs, before and after functionalization with the polymer, measures the degree of covalent attachment between the SWCNTs and poly(vbTMAC).<sup>72</sup> After only five minutes of polymerization followed by functionalization to the SWCNTs the D:G ratio increased by 111 % (Figure 4.9(a) blue trace). When the polymer chains are allowed to grow longer during polymerization, a smaller increase in peak intensity ratio  $I_D/I_G$  can be observed. The longer polymer chains from the 10 min polymerization result in only a 36 % increase

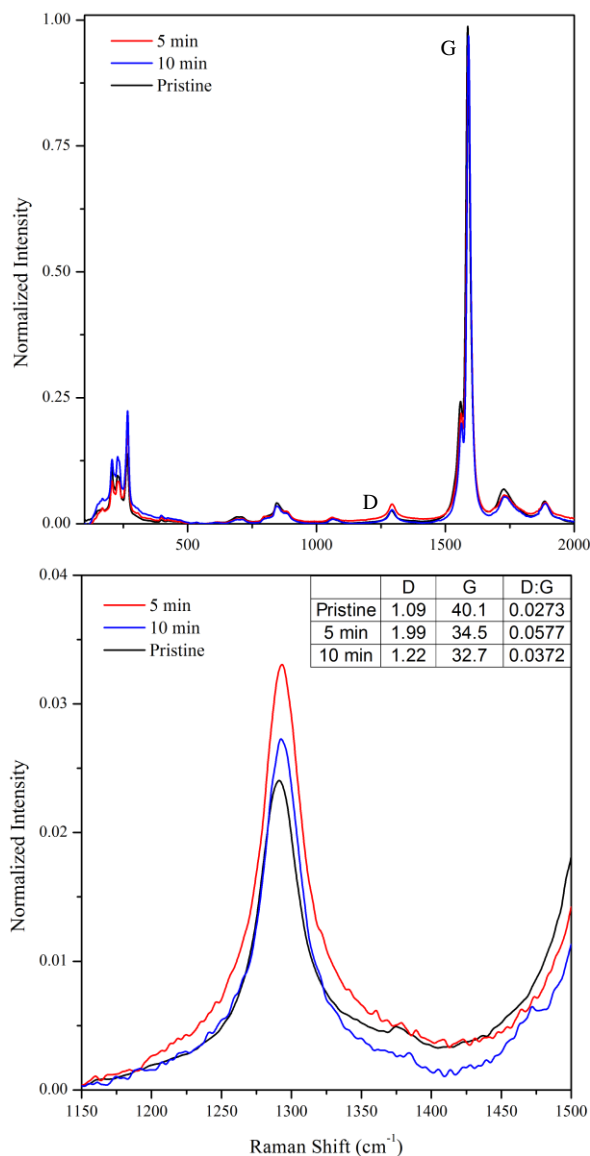


FIGURE 4.9: Raman overlay of pristine SWCNTs (black) and NanoResin. (a) Baseline-normalized Raman spectra overlay of functionalized SWCNTs, after five (red) and ten (blue) minutes of polymerization, and pristine nanotubes. Covalent attachment of polymer to SWCNT is indicated by an increase in the defect band (D-Band). (b) A greater increase in D-Band area observed with shorter polymerization times (shorter polymer chains). This suggests that a greater number of polymer chains covalently attach to the SWCNTs in order to create a conformal polymer coating. Longer polymer chains require fewer attachment sites.

of the D:G ratio which is consistent with fewer chains covalently attached as illustrated by the D band in figure 4.9(b). Since we form a conformal coating along the SWCNTs, as demonstrated in the SEM image (from Section 4.5.4.) of the NanoResin (Figure 4.13(b)), the longer polymer chains cover more area along the SWCNT and therefore, fewer are needed to coat the SWCNT. This is consistent with fewer defects ( $sp^3$  bonds) and the smaller D:G ratio. These data are also consistent with molecular dynamics calculations of short poly(vbTMAC) bound to a SWCNT as shown in figure 4.10. Even with only 12 poly(vbTMAC) strands of 20 units long each there is significant steric crowding on the 10 nm long (6,6) SWCNT. For this model only 1.2% (12 of 984 C atoms) of the SWCNT C atoms are  $sp^3$  hybridized.

Figure 4.11 shows the Raman data from figure 4.9(a) where we focus on the RBMs before and after functionalization. These HiPCO SWCNTs have a small diameter distribution. The five most dominant tube diameters are measured in the RBM spectra where the frequency of the absorption is inversely proportional to the diameter of the tube:<sup>73-74</sup>

$$\omega_{RBM} = \frac{223.5 \text{ cm}^{-1} \text{ nm}}{d_t} + 12.5 \text{ cm}^{-1}. \quad (4.1)$$

We observed that the peak intensity of the larger tubes decreases relative to the other tubes after functionalization. This is consistent with smaller diameter tubes, with higher curvature and bond strain, being more reactive.<sup>75</sup> Un-functionalized tubes, as in these larger ones, are removed during the purification step described above.

#### 4.5.3. Dynamic Light Scattering and Zeta Potential Measurements

The effective diameter and electrophoretic mobility of NanoResin dispersions were measured using a Brookhaven Instruments Corporation Zeta-PALS system with

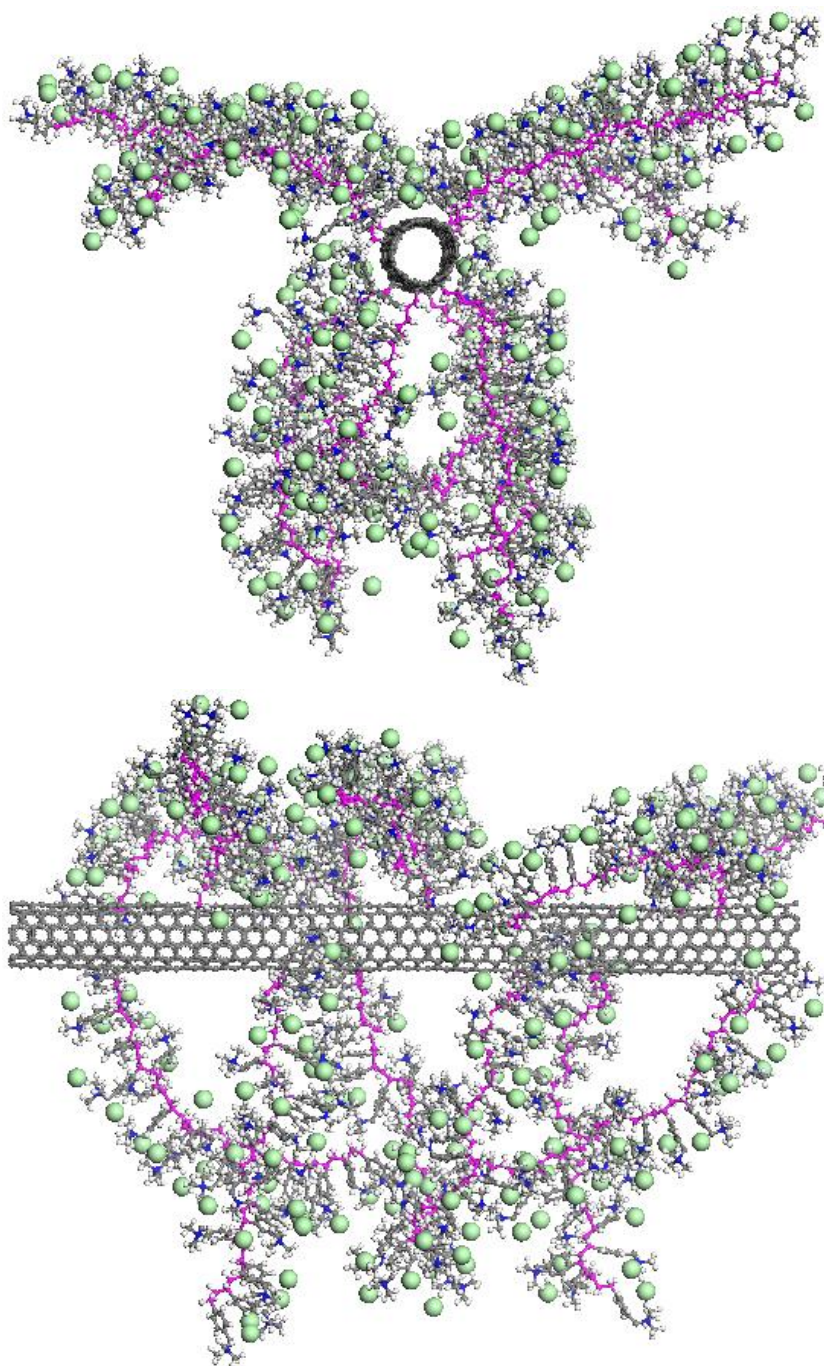


FIGURE 4.10: Molecular dynamics anneal simulation snapshot of 12 poly(vbTMAC) strands (20 units long) covalently bonded to a (6,6) SWCNT. Materials Studio 4.4 UFF after 5 annealing cycles 300 to 500 K and geometry optimization after each. Total simulation time = 100 ps (2 fs steps), NVT.

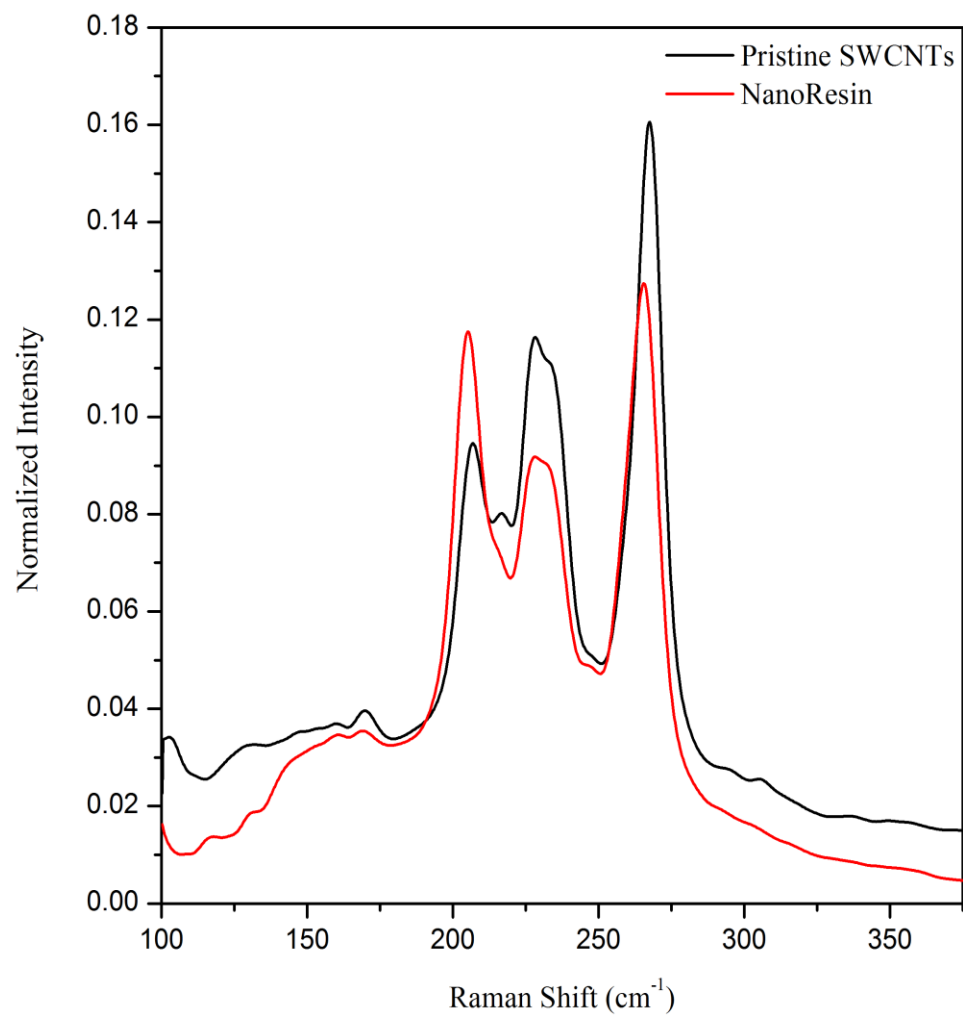


FIGURE 4.11: RMB overlay of pristine SWCNTs (black) and NanoResin (red). Data shows the smaller diameter (higher energy Raman shift) tubes were more likely to be functionalized, compared to larger diameter tubes.

operating voltage set to 10 V<sub>RMS</sub>, and measurements were performed at 25 °C.

NanoResin dispersions of 25 mg/L in water were sonicated prior to measurement.

Multiple runs were averaged after maximum and minimum outliers were discarded. All results are reported as value  $\pm$  standard error, 95%.

The effective hydrodynamic diameter of the individual particles in dispersion was measured to be  $D_h = 339 \pm 2$  nm (all results reported as value  $\pm$  standard error, 95%).

This value is calculated from the Stokes-Einstein relation where the particle is modeled as a sphere. Obviously, the NanoResin tubes are not spheres. If we assume they behave like rigid rods (even though they are actually flexible rods), that have cross-sectional width  $w = 10$  nm wide (as determined by SEM) and length  $L = 1500$  nm, then the calculated hydrodynamic diameter  $D_h$  is  $\sim 320$  nm according to

$$D_h = L / (\ln(L/w) + 0.32), \quad (4.2)$$

which is consistent with the measured value above.<sup>76</sup>

The measured electrophoretic mobility was  $\mu = +1.85 \pm 0.08$  ( $10^{-8}$  m<sup>2</sup> V<sup>-1</sup>s<sup>-1</sup>).

From the electrophoretic mobility, zeta potential was calculated using the Smoluchowski model. In general, there is no valid model relating measured electrophoretic mobility (EPM) of a dispersed SWCNT to the electrostatic potential, the zeta potential, at the slipping plane of the diffuse layer.<sup>77</sup> Typically the Smoluchowski approximation is used to account for the solvent's dielectric constant and viscosity and to calculate the zeta potential.<sup>67</sup> In our system  $\kappa a \sim 6$  where the Debye length  $1/\kappa$  is estimated to be between 20 – 50 nm and the measured radius  $a = D_h/2 = 170$  nm. The NanoResin zeta potential (modeled in figure 4.12) was calculated to be  $\zeta = +24 \pm 1$  mV, which is consistent with a cationic polyelectrolyte coated SWCNT.

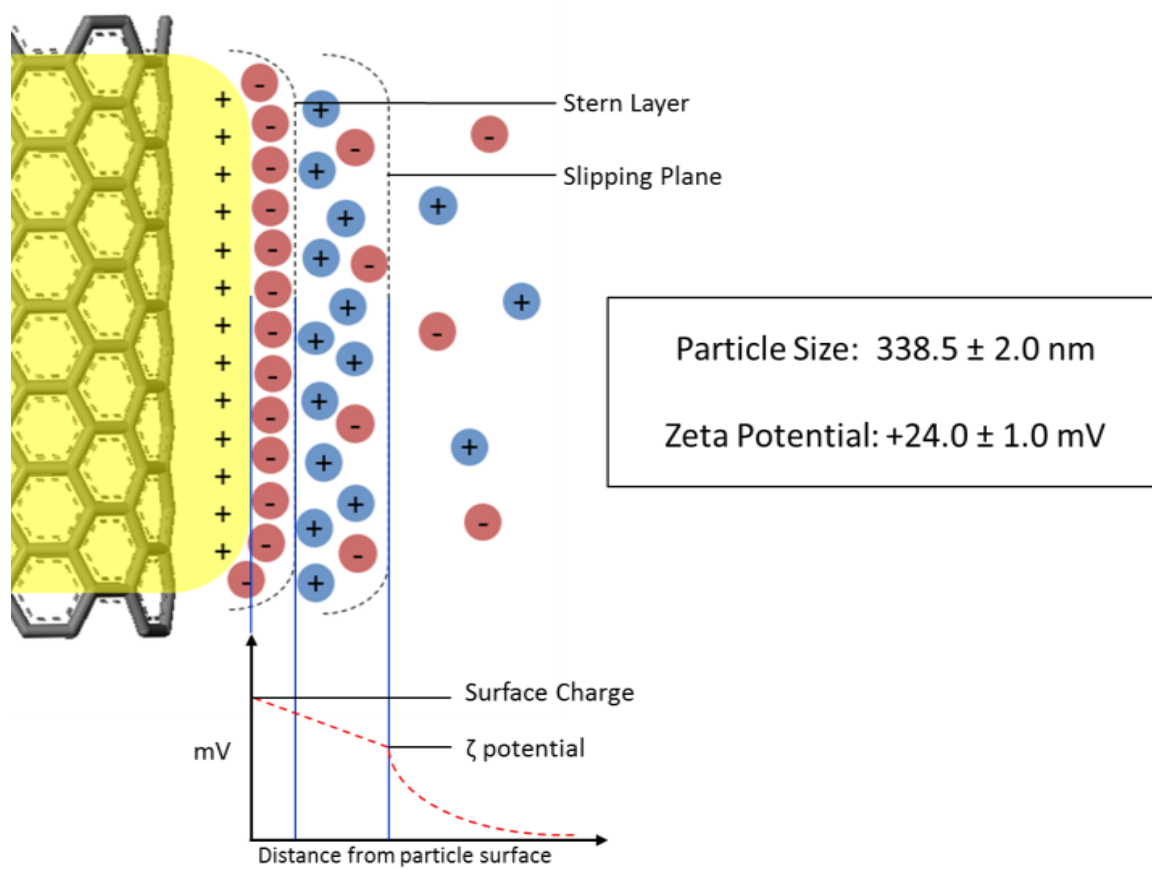


FIGURE 4.12: Electrical double layer representation of NanoResin. The potential measured at the slipping plane is known as the zeta potential.

#### 4.5.4. Scanning Electron Microscopy

To better understand the morphology of the NanoResin, Scanning electron microscopy was employed. Microscopy was necessary for two primary reasons: 1) to see if individual tubes were being functionalized, or if the polymer was simply wrapping around bundles of tubes, and 2) to see if a conformal coating was covering the tubes. This was done by first looking at pristine tubes then looking at NanoResin using the SEM. Figure 4.13(a) shows pristine SWCNTs with diameter  $< 5$  nm. Individual (unbundled) SWCNT diameters are 0.8-1.2 nm. Electron scattering due to the 3 nm wide electron beam makes the tubes appear wider. After functionalization, individual NanoResin tubes have a diameter greater than 10 nm, and a conformal polymer coating along the tube seen in figure 4.13(b).

#### 4.5.5. UV-VIS-NIR Spectroscopy

UV-Vis-NIR was used to determine what percentage of SWCNTs were functionalized during the synthesis; “percent functionalization.” SWCNT concentration in DMF was observed using a Cary 5000 UV-Vis-NIR Spectrophotometer at 1025 nm where only the SWCNTs absorb. We use the extinction coefficient  $\epsilon_{1025} = 0.0247$   $(\text{mg/L})^{-1} \cdot \text{cm}^{-1}$  and the volume of dispersion to calculate the mass of SWCNTs before and after polymer functionalization to the SWCNTs. The percent functionalization, %F, is determined by the mass ratio of SWCNTs collected after purification to that added to the initial reaction. During NanoResin synthesis using the ARGET ATRP method in DMF, functionalization showed a strong dependency of time. After 16 h of functionalization the %F = 81%. This value is ~47% lower for shorter functionalization times of one or four hours.

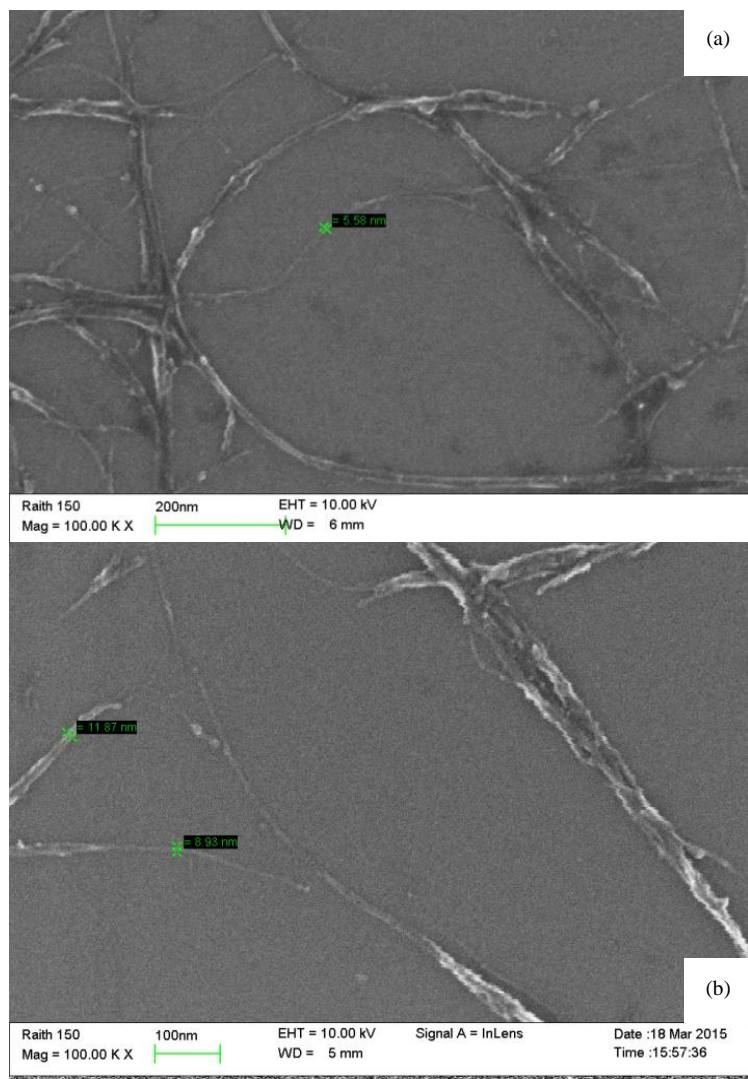


FIGURE 4.13: Electron micrographs of pristine SWCNTs and NanoResin. (a) Scanning Electron Micrograph of pristine SWCNTs. Actual diameters are  $< 3$  nm, but appear larger due to electron beam broadening. (b) Scanning electron micrograph of AER coated SWCNTs showing a conformal polymer coating, as well as an increase in diameter to greater than 10 nm. Magnification and scale bar are the same for both micrographs.

#### 4.5.6. Nuclear Magnetic Resonance Spectroscopy for Polymer Characterization

Polymer characterization proved to be extremely difficult based on the structure of poly(vbTMAC). Commonly used separation techniques are ineffective due to the lack of representative standards for molecular weight analysis. Polystyrene shares the same polymer backbone; however, poly(vbTMAC) has a bulky, charged, functional group on each monomer unit, altering the interactions between the polymer and stationary phase of the column. Dynamic light scattering experiments were able to reveal the point at which bimolecular termination increased, which would mean that monomer conversion had reached the point in which monomer concentration was less than the concentration of active (radical) chains. Once again, this does not provide a true molecular weight. Mass spectrometry (MS) would not work either, as the readout is based on a mass to charge ratio ( $m/z$ ). Poly(vbTMAC) is a polycation; this means that if the charge were known, then the number of monomer units would also be known and molecular weight could be calculated and MS analysis would not be useful.

NMR spectroscopy is an attractive option to monitor conversion, not necessarily MW, due to the change in proton environments between the monomer and polymer. Employing an internal standard that does not interfere with the monomer spectra allows us to quantify the vinylic protons in the monomer spectra as it is converted to polymer. The NMR spectrum of vbTMAC is shown in figure 4.14, and the key changes that are observed are the vinylic protons on the monomer ( $\delta$  6.75 (2H, q), 5.85 (1H, s), and 5.30 (1H, s);  $^1\text{H}$  NMR, 500 MHz,  $\text{D}_2\text{O}$ ). As the monomer is converted to polymer, these proton signals diminish, while the remaining peaks begin to broaden. This broadening is due to the variable chemical environment of each monomer unit resulting in a broadened signal. An internal standard was used to monitor the disappearance of the vinylic protons

during conversion. The internal standard chosen for this experiment was *N,N*-dimethylformamide, as its NMR spectrum consists of one sharp singlet peak at 7.81 ppm (<sup>1</sup>H NMR; 500 MHz, D<sub>2</sub>O). Despite the presence of three vinylic protons on the monomer, only the two terminal signals can be used for analysis since the most downshifted proton signal is distorted by broadening in the polymer spectrum shown in figure 4.15. For the data to be quantitative, an adequate relaxation time must be employed during the measurement to ensure the magnetic excited state of both the internal standard and polymer can return to their equilibrium distributions after pulsing the sample. For these data, a 20 second relaxation delay with eight scans was sufficient. Conversion can be calculated by

$$\alpha = \frac{A_0 - A_t}{A_0} = 1 - \frac{A_t}{A_0} \quad (4.2)$$

where  $\alpha$  is conversion,  $A_0$  is the initial integral area of the average between the two signals at the beginning of the reaction, and  $A_t$  is the integral area at time  $t$ . Multiplying by 100% provides percent conversion. Figure 4.16 displays conversion as a function of time, as well as a kinetics plot for aqueous polymerization, before the addition of SWCNTs. These data were obtained using the NMR characterization method. The linear kinetics plot proves that conversion follows first order kinetics in relation to monomer concentration, as well as a constant concentration of propagating radicals which leads to a narrow range of molecular weights.

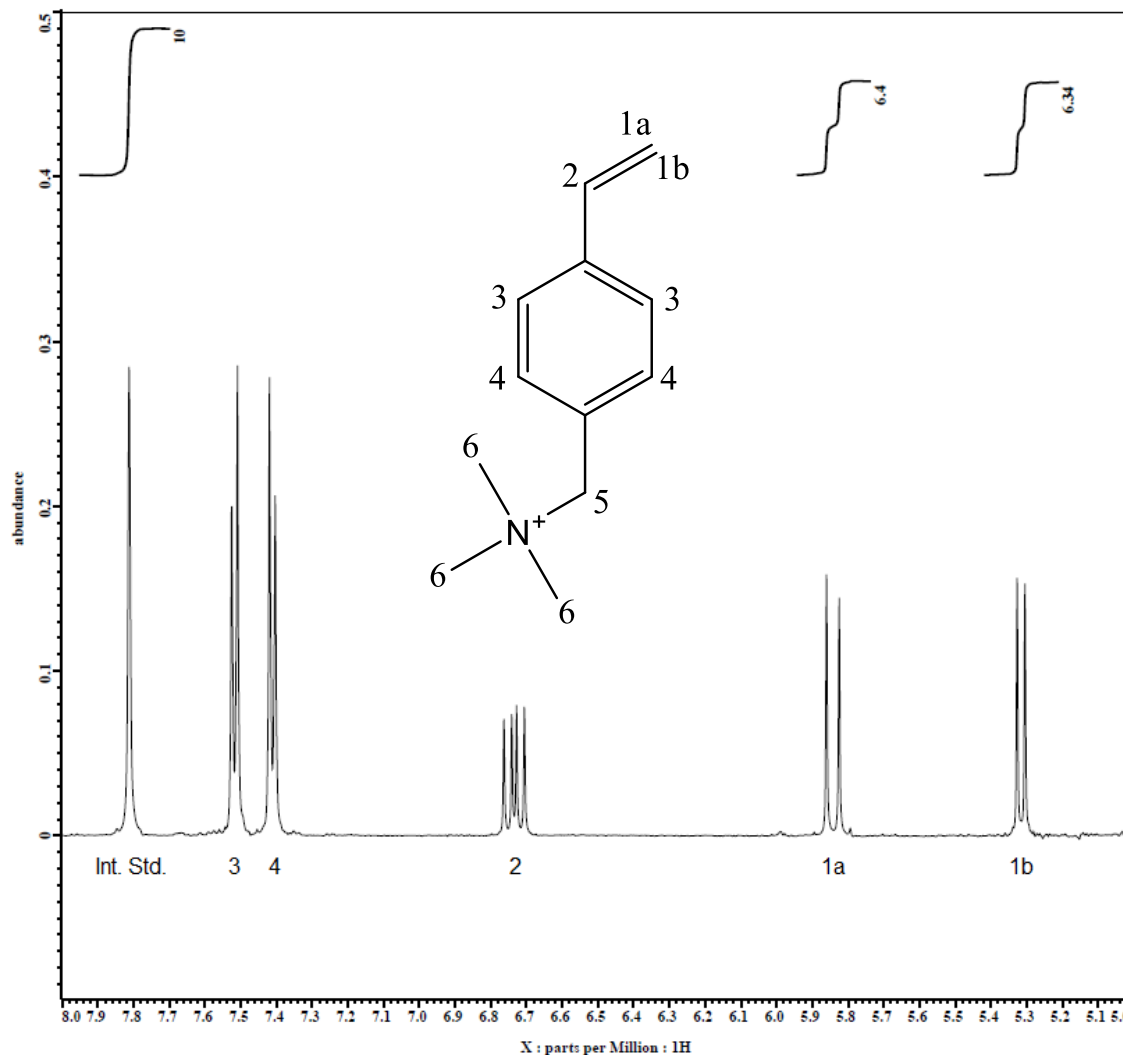


Figure 4.14: Initial NMR spectrum of aqueous ARGET ATRP reaction sample before polymerization of vbTMAC. For conversion of the monomer to the polymer, the vinylic protons ( $\delta$  6.75 (2H, q), 5.85 (1H, s), and 5.30 (1H, s)) will decrease in relation to the internal standard ( $\delta$  7.81 (1H, s)). ( $^1\text{H}$  NMR (500 MHz,  $\text{D}_2\text{O}$ )). The signal from proton 1a is used to monitor monomer conversion based on a ratio between the sample and the initial signal.

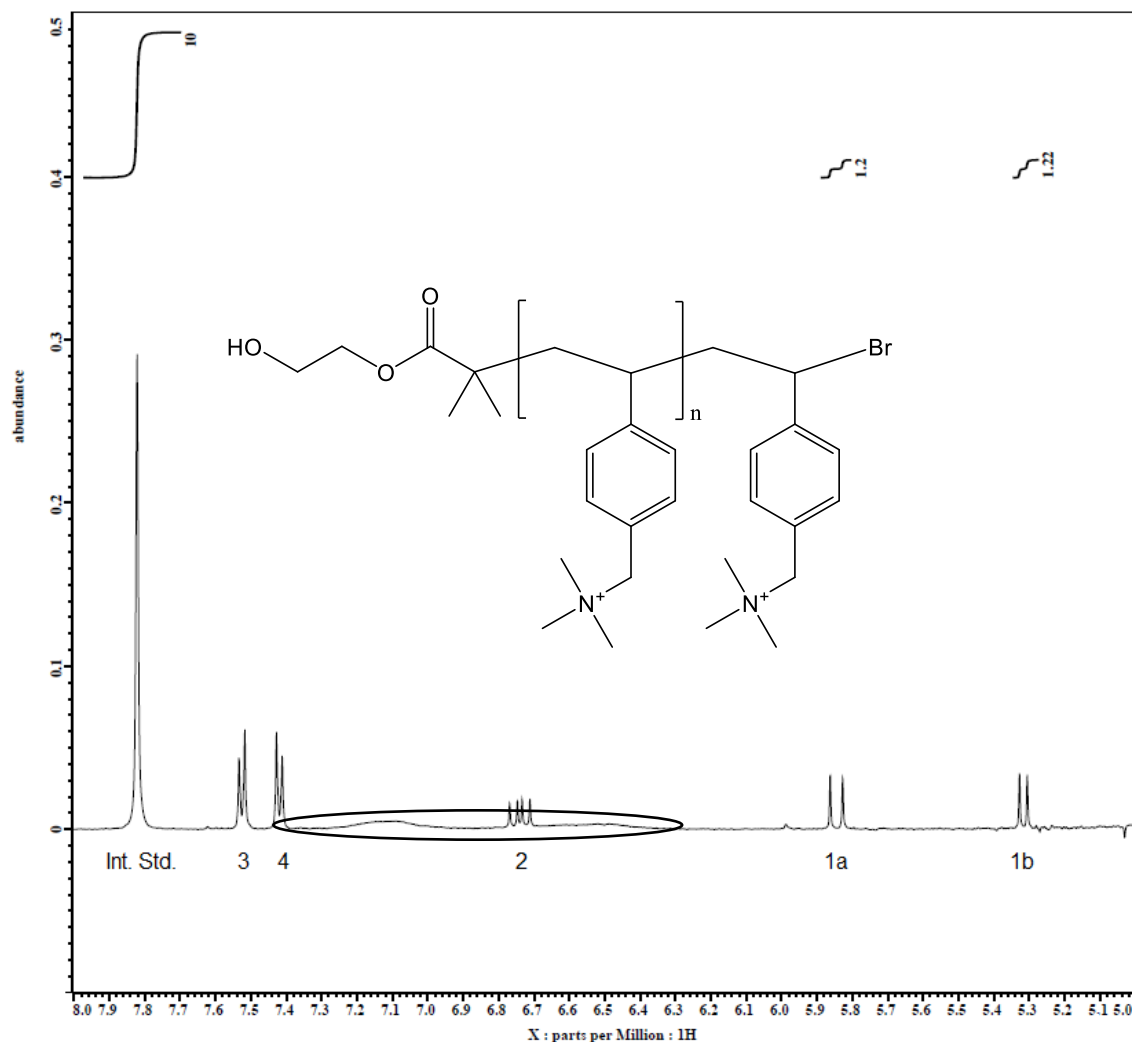


Figure 4.15: NMR spectrum of aqueous ARGET ATRP reaction sample during polymerization of vbTMAC. Broadening of signals can be shown as polymer continues to grow; two of the vinylic proton signals ( $\delta$  5.85 and 5.30 ppm;  $^1\text{H}$  NMR, 300 MHz in  $\text{D}_2\text{O}$ ) are unaltered by this broadening, but shrink in comparison to an internal standard (DMF;  $\delta$  7.81 ppm in  $\text{D}_2\text{O}$ ). These signals, compared to those of the initial sample (Figure 4.13), show that this particular reaction had reached 81% conversion in 20 hours.

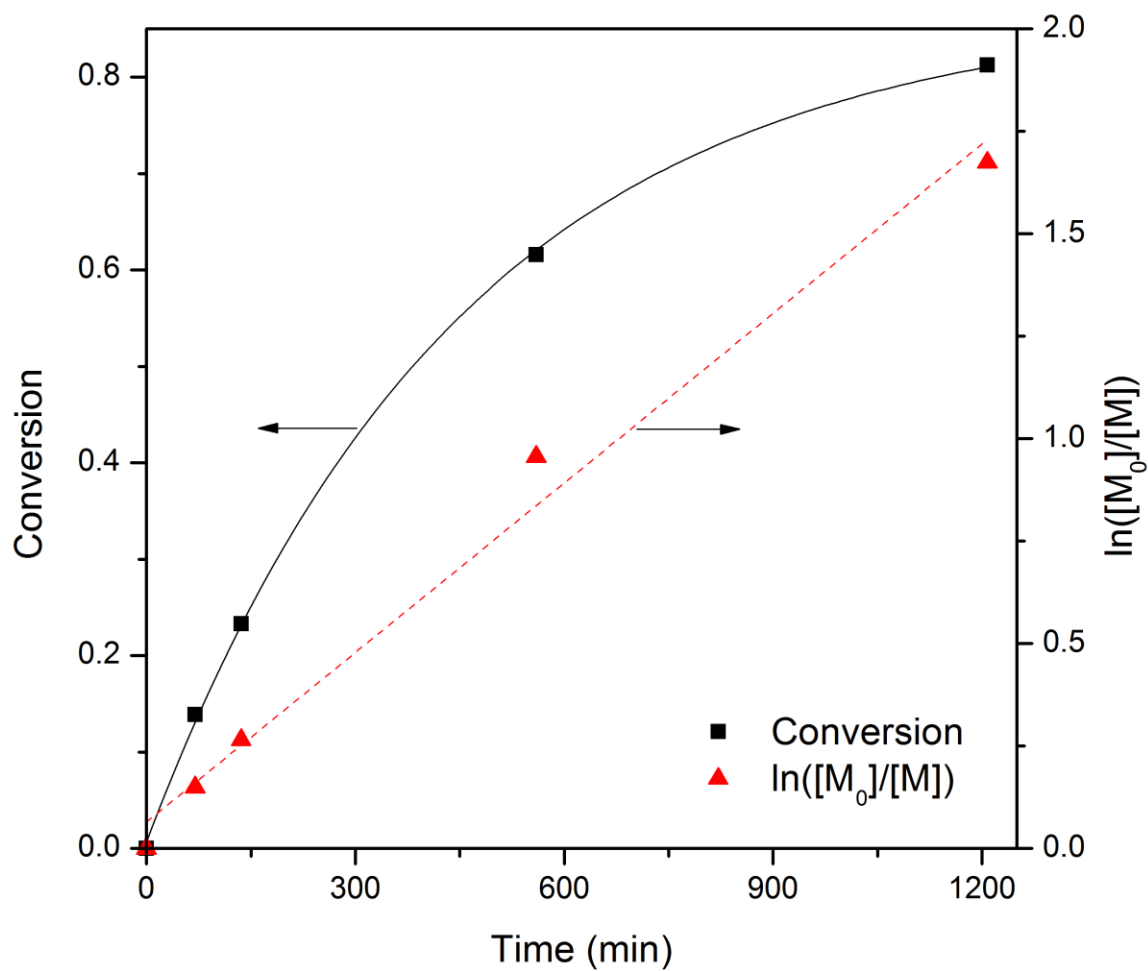


Figure 4.16: Monomer conversion as a function of time (left axis), showing 81% conversion after 1208 minutes for the aqueous NanoResin synthesis. This conversion indicates a polymer MW of 17,200 g/mol. Right axis indicates  $k_{app} = 0.00138 \text{ s}^{-1}$

## CHAPTER 5: COMPARISON OF SELECTED AER TO NANORESIN

Three different surrogate water samples and one natural water sample were used in these experiments. Firstly, a low MW sodium fluorescein solution (NaFL) was used, because of the structural similarities to low molecular weight humic substances (see figure 5.1), as well as the strong absorbance at 490 nm ( $\epsilon_{490} = 0.3576 \pm 0.0106$  (mg-C/L) $^{-1} \cdot \text{cm}^{-1}$  allowing low residual concentrations (with a detection limit below 0.001 mg-C/L). Additionally, it is these low molecular weight (200-400 g/mol), DBP precursors, which are most recalcitrant to coagulation and granular activated carbon (GAC) treatment,<sup>17</sup> that are being targeted by our materials. Treatment of aqueous NaFL with standard coagulation with aluminum sulfate at a dose of 3 mg/L as Al at pH 6.3 removed only about 5% of NaFL from a solution (Table 5.1). Secondly, a low SUVA surrogate was prepared from instant coffee powder (MW profile can be shown in figure 5.2), with typical initial DOC concentration of 8.60 mg/L, and a UV254 absorbance of 0.1789 (2.08 L·mg $^{-1}$ ·m $^{-1}$  SUVA). Along with low MW NOM, low SUVA NOM is very difficult to remove by coagulation or any other means to water treatment. Thirdly, a high SUVA surrogate was prepared from ECO Super Hume – 17% Humic Acid (13% fulvic, 4% humic), with typical initial DOC concentration of 11.28 mg/L, and a UV254 absorbance of 0.470 (4.16 L·mg $^{-1}$ ·m $^{-1}$  SUVA). Total organic carbon was monitored by a Shimadzu TOC-L/CPN using standard method 5310 B.<sup>78</sup>

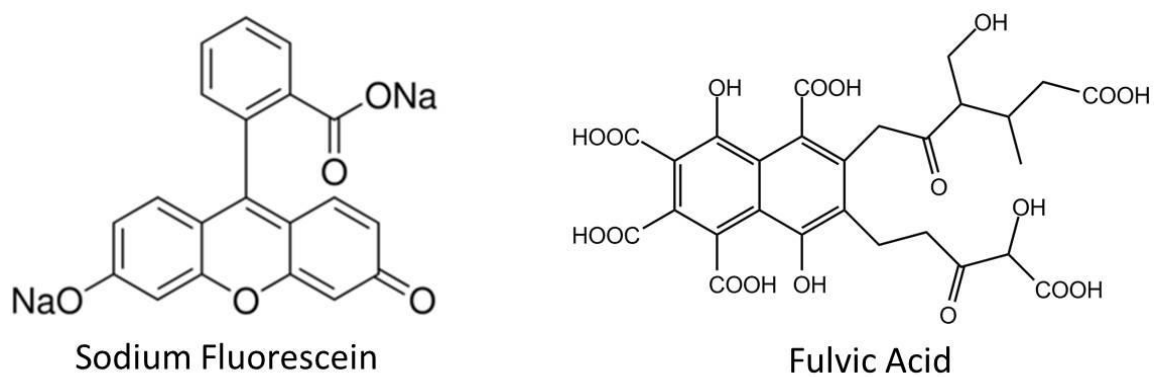


FIGURE 5.1: Sodium fluorescein was chosen as a surrogate molecule for NOM due to structural similarities to fulvic acids and strong absorbance in the visible region. A large majority of NOM has either carboxylate or phenolate groups, or both, leaving them as negatively charged species in water.

TABLE 5.1: Coagulation data for low MW surrogate, sodium fluorescein. About 5% of the surrogate could be removed via coagulation. Showing the difficulty found in removing these types of low MW compounds from drinking water sources using coagulation.

Sample	UV254		DOC [mg-c/L]		SUVA
	Avg. (n=3)	Stdv	Avg. (n=3)	Stdv	
<b>NaFL in Water</b>	0.557	0.00239	7.93	0.0189	7.03
<b>Post Coagulation</b>	0.527	0.00656	7.54	0.0796	6.99
<b>Removal [%]</b>	5.4		4.9		----

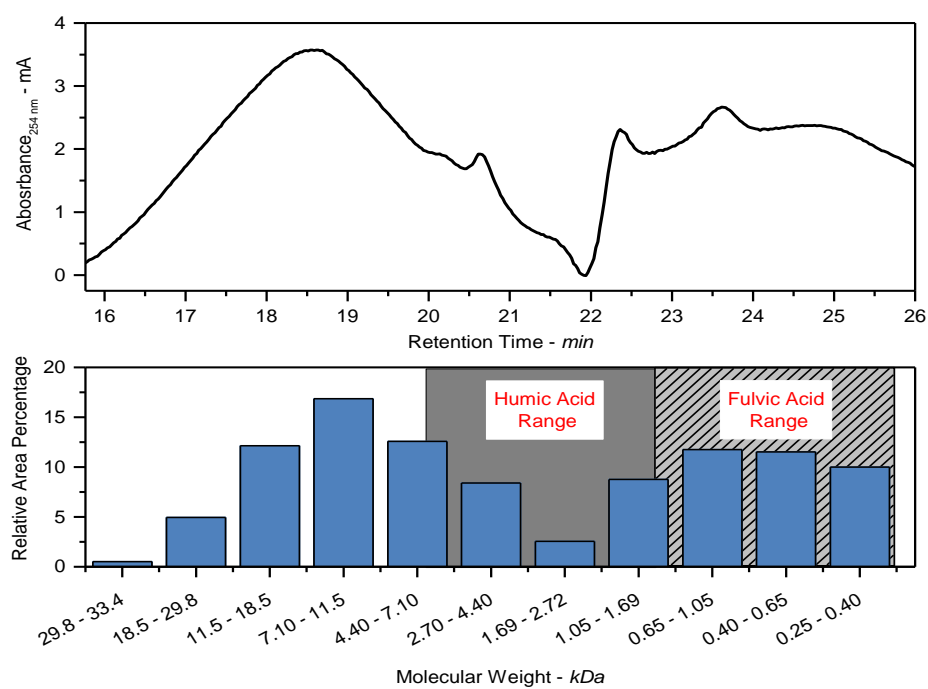


FIGURE 5.2: Molecular weight profile of instant coffee mix used as low SUVA surrogate. Data obtained via HPLC-SEC.

## 5.1. Adsorption Experiments

### 5.1.1. NOM Removal via Adsorbent Incubation

A known mass of adsorbent material was mixed with to a surrogate solution of known concentration in a low retention polypropylene microcentrifuge tube or glass vial for larger samples. For incubation studies of less than one minute specific conditioning steps were followed. For MIEX<sup>®</sup>, resin samples were swelled in water before use. DOWEX<sup>®</sup> samples were conditioned according to the procedure developed by Humbert et al.<sup>17</sup> NOM samples were allowed to incubate, at 22 °C, for various time periods before removing the adsorbent and measuring the final NOM concentration.

### 5.1.2. Surrogate Adsorption via “Fast Filtration”

A known mass of NanoResin was deposited on an alumina membrane with a glass microfiber prefilter. Slowly pushing the NanoResin dispersion through the alumina membrane resulted in a smooth uniform film. The NanoResin film thickness across the membrane was self-limiting. Since the membrane resistance increases (decreasing flux) with the film thickness, heterogeneity is minimized. Control studies found no adsorption of NOM to filtration apparatus without addition of NanoResin. Sodium fluorescein, of a known volume and concentration, was then pushed through the adsorbent using a syringe. The back pressure was low enough for easy manual compression of the syringe (~1 atm backpressure) in less than 10 seconds. The concentration of the filtrate was then measured and compared to the initial NOM concentration. Process depicted in figure 5.3.

### 5.1.3. Surrogate Adsorption via Film Incubation

A known mass of NanoResin was deposited onto a polypropylene support membrane then placed into a glass vial with the NanoResin film facing the solution. A

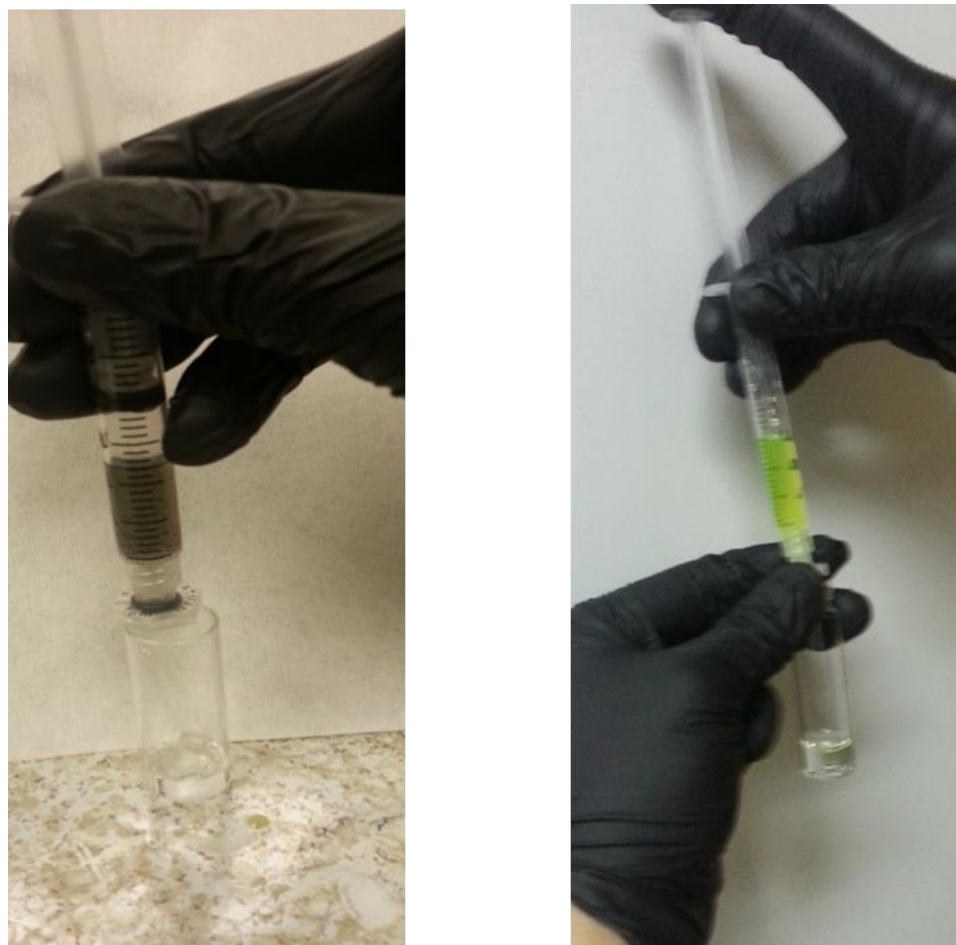


FIGURE 5.3: (a) Preparation of a “fast filtration” membrane. Membrane prepared by depositing a known amount of NanoResin on alumina membrane. (b) Fast filtration adsorption experiment. A low MW surrogate of a known concentration is pushed through a NanoResin membrane. Concentration of the effluent is considerably lower than the influent indicating significant removal of the surrogate.

surrogate solution of known concentration was added to the vial. Samples were allowed to incubate in a tube rotator for five minutes before separating the surrogate solution from the adsorbent, and measuring the final NOM concentration.

#### 5.1.4. DOC Removal from Myrtle Beach, SC NOM Concentrate

A concentrated NOM sample from Myrtle Beach, SC was obtained, and diluted to a known DOC concentration. A NanoResin film, of a known mass, deposited on a polypropylene support membrane, was incubated in the sample for five minutes. DOC concentration was measured before and after incubation, and percent removal was obtained.

#### 5.1.5. Regeneration and Reuse of NanoResin

A known mass of NanoResin was deposited on a support membrane. The nano-AER film was placed inside of a glass vial with a brine solution (2.0 M NaCl) and allowed to incubate for five minutes to ensure the sample had reached ion-exchange equilibrium. Brine was then removed and the film and vial were rinsed with several aliquots of milli-Q water to remove all traces of brine as determined by conductivity measurements. Once clean, the water was removed and a known volume of a NaFL solution with a known concentration was added and allowed to incubate for five minutes. After incubation was complete, the final concentration of the NOM surrogate was measured. This process was repeated 15 times (Figure 5.4).

## 5.2. Results and Discussion

### 5.2.1. Adsorption Kinetics of a Low MW Surrogate

In figure 5.5, we plot the sorption kinetics of the NaFL surrogate DOC onto NanoResin where the loading  $q$ , in mg-C adsorbate per g adsorbent, is measured as a

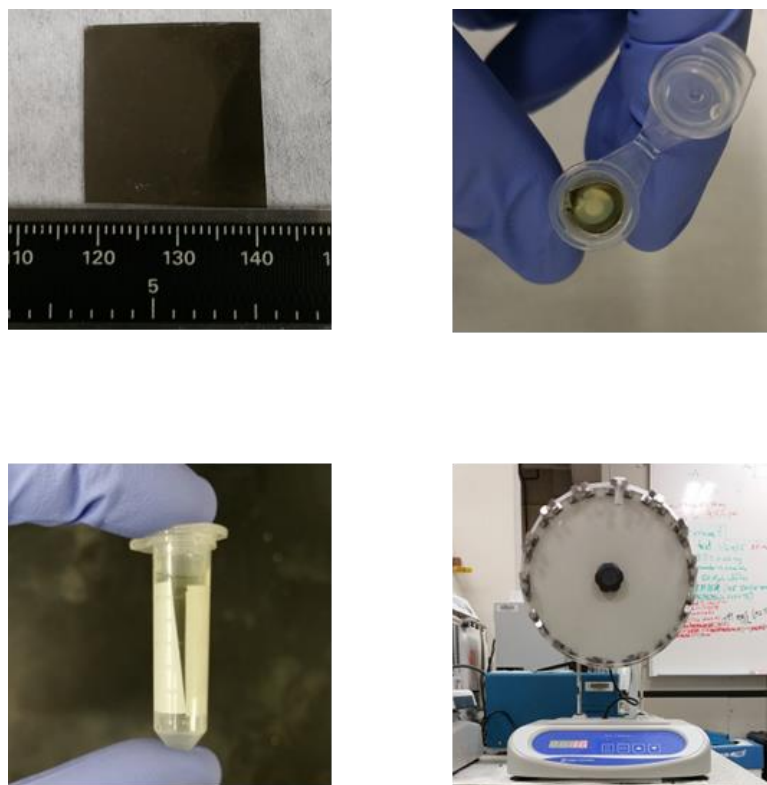


FIGURE 5.4: NanoResin regeneration experiment. (Clockwise from top left) A NanoResin film was prepared on a support membrane. The film was deposited into a NOM surrogate solution and allowed to incubate on a tube rotator. At the end of incubation, adsorption was measured. Film was then placed in a brine solution to desorb NOM. This process was repeated fifteen times and results are shown in figure 5.12.

function of incubation time. A “pseudo-equilibrium” is reached for the NanoResin after about ten seconds of incubation. Comparatively, it takes more than 40 minutes for commercially available AERs to approach equilibrium. This is a consequence of the nanoscale nature of the NanoResin material. As particle size decreases, surface area (per mass) for adsorption increases, and the mass transfer length decreases; thus, the rate of ion exchange increases. Internal diffusion of the adsorbate into the NanoResin is practically negligible due to the small thickness (~5 nm of resin), as well as a lack of cross-linking of the polymer strands. This results in a completely open resin matrix, making adsorption essentially a diffusion-limited process, as illustrated in figure 5.6.<sup>22</sup> This open resin structure differentiates NanoResin from commercial resins because they must be cross-linked in order to form an actual resin bead that will not just dissolve in water. Cross-linking in commercial resins forms pores of different sizes, and the degree of crosslinking directly affects the size of the pores. There are two commonly used types of resins; microreticular (gel) resins, which have 4-10% of a crosslinker (divinyl benzene (DVB) is used with styrenic polymers), and macroreticular resins which have 20-25% cross-linking. While introducing pores to the resin structure significantly increases surface area and the number of active exchange sites, it significantly slows sorption kinetics because ions have to diffuse in and out of the resin structure. The idea that our materials have a completely open resin structure eliminates intraparticle diffusion and allows NanoResin to work as a contact resin. In figure 5.7, we compare adsorption of low MW

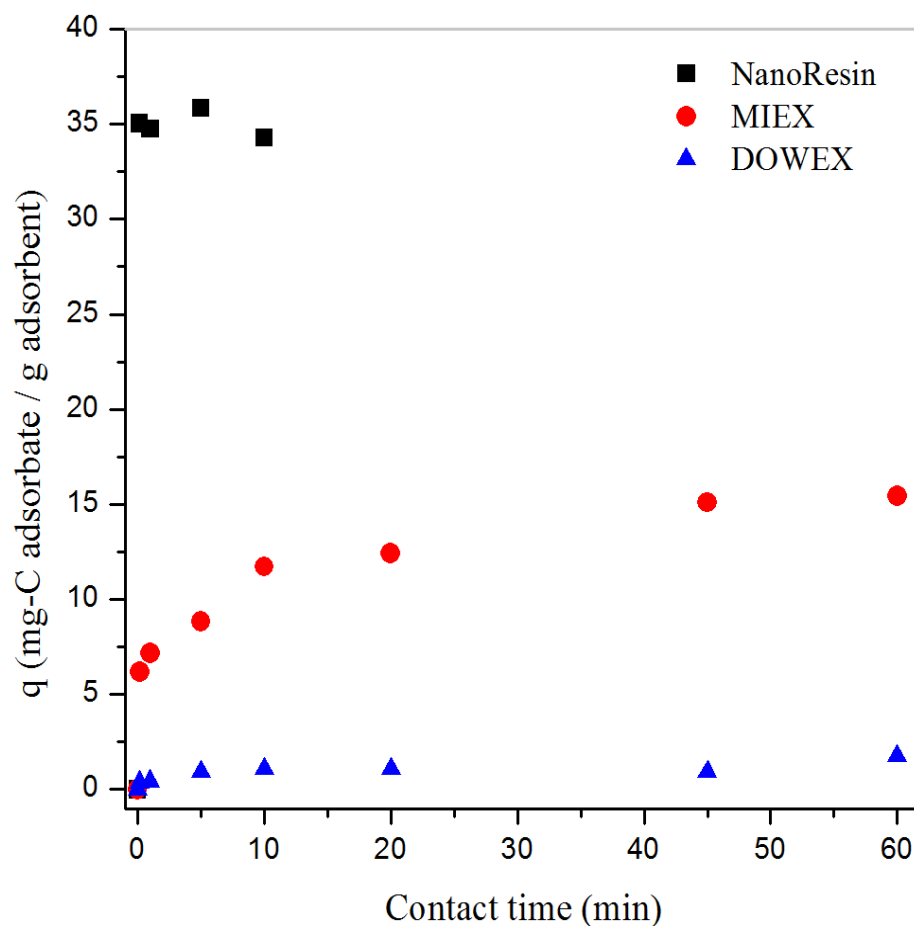


FIGURE 5.5: Kinetic removal of low MW surrogate. Initial DOC concentration of 6.51 mg-C/L for each experiment. Contact time,  $t = 0$ , represents control experiments with no adsorbent added. NanoResin reached equilibrium in less than 60 seconds, whereas MIEX® reached equilibrium within one hour. DOWEX® 21K takes greater than 24 hours to reach equilibrium.

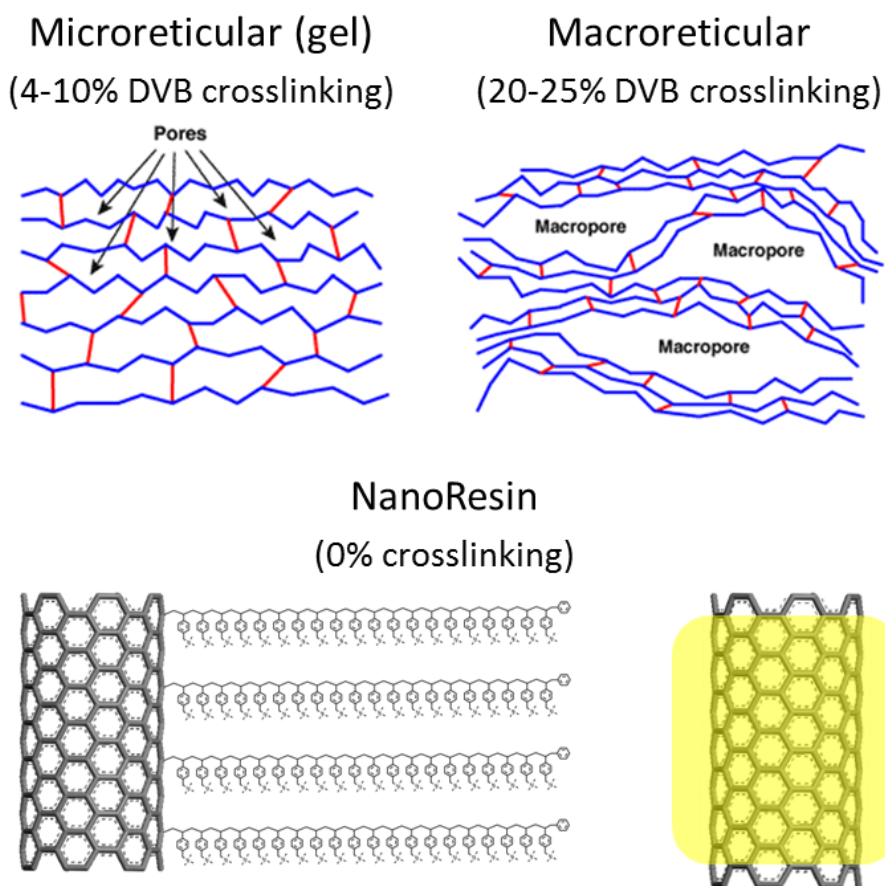


FIGURE 5.6: Gel and macroreticular resin structures compared to open NanoResin structure. Pores in gel and macroreticular structures introduce intraparticle diffusion, which significantly lowers sorption kinetics. NanoResin has a completely open resin structure, meaning that all active sites are on the surface so the resin can act as a contact resin, significantly increasing sorption kinetics.

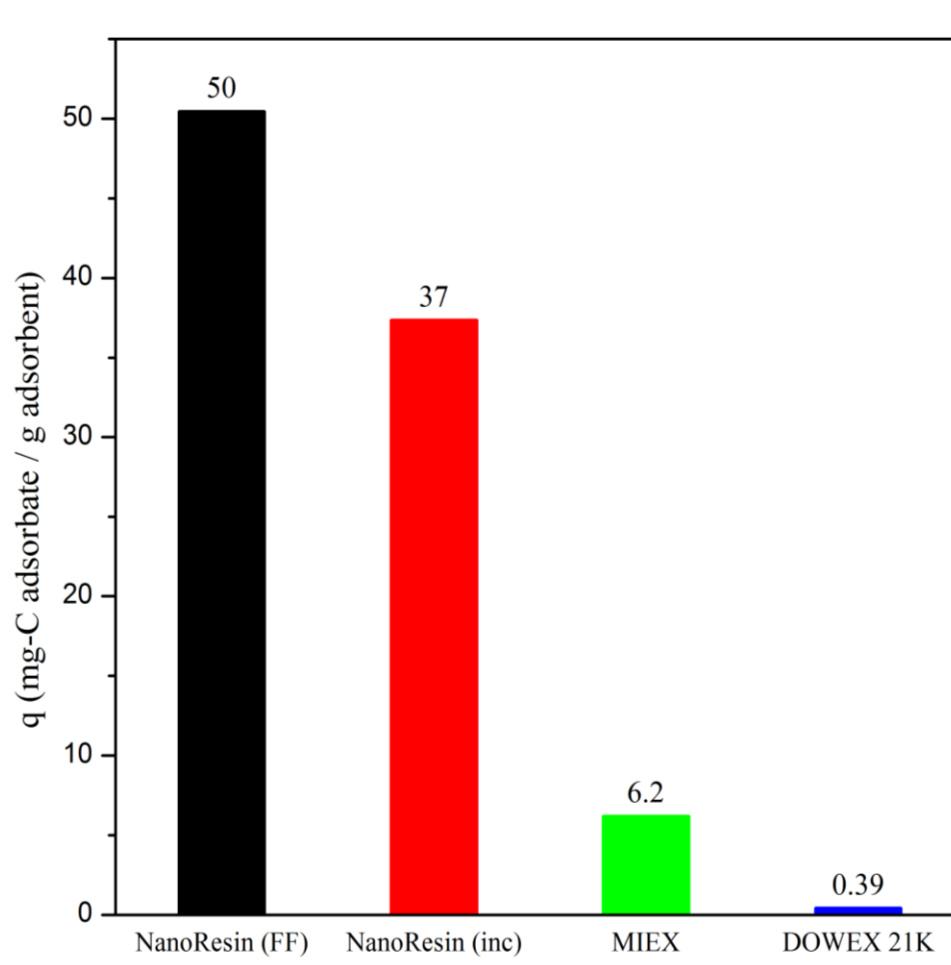


FIGURE 5.7: A comparison of NanoResin adsorption (fast filtration and incubation) to MIEX® and DOWEX® 21K adsorption via incubation after 10 seconds. NaFL NOM adsorbate binds much more efficiently to NanoResin due to the increase in surface area.

TABLE 5.2: Raw data from figure 5.7, low MW surrogate (sodium fluorescein) adsorption after 10 second incubation.

<b>Adsorbent Media</b>	<b>Initial Surrogate Conc. <math>c_i</math> (mg-C/L)</b>	<b>Final Surrogate Conc. <math>c_f</math> (mg-C/L)</b>	<b>Surrogate Volume (mL)</b>	<b>NaFL removed (mg-C)</b>	<b>Mass of Adsorbent (mg)</b>	<b>q (mg-C adsorbate / g adsorbent)</b>
<b>NanoResin (FF)</b>	5.01	2.24	3.00	$8.31 \times 10^{-3}$	0.17	50
<b>NanoResin (inc)</b>	6.70	5.03	1.75	$2.91 \times 10^{-3}$	0.078	37
<b>MIEX<sup>®</sup></b>	6.51	5.93	1.75	$1.09 \times 10^{-3}$	0.18	6.2
<b>Dowex<sup>®</sup></b>	6.51	6.49	1.75	$8.55 \times 10^{-5}$	0.22	0.16

NOM surrogate (NaFL) during a 10 second exposure to either NanoResin, MIEX<sup>®</sup>, or DOWEX<sup>®</sup> 21K. The initial NOM concentration for each trial was held constant and the specific loading capacity  $q$  was measured for different processes and different materials (see table 5.2 for raw data). For each experiment a controlled mass of NOM was interacted with the adsorbent. The specific loading capacity of the resins are reported as  $q$  in mg-C adsorbate per g adsorbent. Fast filtration through a NanoResin thin film had the highest specific adsorption where 0.16 mg of NanoResin removed  $8.31 \times 10^{-3}$  mg-C of NaFL, with a specific capacity  $q = 50$  mg-C/g. A 0.35 mg sample of MIEX<sup>®</sup> removed only  $0.14 \times 10^{-3}$  mg-C of NaFL under the same conditions. A 10 second incubation in dispersed NanoResin yielded  $q = 37$  mg-C/g whereas, the same incubation in dispersed MIEX<sup>®</sup> and DOWEX<sup>®</sup> 21K yielded a specific capacity of only 6.2 mg-C/g and 0.39 mg-C/g respectively. The high SSA and open structure of the NanoResin make it an attractive material for the rapid removal of refractory NOM.

### 5.2.2. Adsorption of a Low MW NOM Surrogate

High-capacity adsorption of low MW surrogate sodium fluorescein was observed with NanoResin in comparison to MIEX<sup>®</sup> and DOWEX<sup>®</sup> 21K, as shown in figure 5.8. Here, we show adsorption isotherms for each type of resin. We plot the surrogate specific loading  $q_e$  against the equilibrium concentration  $C_e$ . The data (in black) illustrate the performance of NanoResin. The larger  $q_e$  for the NanoResin adsorption isotherm is a result of the vast SSA and open resin matrix. Since the adsorbate does not have to diffuse through pores in the resin, adsorption is extraordinarily fast. In figure 5.8, we focus on the low concentration portion of the adsorption isotherms and allowed all materials to incubate with the NOM for 15 hours. We report the Freundlich constant  $K_f$  and exponent

$1/n_f$  from non-linear fitting of the data to the function  $q_e = K_f C_e^{(1/n_f)}$  where  $K_f$  and  $1/n_f$  represent the adsorption capacity and binding strength, respectively. From these data, the  $K_f$  for NanoResin is  $116 \pm 3 \text{ (mg-C/g)(mg-C/L)}^{-1}$ , and is  $33 \pm 3 \text{ (mg-C/g)(mg-C/L)}^{-1}$  for MIEX<sup>®</sup>. The DOWEX<sup>®</sup> 21K is a cross-linked, low SSA material. Between 15 and 24 hours of incubation the material adsorbs just 3% more NOM and as such we are measuring a pseudo-equilibrium isotherm in figure 5.8 for DOWEX with  $K_f = 8.8 \pm 2 \text{ (mg-C/g)(mg-C/L)}^{-1}$ . We also compare the NanoResin to previous literature studies of NOM adsorption onto un-functionalized multi-walled carbon nanotubes<sup>79</sup> (MWCNTs) with  $K_f \sim 6 \text{ (mg-C/g)(mg-C/L)}^{-1}$ , and GAC<sup>80</sup> with  $K_f \sim 8 - 11 \text{ (mg-C/g)(mg-C/L)}^{-1}$ . These MWCNT and GAC results are based on humic substance NOM, which differs from the NaFL we used in our adsorption isotherm study. While MWCNTs and GAC both have very high SSA, the lack of ion-ion attraction between adsorbate and adsorbent (both are slightly negative) contributes to the low  $K_f$ .

The increase in accessible ion-exchange surface area, while increasing the surface area to mass ratio, allows NanoResin to adsorb a significantly greater amount of adsorbate, per mass. The larger  $q_e$  near  $C_{eq} = 0$  shows that the NanoResin can remove NOM more effectively even at very low concentrations (where traditional GAC treatment fails). Even after very long incubation time, and higher resin dose, MIEX<sup>®</sup> and DOWEX<sup>®</sup> 21K are not as effective at removal of low MW NOM. Removal of NOM to very low concentrations requires a large binding strength between the NOM and the adsorbent. The Freundlich exponent,  $1/n_f$ , was also determined by fitting the data in figure 5.8 to the Freundlich isotherm. The binding strength of the NanoResin material is larger than that for the other resin materials, and for NOM adsorbed to un-functionalized

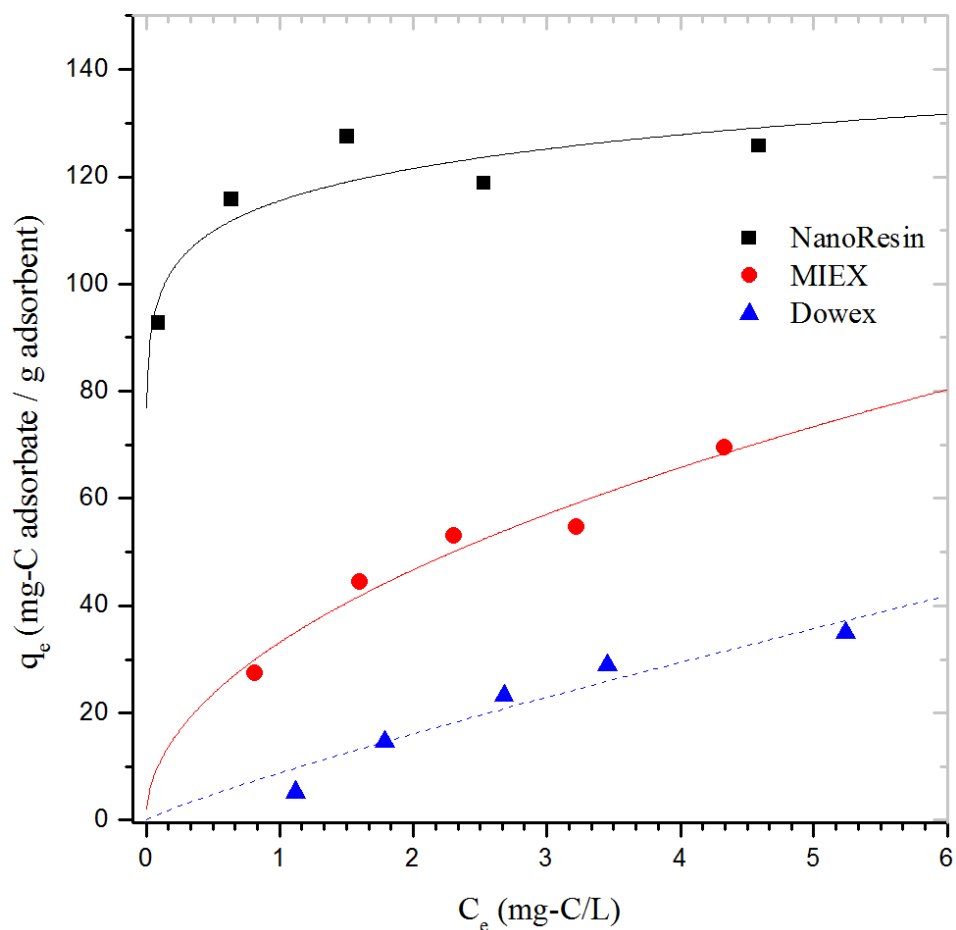


FIGURE 5.8: Adsorption isotherm comparison of commercially available adsorbents to NanoResin. All data are compared with a similar resin dose and adsorbent mass. As surface area increases (DOWEX® 21K < MIEX® < NanoResin), more adsorbate can be bound per mass, much more efficiently. All samples were allowed to incubate for 15 hours. NanoResin and MIEX® are at equilibrium within one hour. Solid line is from fitting the Freundlich isotherm to the data. Dashed line is a non-equilibrium fit to the Freundlich for DOWEX 21K.

MWCNTs or GAC. The values for  $1/n_f$  were  $0.073 \pm 0.02$ ,  $0.49 \pm 0.07$ ,  $0.87 \pm 0.17$ , for the NanoResin, MIEX<sup>®</sup>, DOWEX<sup>®</sup> 21K respectively, where the smaller value is associated with a stronger binding constant. We also compare our data to recent literature reports of  $1/n_f$  being  $0.3 \pm 0.1$  and  $1.3 \pm 0.1$ , for MWCNTs<sup>79</sup> and GAC<sup>80</sup> respectively. Log-log representation of the data is shown in figure 5.9. Photographs of NaFL removal is shown in figure 5.10 with the 1.2 mg-C/L control sample on the left, followed by the NanoResin dispersion, MIEX<sup>®</sup>, and DOWEX<sup>®</sup> 21K after incubating on a tube rotator for 15 hours.

### 5.2.3. Adsorption of Low and High SUVA Surrogates

We compared surrogate NOM removal from both low and high SUVA samples. MIEX<sup>®</sup> is compared to two different NanoResin samples; one prepared by film incubation, and the other by dispersing the NanoResin and incubating the sample. All samples were allowed to incubate for 15 minutes to simulate the published pseudo-equilibrium time for MIEX<sup>®</sup>.<sup>17</sup> Results were measured using both UV254 absorption, as well as TOC analysis, before and after incubation to determine the amount of surrogate removed by each resin. Control studies without resin found no significant removal of NOM. From these data, the NanoResin again shows increased adsorption capacity over the commercial resin in both high and low SUVA samples. All of the 15 minute incubation data are summarized in tables 5.4A and 5.4B. From TOC analysis, 0.30 mg of NanoResin film measured a specific adsorption  $q_e = 32.5$  mg-C/g. For a similar resin dose, the MIEX<sup>®</sup> sample had a specific adsorption of only 7.9 mg-C/g. The dispersed NanoResin sample showed the greatest removal of UV254 absorbing NOM. The raw data in table 5.4A shows that the measured change in UV254 absorbance,  $\Delta A_{254}$ , for

TABLE 5.3: Raw data from figure 5.8, low molecular weight surrogate (sodium fluorescein) adsorption isotherm.

Adsorbent Media	Initial Surrogate Concentration (mg-C/L)	Final Surrogate Concentration; $c_{eq}$ (mg-C/L)	Surrogate Volume (mL)	Mass of Adsorbent (mg)	$q_e$ (mg adsorbate/g adsorbent)
<b>NanoResin</b>	1.20	0.0915	15.0	0.18	92.7
	2.04	0.636	15.0	0.18	116
	3.05	1.50	15.0	0.18	127
	3.91	2.53	15.0	0.17	119
	6.10	4.59	15.0	0.17	126
<b>MIEX<sup>®</sup></b>	1.20	0.815	15.0	0.22	27.4
	2.04	1.60	15.0	0.15	44.5
	3.05	2.31	15.0	0.21	53.1
	3.91	3.22	15.0	0.19	54.6
	6.10	4.34	15.0	0.37	69.6
<b>Dowex<sup>®</sup></b>	1.20	1.12	15.0	0.27	5.26
	2.04	1.79	15.0	0.26	14.7
	3.05	2.68	15.0	0.24	23.3
	3.91	3.45	15.0	0.24	28.9
	6.10	5.24	15.0	0.35	34.9

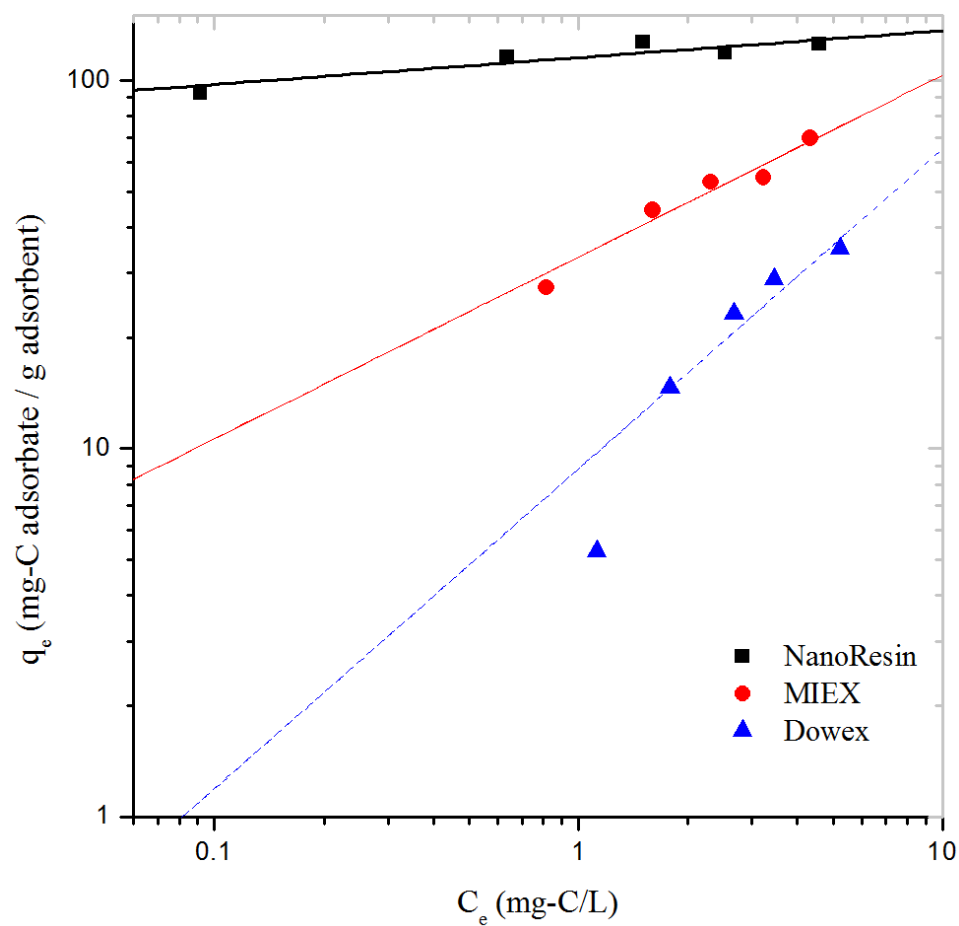


Figure 5.9: Adsorption isotherm of low MW NaFL surrogate, plotted as a log-log graph, comparing commercially available adsorbents to NanoResin. All data are compared with a similar resin dose and adsorbent mass. As surface area increases (DOWEX<sup>®</sup> 21K < MIEX<sup>®</sup> < NanoResin), more adsorbate can be bound per mass, much more efficiently. All samples were allowed to incubate for 15 hours. NanoResin and MIEX<sup>®</sup> are at equilibrium within one hour. Solid line is from fitting the Freundlich isotherm to the data. Dashed line is a non-equilibrium fit to the Freundlich for DOWEX<sup>®</sup> 21K.

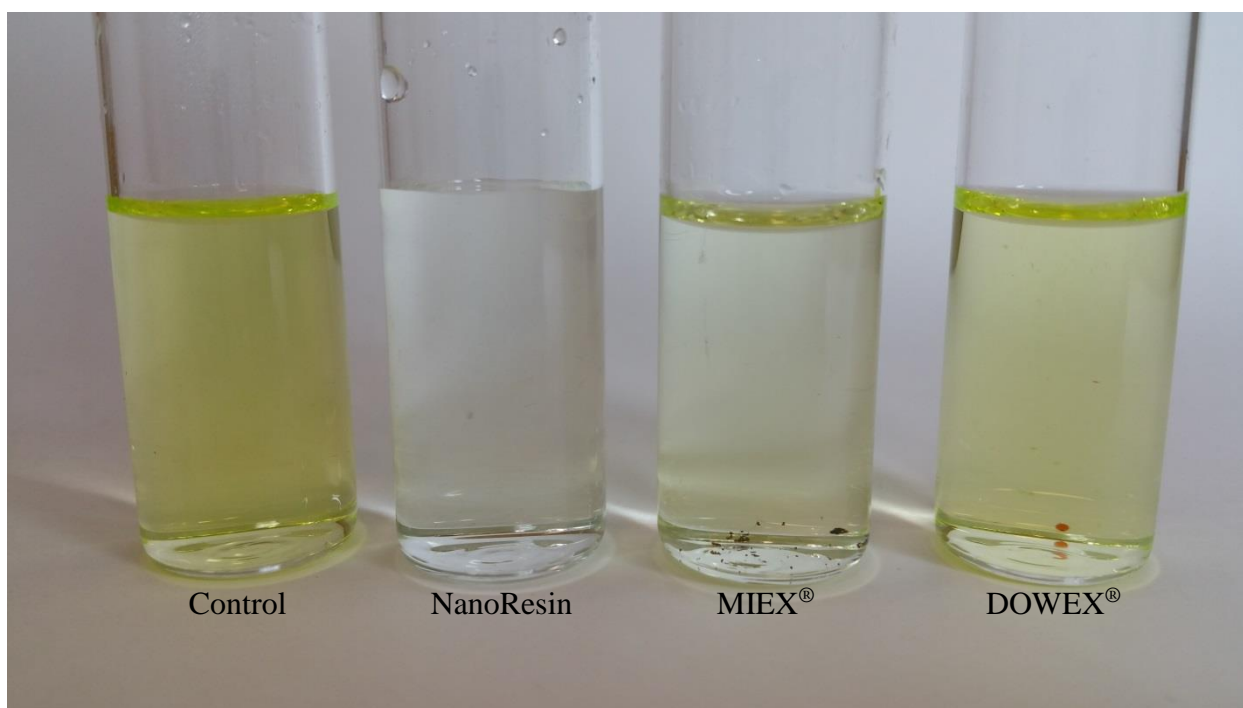


Figure 5.10: Photo of NaFL removal is with the 1.2 mg-C/L control sample on the left, followed by the NanoResin dispersion, MIEX<sup>®</sup>, and DOWEX<sup>®</sup> after incubating on a tube rotator for 15 hours. All samples had similar adsorbent masses.

the NanoResin dispersion incubation was three times that of the  $\Delta A_{254}$  for MIEX<sup>®</sup>, even with six times less NanoResin mass added. We normalized the UV<sub>254</sub> removal by dividing by resin mass and tabulated the  $\Delta A_{254}$  per gram and the % difference per gram of resin. The NanoResin dispersion significantly outperforms the NanoResin film and the MIEX<sup>®</sup> beads, where % difference per g resin is  $1.47 \times 10^5$ ,  $1.35 \times 10^5$ , and  $2.3 \times 10^3$  %/g respectively. This increased adsorption capacity is due to the rapid ion exchange equilibration and increased binding sites based on the larger SSA and open resin matrix of the NanoResin material.

We also compared the NanoResin dispersion to the MIEX<sup>®</sup> dispersion for high SUVA adsorption using similar resin dose and listed in table 5.5. A 0.51 mg sample of NanoResin had a  $\Delta A_{254} = 0.136$  and a % difference UV<sub>254</sub> of 94%. A 2.5 mg sample of MIEX<sup>®</sup> had a  $\Delta A_{254} = 0.0108$  giving a % difference UV<sub>254</sub> from MIEX<sup>®</sup> of only 2.3% NOM removed. Photographs of low and high SUVA removal is shown in figure 5.11 with the control sample on the right of each photograph and the solution after a 15 minute incubation with NanoResin dispersion, on a tube rotator, on the left. These data show the intrinsic ability of the NanoResin to remove both low and high SUVA types of refractory NOM with little discrimination over size or aromatic character. The reduced capability of MIEX<sup>®</sup> to remove the high SUVA NOM is likely related to the pore structure of the resin material. Larger molecules can sterically block others from binding to available sites. However, the open resin structure of the NanoResin enables easier access to the IEX sites along the SWCNT-poly(vbTMAC) microstructure. In table 5.6A and 5.6B, we report data from five minute incubation studies. While the dispersed NanoResin still exhibits high capacity, rapid removal of the NOM, the NanoResin thin

TABLE 5.4A: Raw data from 15 minute, low SUVA surrogate adsorption experiments.  
 \*NanoResin film data collected by averaging five separate adsorption experiments, regenerating, and rinsing between each.

Adsorbent Media	Mass of Adsorbent (mg)	UV254 initial	UV254 Removal (initial – final)	(UV removal) / (g adsorbent) (A.U./g)	UV254 % difference	(UV254 % difference) / (g adsorbent)
NanoResin Dispersion	0.51	0.0447	0.0339	65.9	75.9	1.47E5
NanoResin Film*	0.30	0.1481	0.0183	40.2	11.0	1.35E5
MIEX®	3.39	0.1789	0.0105	3.10	5.87	1.73E3
	3.15	0.1789	0.0159	5.05	8.89	2.82E3

TABLE 5.4B: Raw data from 15 minute, low SUVA surrogate adsorption experiments.  
 \*NanoResin film data collected by combining five separate adsorption experiments, regenerating, and rinsing between each.

Adsorbent Media	Mass of Adsorbent (mg)	Initial Surrogate Conc. $C_{eq}$ (mg-C/L)	Final Surrogate Conc. $C_{eq}$ (mg-C/L)	TOC % difference	(% difference TOC) / (g adsorbent)	$q_e$ (mg-C NOM) / (g adsorbent)
NanoResin Film*	1.49	7.58	6.20	18.2	122	32.5
MIEX®	3.39	8.60	8.03	6.63	19.6	6.19
	3.15	8.60	7.71	10.3	32.8	9.56

thin film is less effective at the shorter times. This is again related to the transport of NOM into the thin film material. As with MIEX<sup>®</sup> beads dispersed in water, the NOM must still diffuse into the film to bind. These data further support our model shown in figure 4.9, where the dispersed NanoResin effectively exposes its IEX sites to the solution, while the SWCNT scaffold maintains the material's morphology. Without the SWCNT scaffold, the polymer strands would simply form a resin bead, decreasing the SSA. Moreover, the SWCNT scaffold enables the material to be more easily recovered and thereby, reused.

#### 5.2.4. Adsorption of Myrtle Beach, SC NOM Concentrate

A concentrated NOM sample from Myrtle Beach, SC was diluted to a DOC of 11.52 mg-C/L, with a UV254 absorbance of 0.396, giving a SUVA of 4.36 L·mg<sup>-1</sup>·m<sup>-1</sup>. The adsorption capabilities of a NanoResin film were measured and the UV254 and TOC results are included in tables 5.7A and 5.7B respectively. After a five minute incubation with a 0.34 mg NanoResin film, the UV254 fell from  $A_{254} = 0.5026$  to  $A_{254} = 0.1041$ , a 20.7% reduction. The NanoResin also effectively reduced the TOC of the natural water sample. The surrogate concentration dropped from 11.5 mg-C/L to 9.17 mg-C/L after a five minute incubation, a 20.4% reduction. After incubation, the SUVA was measured to be 4.35 L·mg<sup>-1</sup>·m<sup>-1</sup>, where we found effectively no change in SUVA from the initial sample. This indicates that the NanoResin shows little preference over hydrophilic and hydrophobic compounds; universally removing NOM until all active sites have been exchanged. This behavior is consistent with our polymerization mechanism and functionalization which leads to a nanoscale thin film that does not contain polymer branching or crosslinking between strands. These data are also consistent with our

TABLE 5.5: Raw data from 15 minute, high SUVA surrogate adsorption experiments.

<b>Adsorbent Media</b>	<b>Mass of Adsorbent (mg)</b>	<b>UV254 initial</b>	<b>UV254 Removal (initial – final)</b>	<b>(UV removal) / (g adsorbent) (A.U./g)</b>	<b>UV254 % difference</b>	<b>(UV254 % difference) / (g adsorbent)</b>
<b>NanoResin Dispersion</b>	0.51	0.1452	0.1363	265	93.9	1.82E5
	0.51	0.1452	0.1368	266	94.2	1.83E5
<b>MIEX®</b>	2.55	0.4697	0.0109	4.27	2.32	910.
	2.49	0.4697	0.0107	4.30	2.28	915

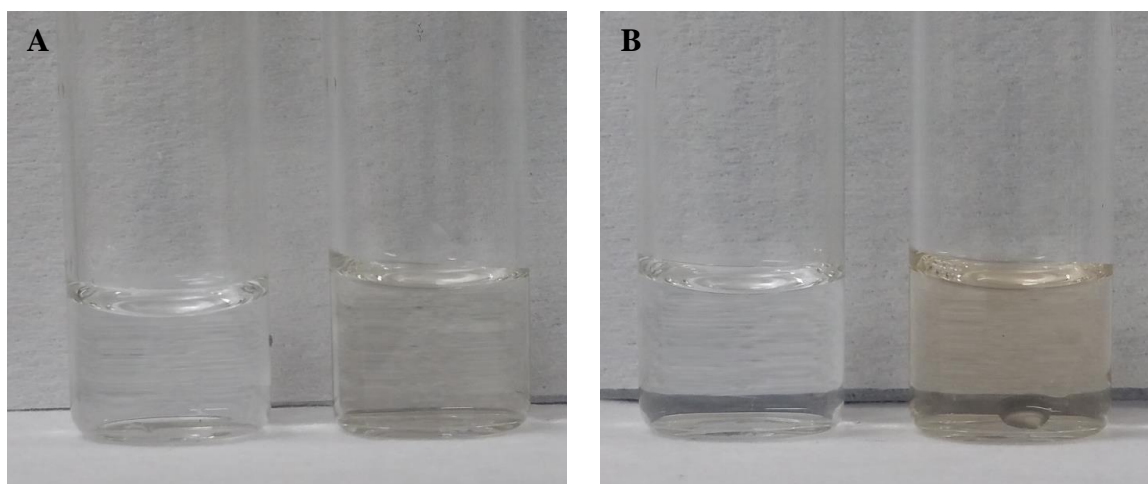


Fig. 5.11: 15 minute incubation of NanoResin dispersion with low SUVA 7.58 mg-C/L (A) and high SUVA (B). Initial concentration of low SUVA sample in (A) is 8.60 mg-C/L (right). Incubated sample on the (left). Initial concentration of high SUVA sample in (B) is 11.28 mg-C/L (right). Incubated sample on the ( left).

TABLE 5.6A: Raw data for the low SUVA surrogate adsorption experiments. All samples were allowed to incubate for five minutes.

Adsorbent Media	Mass of Adsorbent (mg)	UV254 initial	UV254 Removal (initial – final)	(UV removal)/ (g adsorbent) (A.U./g)	UV254 % difference	(UV254 % difference) / (g adsorbent)
<b>NanoResin Dispersion</b>	0.23	0.0817	0.0521	230.	63.8	2.81E5
<b>NanoResin Film</b>	0.35	0.188	0.0500	142	26.6	7.57E4
<b>MIEX®</b>	0.59	0.188	0.0140	23.7	7.45	1.26E4

TABLE 5.6B: Raw data for the low SUVA surrogate adsorption experiments. All samples were allowed to incubate for five minutes.

Adsorbent Media	Mass of Adsorbent (mg)	Initial Surrogate Conc.; $C_{eq}$ (mg-C/L)	Final Surrogate Conc.; $C_{eq}$ (mg-C/L)	TOC % difference	(% diff TOC)/ (g adsorbent)	$q_e$ (mg-C NOM) / (g adsorbent)
<b>NanoResin Film</b>	0.35	8.90	6.22	30.1	86000	53.4
<b>MIEX®</b>	0.59	8.90	6.99	21.5	36400	22.6

TABLE 5.7A: Raw UV254 data from section 5.2.4: Adsorption of Myrtle Beach, SC NOM concentrate onto NanoResin. Samples incubated for five minutes.

Adsorbent Media	Mass of Adsorbent (mg)	UV254 initial	UV254 Removal (initial – final)	(UV removal) / (g adsorbent) (A.U./g)	UV254 % difference	(UV254 % difference) / (g adsorbent)
<b>NanoResin Film</b>	0.34	0.5026	0.1041	303	20.7	6.02E4

TABLE 5.7B: Raw TOC data from section 5.2.4: Adsorption of Myrtle Beach, SC NOM concentrate onto NanoResin. Samples incubated for five minutes.

Adsorbent Media	Mass of Adsorbent (mg)	Initial Surrogate Conc.; $c_{eq}$ (mg-C/L)	Final Surrogate Conc.; $c_{eq}$ (mg-C/L)	TOC % difference	(% diff TOC) / (g adsorbent)	$q_e$ (mg-C NOM) / (g adsorbent)
<b>NanoResin Film</b>	0.34	11.5	9.17	20.4	5.93E4	235

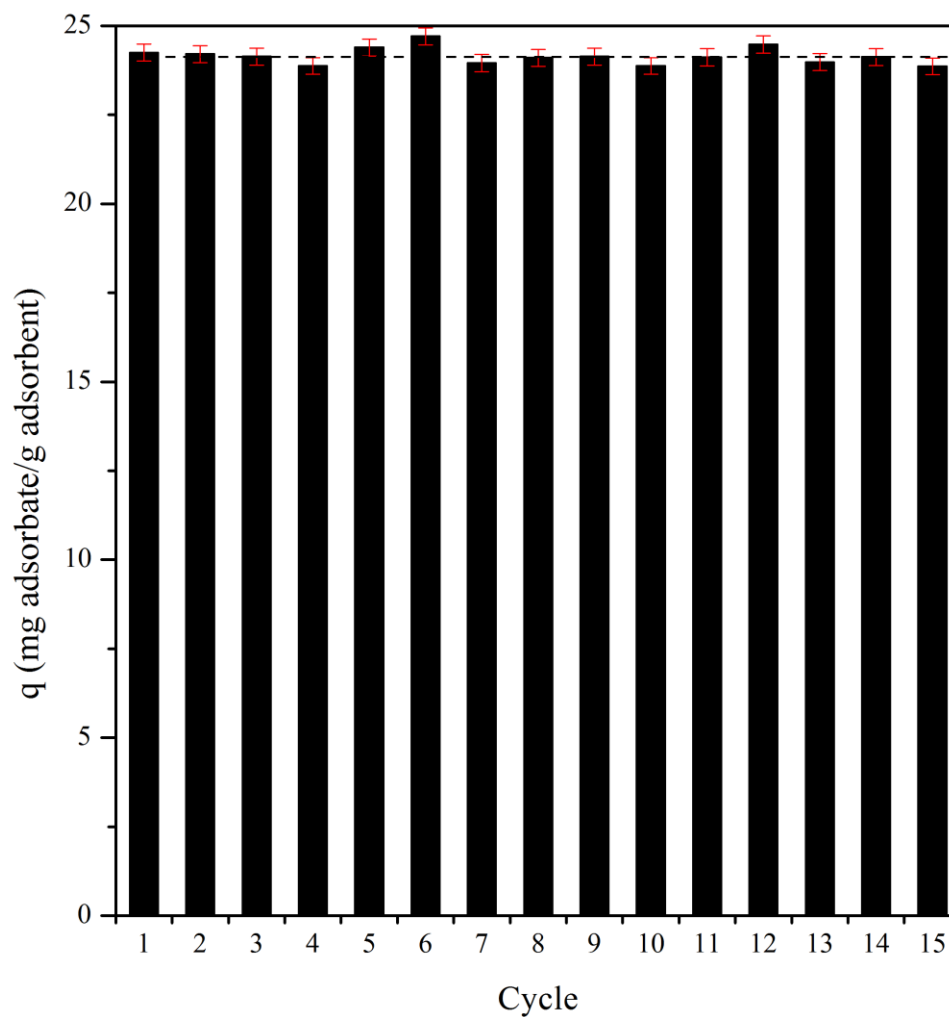


FIGURE 5.12: Regeneration cycles for a NanoResin thin film. After surrogate NOM adsorption, the NanoResin is exposed to 2.0 M NaCl(aq). No perceptible degradation within experimental uncertainty where  $q$  versus cycle has a slope of  $-0.057 \pm 0.06$  %/cycle. Result  $\pm$  95% standard error.

with our molecular dynamics calculations of this open microstructure model.

#### 5.2.5. Regeneration and Reuse of NanoResin

To probe the regeneration efficiency of the NanoResin, a brine solution (2.0 M NaCl) was used to desorb NOM from NanoResin deposited on a support membrane. Excess brine was rinsed away with milli-Q water until conductivity measurements showed no residual NaCl, before adding the surrogate low MW NOM. After a five minute incubation with the NanoResin film, the specific adsorption  $q_e$  was measured. The sample NanoResin film was then regenerated with brine and the experiment repeated. It was found that through 15 adsorption/regeneration cycles, at neutral pH, the NanoResin maintained the same adsorption capacity without perceptible degradation within experimental uncertainty where  $q_e$  versus cycle has a slope of  $(-0.057 \pm 0.06)$  %/cycle; as shown in figure 5.12. Using a surrogate (NaFL) DOC concentration of 2.28 mg-C/L, it was found that NanoResin could effectively adsorb the surrogate, and just as efficiently, desorb it in a brine solution. This demonstrates that NanoResin can be regenerated and reused for the removal of NOM. This open polymer microstructure of NanoResin differs significantly from the crosslinked resin in MIEX<sup>®</sup> or DOWEX<sup>®</sup>. We observe that DOWEX<sup>®</sup> resin beads fracture and degrade after regeneration in brine, and cannot be considered a sustainable water purification material.

## CHAPTER 6: CONCLUSIONS AND FUTURE WORK

Single-walled carbon nanotubes, covalently functionalized with a Strong Base Type I anion exchange resin, were synthesized using a robust polymerization mechanism (ARGET ATRP). This allows for exploitation of the very large SSA intrinsic to SWNCTs to be coupled with the enhanced NOM removal capability of the quaternary ammonium AER. This novel NanoResin is dispersible in aqueous systems, where it can rapidly remove a broad spectrum of NOM types, while maintaining high adsorption capacity throughout numerous regeneration cycles. The NanoResin outperformed commercial resins and GAC at NOM removal. Furthermore, we have demonstrated rapid removal of low MW NOM after a 10 second exposure to both the dispersed material and by fast filtration through a NanoResin thin film. Enhanced adsorption of refractory NOM (low MW, low SUVA) compared to commercial AER has been effectively demonstrated by these novel nanomaterials. This effectiveness is due to the vast specific surface area of the nano-AER and the completely open resin matrix. The open resin matrix eliminates intraparticle diffusion of adsorbates, and the rate of adsorption is limited only by solvent diffusion; thus, these nanomaterials act as a “contact resin,” reaching IEX equilibrium within 10 seconds. The ability to remove potentially hazardous DBP precursors, while being easily regenerated, is a sustainable solution to a very difficult environmental problem.

Future work focuses on optimization of aqueous polymer synthesis and SWCNT functionalization. Once synthesis is well controlled, alterations can be made to maximize adsorption characteristics of the resin. Currently, all adsorption studies have been completed using surrogate NOM, or NOM concentrate, studies using real water samples with TOC/UV254 analysis are necessary to further validate actual effectiveness as a tool for water purification. As a cost savings measure, cheaper scaffolding materials are being considered. SWCNTs are > \$500/g currently, materials like carbon nanofibers (\$3/g) are currently being explored as a nanostructured carbon alternative. Nanostructured carbon is ideal for NanoResin synthesis since functionalization happens via the same mechanism of polymer propagation allowing for a one-pot synthesis. Changing the resin specificity is another project that needs to be explored to change the types of adsorbates that can be removed.

## REFERENCES

- (1) Reckhow, D. A.; Singer, P. C., The removal of organic halide precursors by preozonation and alum coagulation. *Journal American Water Works Association* **1984**, *76* (4), 151-157.
- (2) Christman, R. F.; Norwood, D. L.; Millington, D. S.; Johnson, J. D.; Stevens, A. A., Identity and yields of major halogenated products of aquatic fulvic acid chlorination. *Environmental Science & Technology* **1983**, *17* (10), 625-628.
- (3) USEPA Basic Information about Disinfection Byproducts in Drinking Water: Total Trihalomethanes, Haloacetic Acids, Bromate, and Chlorite.  
<http://water.epa.gov/drink/contaminants/basicinformation/disinfectionbyproducts.cfm> (accessed 09/11/2015).
- (4) Bond, T.; Goslan, E. H.; Parsons, S. A.; Jefferson, B., Disinfection by-product formation of natural organic matter surrogates and treatment by coagulation, MIEX (R) and nanofiltration. *Water Research* **2010**, *44* (5), 1645-1653.
- (5) Rose, J. B. TTHM in Drinking Water: The Flint, Michigan Story, A Lesson for Us All *Water and Health* [Online], 2015. <http://www.waterandhealth.org/tthm-drinking-water-flint-michigan-story-lesson/> (accessed March 11, 2016).
- (6) USEPA Microbials and Disinfection Byproducts (MDBP) Tools: Microbials and Disinfection Byproducts Rules.  
<http://water.epa.gov/lawsregs/rulesregs/sdwa/mdbp/tools.cfm> (accessed 10/01/2015).
- (7) Bolto, B.; Dixon, D.; Eldridge, R.; King, S.; Linge, K., Removal of natural organic matter by ion exchange. *Water Research* **2002**, *36* (20), 5057-5065.
- (8) Tan, Y. R.; Kilduff, J. E., Factors affecting selectivity during dissolved organic matter removal by anion-exchange resins. *Water Research* **2007**, *41* (18), 4211-4221.
- (9) Drikas, M.; Dixon, M.; Morran, J., Long term case study of MIEX pre-treatment in drinking water; understanding NOM removal. *Water Research* **2011**, *45* (4), 1539-1548.
- (10) Humbert, H.; Gallard, H.; Jacquemet, V.; Croue, J.-P., Combination of coagulation and ion exchange for the reduction of UF fouling properties of a high DOC content surface water. *Water Research* **2007**, *41* (17), 3803-3811.

- (11) Wang, H. T.; Keller, A. A.; Clark, K. K., Natural organic matter removal by adsorption onto magnetic permanently confined micelle arrays. *Journal of Hazardous Materials* **2011**, *194*, 156-161.
- (12) Hruska, J.; Kram, P.; McDowell, W. H.; Oulehle, F., Increased Dissolved Organic Carbon (DOC) in Central European Streams is Driven by Reductions in Ionic Strength Rather than Climate Change or Decreasing Acidity. *Environmental Science & Technology* **2009**, *43* (12), 4320-4326.
- (13) Joseph, L.; Flora, J. R. V.; Park, Y. G.; Badawy, M.; Saleh, H.; Yoon, Y., Removal of natural organic matter from potential drinking water sources by combined coagulation and adsorption using carbon nanomaterials. *Separation and Purification Technology* **2012**, *95*, 64-72.
- (14) Cornelissen, E. R.; Moreau, N.; Siegers, W. G.; Abrahamse, A. J.; Rietveld, L. C.; Grefte, A.; Dignum, M.; Amy, G.; Wessels, L. P., Selection of anionic exchange resins for removal of natural organic matter (NOM) fractions. *Water Research* **2008**, *42* (1-2), 413-423.
- (15) Qi, S. Y.; Schideman, L. C.; Boyer, T. H., Determining Minimum Ion Exchange Resin Usage for NOM Removal. *Journal of Environmental Engineering-Asce* **2012**, *138* (10), 1058-1066.
- (16) Swietlik, J.; Dabrowska, A.; Raczyk-Stanislawiak, U.; Nawrocki, J., Reactivity of natural organic matter fractions with chlorine dioxide and ozone. *Water Research* **2004**, *38* (3), 547-558.
- (17) Humbert, H.; Gallard, H.; Suty, H.; Croue, J. P., Performance of selected anion exchange resins for the treatment of a high DOC content surface water. *Water Research* **2005**, *39* (9), 1699-1708.
- (18) Boening, P. H.; Beckmann, D. D.; Snoeyink, V. L., Activated carbon versus resin adsorption of humic substances. *Journal American Water Works Association* **1980**, *72* (1), 54-59.
- (19) Bolto, B.; Dixon, D.; Eldridge, R.; King, S., Removal of THM precursors by coagulation or ion exchange. *Water Research* **2002**, *36* (20), 5066-5073.
- (20) Weber, W. J.; Vanvliet, B. M., Synthetic adsorbents and activated carbons for water-treatment – overview and experimental comparisons. *Journal American Water Works Association* **1981**, *73* (8), 420-426.
- (21) Bolto, B.; Dixon, D.; Eldridge, R., Ion exchange for the removal of natural organic matter. *Reactive & Functional Polymers* **2004**, *60*, 171-182.

- (22) Crittenden, J. C.; Montgomery Watson, H.; Wiley, I., MWH's water treatment principles and design. **2012**, 1283.
- (23) Heo, J.; Kim, H.; Her, N.; Lee, S.; Park, Y. G.; Yoon, Y., Natural organic matter removal in single-walled carbon nanotubes-ultrafiltration membrane systems. *Desalination* **2012**, *298*, 75-84.
- (24) Singer, P. C.; Schneider, M.; Edwards-Brandt, J.; Budd, G. C., MIEX for removal of DBP precursors: Pilot-plant findings. *Journal American Water Works Association* **2007**, *99* (4), 128-139.
- (25) Wang, J. S.; Matyjaszewski, K., CONTROLLED LIVING RADICAL POLYMERIZATION - HALOGEN ATOM-TRANSFER RADICAL POLYMERIZATION PROMOTED BY A CU(I)CU(II) REDOX PROCESS. *Macromolecules* **1995**, *28* (23), 7901-7910.
- (26) Minisci, F., FREE-RADICAL ADDITIONS TO OLEFINS IN PRESENCE OF REDOX SYSTEMS. *Accounts of Chemical Research* **1975**, *8* (5), 165-171.
- (27) Matyjaszewski, K.; Xia, J. H., Atom transfer radical polymerization. *Chemical Reviews* **2001**, *101* (9), 2921-2990.
- (28) Matyjaszewski, K.; American Chemical, S.; Division of Polymer, C.; American Chemical, S.; Meeting, *Controlled radical polymerization*. American Chemical Society: Washington, DC, 1998.
- (29) Tang, W.; Tsarevsky, N. V.; Matyjaszewski, K., Determination of equilibrium constants for atom transfer radical polymerization. *Journal of the American Chemical Society* **2006**, *128* (5), 1598-1604.
- (30) Patten, T. E.; Matyjaszewski, K., Atom transfer radical polymerization and the synthesis of polymeric materials. *Advanced Materials* **1998**, *10* (12), 901-+.
- (31) Matyjaszewski, K.; Sumerlin, B. S.; Tsarevsky, N. V.; American Chemical, S.; Division of Polymer, C., *Progress in controlled radical polymerization mechanisms and techniques*. American Chemical Society: Washington, DC, 2012.
- (32) Coessens, V.; Pintauer, T.; Matyjaszewski, K., Functional polymers by atom transfer radical polymerization. *Progress in Polymer Science* **2001**, *26* (3), 337-377.
- (33) Tang, W.; Kwak, Y.; Braunecker, W.; Tsarevsky, N. V.; Coote, M. L.; Matyjaszewski, K., Understanding atom transfer radical polymerization: Effect of ligand and initiator structures on the equilibrium constants. *Journal of the American Chemical Society* **2008**, *130* (32), 10702-10713.

- (34) Matyjaszewski, K.; Gobelt, B.; Paik, H. J.; Horwitz, C. P., Tridentate nitrogen-based ligands in Cu-based ATRP: A structure-activity study. *Macromolecules* **2001**, *34* (3), 430-440.
- (35) Tsarevsky, N. V.; Matyjaszewski, K., "Green" atom transfer radical polymerization: From process design to preparation of well-defined environmentally friendly polymeric materials. *Chemical Reviews* **2007**, *107* (6), 2270-2299.
- (36) Matyjaszewski, K., Transition metal catalysis in controlled radical polymerization: Atom transfer radical polymerization. *Chemistry-a European Journal* **1999**, *5* (11), 3095-3102.
- (37) Eckenhoff, W. T.; Pintauer, T., Atom transfer radical addition (ATRA) catalyzed by copper complexes with tris 2-(dimethylamino)ethyl amine (Me6TREN) ligand in the presence of free-radical diazo initiator AIBN. *Dalton Transactions* **2011**, *40* (18), 4909-4917.
- (38) Simakova, A.; Averick, S. E.; Konkolewicz, D.; Matyjaszewski, K., Aqueous ARGET ATRP. *Macromolecules* **2012**, *45* (16), 6371-6379.
- (39) Horn, M.; Matyjaszewski, K., Solvent Effects on the Activation Rate Constant in Atom Transfer Radical Polymerization. *Macromolecules* **2013**, *46* (9), 3350-3357.
- (40) Kamigaito, M.; Ando, T.; Sawamoto, M., Metal-catalyzed living radical polymerization. *Chemical Reviews* **2001**, *101* (12), 3689-3745.
- (41) Burdge, J., *Chemistry*. Second ed.; McGraw-Hill Companies, Incorporated: 2010.
- (42) Seeliger, F.; Matyjaszewski, K., Temperature Effect on Activation Rate Constants in ATRP: New Mechanistic Insights into the Activation Process. *Macromolecules* **2009**, *42* (16), 6050-6055.
- (43) Mueller, L.; Jakubowski, W.; Matyjaszewski, K.; Pietrasik, J.; Kwiatkowski, P.; Chaladaj, W.; Jurczak, J., Synthesis of high molecular weight polystyrene using AGET ATRP under high pressure. *European Polymer Journal* **2011**, *47* (4), 730-734.
- (44) Schroeder, H.; Buback, M.; Shaver, M. P., Kinetics of Amine-Bis(phenolate) Iron-Mediated ATRP Up to High Pressure. *Macromolecules* **2015**, *48* (17), 6114-6120.
- (45) Braunecker, W. A.; Matyjaszewski, K., Controlled/living radical polymerization: Features, developments, and perspectives. *Progress in Polymer Science* **2007**, *32* (1), 93-146.

- (46) Matyjaszewski, K. Atom Transfer Radical Polymerization. <http://www.cmu.edu/maty/chem/fundamentals-atrp/atrp.html>.
- (47) Jakubowski, W.; Min, K.; Matyjaszewski, K., Activators regenerated by electron transfer for atom transfer radical polymerization of styrene. *Macromolecules* **2006**, *39* (1), 39-45.
- (48) Min, K.; Gao, H. F.; Matyjaszewski, K., Use of ascorbic acid as reducing agent for synthesis of well-defined polymers by ARGET ATRP. *Macromolecules* **2007**, *40* (6), 1789-1791.
- (49) Smolne, S.; Buback, M., Kinetic Investigations of Cu-Mediated ATRP in Aqueous Solution. *Macromolecular Chemistry and Physics* **2015**, *216* (8), 894-902.
- (50) Fantin, M.; Isse, A. A.; Gennaro, A.; Matyjaszewski, K., Understanding the Fundamentals of Aqueous ATRP and Defining Conditions for Better Control. *Macromolecules* **2015**, *48* (19), 6862-6875.
- (51) Richardson, S. D.; Plewa, M. J.; Wagner, E. D.; Schoeny, R.; DeMarini, D. M., Occurrence, genotoxicity, and carcinogenicity of regulated and emerging disinfection by-products in drinking water: A review and roadmap for research. *Mutation Research/Reviews in Mutation Research* **2007**, *636* (1-3), 178-242.
- (52) Boyer, T. H.; Singer, P. C., Bench-scale testing of a magnetic ion exchange resin for removal of disinfection by-product precursors. *Water Research* **2005**, *39* (7), 1265-1276.
- (53) Singer, P. C., CONTROL OF DISINFECTION BY-PRODUCTS IN DRINKING-WATER. *Journal of Environmental Engineering-Asce* **1994**, *120* (4), 727-744.
- (54) Krasner, S. W.; Weinberg, H. S.; Richardson, S. D.; Pastor, S. J.; Chinn, R.; Scilimenti, M. J.; Onstad, G. D.; Thruston, A. D., Occurrence of a new generation of disinfection byproducts. *Environmental Science & Technology* **2006**, *40* (23), 7175-7185.
- (55) Matilainen, A.; Vepsäläinen, M.; Sillanpää, M., Natural organic matter removal by coagulation during drinking water treatment: A review. *Advances in Colloid and Interface Science* **2010**, *159* (2), 189-197.
- (56) Wang, Y.; Gao, B.-Y.; Chu, Y.-B.; Zhou, X.-Z.; Wang, Q., Removal of natural organic matter (NOM) by the coagulation-ultrafiltration system using an inorganic-organic composite coagulant. *Desalination and Water Treatment* **2011**, *32* (1-3), 187-193.

- (57) Bongiovani, M. C.; Camacho, F. P.; Coldebella, P. F.; Valverde, K. C.; Nishi, L.; Bergamasco, R., Removal of natural organic matter and trihalomethane minimization by coagulation/flocculation/filtration using a natural tannin. *Desalination and Water Treatment* **2016**, *57* (12), 5406-5415.
- (58) Rondeau, V.; Jacqmin-Gadda, H.; Commenges, D.; Helmer, C.; Dartigues, J.-F., Aluminum and Silica in Drinking Water and the Risk of Alzheimer's Disease or Cognitive Decline: Findings From 15-Year Follow-up of the PAQUID Cohort. *American Journal of Epidemiology* **2009**, *169* (4), 489-496.
- (59) Peplow, M. The toxic tale of the Flint water crisis. <http://www.rsc.org/chemistryworld/2016/02/flint-toxic-water-crisis-lead>.
- (60) Lee, N. H.; Amy, G.; Croue, J. P.; Buisson, H., Identification and understanding of fouling in low-pressure membrane (MF/UF) filtration by natural organic matter (NOM). *Water Research* **2004**, *38* (20), 4511-4523.
- (61) Zularisam, A. W.; Ismail, A. F.; Salim, R., Behaviours of natural organic matter in membrane filtration for surface water treatment - a review. *Desalination* **2006**, *194* (1-3), 211-231.
- (62) Velten, S.; Knappe, D. R. U.; Traber, J.; Kaiser, H.-P.; von Gunten, U.; Boller, M.; Meylan, S., Characterization of natural organic matter adsorption in granular activated carbon adsorbers. *Water Research* **2011**, *45* (13), 3951-3959.
- (63) Cheng, W.; Dastgheib, S. A.; Karanfil, T., Adsorption of dissolved natural organic matter by modified activated carbons. *Water Research* **2005**, *39* (11), 2281-2290.
- (64) Dastgheib, S. A.; Karanfil, T.; Cheng, W., Tailoring activated carbons for enhanced removal of natural organic matter from natural waters. *Carbon* **2004**, *42* (3), 547-557.
- (65) Humbert, H.; Gallard, H.; Suty, H.; Croue, J.-P., Natural organic matter (NOM) and pesticides removal using a combination of ion exchange resin and powdered activated carbon (PAC). *Water Research* **2008**, *42* (6-7), 1635-1643.
- (66) Singer, P. C.; Bilyk, K., Enhanced coagulation using a magnetic ion exchange resin. *Water Research* **2002**, *36* (16), 4009-4022.
- (67) Ameen, A. A.; Giordano, A. N.; Alston, J. R.; Forney, M. W.; Herring, N. P.; Kobayashi, S.; Ridlen, S. G.; Subaran, S. S.; Younts, T. J.; Poler, J. C., Aggregation kinetics of single-walled carbon nanotubes investigated using mechanically wrapped multinuclear complexes: probing the tube-tube repulsive barrier. *Physical Chemistry Chemical Physics* **2014**, *16* (12), 5855-5865.

- (68) Matyjaszewski, K., Atom Transfer Radical Polymerization (ATRP): Current Status and Future Perspectives. *Macromolecules* **2012**, *45* (10), 4015-4039.
- (69) Wade, L. G., *Organic Chemistry - Eighth Edition*. Prentice Hall ; Pearson Education [distributor]: Upper Saddle River, N.J.; London, 2012.
- (70) Dresselhaus, M. S.; Dresselhaus, G.; Saito, R.; Jorio, A., Raman spectroscopy of carbon nanotubes. *Physics Reports-Review Section of Physics Letters* **2005**, *409* (2), 47-99.
- (71) Hennrich, F.; Krupke, R.; Lebedkin, S.; Arnold, K.; Fischer, R.; Resasco, D. E.; Kappes, M., Raman spectroscopy of individual single-walled carbon nanotubes from various sources. *Journal of Physical Chemistry B* **2005**, *109* (21), 10567-10573.
- (72) Wu, H.-X.; Tong, R.; Qiu, X.-Q.; Yang, H.-F.; Lin, Y.-H.; Cai, R.-F.; Qian, S.-X., Functionalization of multiwalled carbon nanotubes with polystyrene under atom transfer radical polymerization conditions. *Carbon* **2007**, *45* (1), 152-159.
- (73) Chaturvedi, H.; Giordano, A. N.; Kim, M.-J.; MacDonnell, F. M.; Subaran, S. S.; Poler, J. C., "Mechanically Docked" Metallodendrimers about Single-Walled Carbon Nanotubes. *J. Phys. Chem. C* **2009**, *113* (26), 11254-11261.
- (74) Bachilo, S. M.; Strano, M. S.; Kittrell, C.; Hauge, R. H.; Smalley, R. E.; Weisman, R. B., Structure-assigned optical spectra of single-walled carbon nanotubes. *Science* **2002**, *298* (5602), 2361-2366.
- (75) Chen, Z. F.; Thiel, W.; Hirsch, A., Reactivity of the convex and concave surfaces of single-walled carbon nanotubes (SWCNTs) towards addition reactions: Dependence on the carbon-atom pyramidalization. *Chemphyschem* **2003**, *4* (1), 93-+.
- (76) Nair, N.; Kim, W.-J.; Braatz, R. D.; Strano, M. S., Dynamics of surfactant-suspended single-walled carbon nanotubes in a centrifugal field. *Langmuir* **2008**, *24* (5), 1790-1795.
- (77) Delgado, A. V.; González-Caballero, F.; Hunter, R. J.; Koopal, L. K.; Lyklema, J., Measurement and interpretation of electrokinetic phenomena. *J. Colloid Interface Sci.* **2007**, *309* (2), 194-224.
- (78) Lenore, S. C.; Arnold, E. G.; Andrew, D. E., Standard methods for the examination of water and wastewater. *American Public Health Association. American Water Works Association and World Environment Federation. 20th Edition, Washington DC* **1998**.

- (79) Hyung, H.; Kim, J.-H., Natural Organic Matter (NOM) Adsorption to Multi-Walled Carbon Nanotubes: Effect of NOM Characteristics and Water Quality Parameters. *Environmental Science & Technology* **2008**, *42* (12), 4416-4421.
- (80) Al-Naseri, S. K.; Abbas, T. R., Predicting NOM Removal by Fixed-Bed GAC Adsorbers. *Jordan Journal of Civil Engineering* **2009**, *3* (2), 172-183.

## APPENDIX A: AQUEOUS NANORESIN SYNTHESIS

Great focus has been placed on the solvent choice for ATRP. It is desirable to move away from commonly used organic solvents, such as DMF or acetonitrile, to “green” solvents such as water. For NanoResin synthesis, it was also made necessary to switch to water, instead of DMF, due to ion-dipole interactions between the very polar DMF and the ion exchange sites on the NanoResin.

NanoResin synthesis can be broken down into two distinct parts: polymerization and functionalization (attaching polymer to SWCNTs). It was necessary to first explore the polymerization portion to see if synthesis was possible. The route chosen for synthesis of poly(vinylbenzyl trimethylammonium chloride) is has been given above in section 4.3.3; however, functionalization has not been as facile as with synthesis in DMF. In DMF, greater the 80% of SWCNTs were functionalized. Contrarily, in water, the greatest degree of functionalization we have obtained is 18%.

A variety of parameters must be considered to achieve greater percent functionalization; time, temperature, polymer length, and ascorbic acid feed rate/concentration have been of the greatest focus. All syntheses were performed under idealARGET ATRP conditions.<sup>47</sup> All solutions were sparged with Ar for fifteen minutes before use, and each reaction was done on a Schlenk line under Ar. Below, each experimental setup, and result has been outlined.

### A.1. JCP-46D-88

In a dry 100 mL Schlenk flask, 1.99 g of vbTMAC was dissolved into water (4.00 mL). The resulting mixture was stirred until fully dissolved.  $\text{CuBr}_2$  (0.945  $\mu\text{mol}$ ) and TPMA (42.5  $\mu\text{mol}$ ) were added, followed by the addition of HEBiB (13.7  $\mu\text{L}$ , 94.5  $\mu\text{mol}$ ). The reaction flask was then placed into a 90 °C oil bath. To start the reaction, AA (37.8  $\mu\text{mol}$ ) was added to the flask. Meanwhile, 2.86 mg of SWCNT were added to 10.0 mL of water and sonicated at 8 W for 15 minutes. Polymerization was allowed to proceed for 30 minutes. The catalyst and reducing agent were then recharged (same as above) and the SWCNTs were added. The catalyst and reducing agent were recharged after 80 minutes, 13 hours and 20 minutes, 18 hours and 30 minutes, and last after 23 hours and 25 minutes. The reaction was stopped after 45 hours of functionalization. After cleanup, it was found that 15.5% of the tubes had been functionalized.

### A.2. JCP-46D-96

In a dry 100 mL Schlenk flask, under argon, vbTMAC (1.00 g, 4.72 mmol) was dissolved into water (10.000 mL). The resulting mixture was stirred until fully dissolved.  $\text{CuBr}_2$  (0.236  $\mu\text{mol}$ ) and TPMA (14.2  $\mu\text{mol}$ ) in water (0.942 mL) was added, followed by the addition of HEBiB (6.85  $\mu\text{L}$ , 47.2  $\mu\text{mol}$ ). The reaction flask was then placed into a 98 °C oil bath. A 1.6 mM AA solution was then fed into the reaction solution with a syringe pump at a rate of 6.8  $\mu\text{L}/\text{min}$  (11 nmol/min) to initiate polymerization while maintaining a low concentration of active radicals. Polymerization was allowed to proceed for 1208 minutes. SWCNTs (4.50 mg) were then added to water (5.00 mL) and tip sonicated at 10 W for 10 minutes before adding to the reaction mixture. The tip sonicator was then added to one of neck on the round bottom flask and sealed with aluminum foil and parafilm. The vessel was not perfectly sealed, so some volume was

lost. The reaction was sonicated at 5 W for 183 minutes before the sonicator was removed and the reaction vessel sealed. The reaction was stopped after 24 hours of functionalization, and after purification 15.1% of the tubes had been functionalized.

#### A.3. JCP-46D-109

In a dry 500 mL Schlenk flask, under argon, vbTMAC (0.5006 g) was dissolved into water (5.00 mL). The resulting mixture was stirred until fully dissolved.  $\text{CuBr}_2$  (0.118  $\mu\text{mol}$ ) and TPMA (1.96 mg) were added, followed by the addition of HEBiB (3.42  $\mu\text{L}$ ). The reaction flask was then placed into a 98 °C oil bath. A 23 mM AA solution was then fed into the reaction solution with a syringe pump at a rate of 0.68  $\mu\text{L}/\text{min}$  (16 nmol/min) to initiate polymerization while maintaining a low concentration of active radicals. Polymerization was allowed to proceed for 159 minutes. SWCNTs (3.86 mg) were then added to water (5.00 mL) and tip sonicated at 10 W for 5 minutes before adding to the reaction mixture. The tip sonicator was then added to one of neck on the round bottom flask and sealed with aluminum foil and parafilm. The vessel was not perfectly sealed, after three hours all solvent had evaporated and only dried tubes remained. In attempt to restart the reaction, 20 mL of degassed water was added, along with  $\text{CuBr}_2$  and TPMA (in the same ratio as above). The reaction was stopped after 68 hours of functionalization, and after purification 6.07% of the tubes had been functionalized.

#### A.4. JCP-49D-26

In a dry 500 mL Schlenk flask, under argon, vbTMAC (1.5028 g) was dissolved into water (16.1 mL). The resulting mixture was stirred until fully dissolved.  $\text{CuBr}_2$  (0.354  $\mu\text{mol}$ ) and TPMA (6.17 mg) were added, followed by the addition of HEBiB (10.27  $\mu\text{L}$ ). The reaction flask was then placed into a 94 °C oil bath. A 23 mM AA

solution was then fed into the reaction solution with a syringe pump at a rate of 2.11  $\mu\text{L}/\text{min}$  (48 nmol/min) to initiate polymerization while maintaining a low concentration of active radicals. Polymerization was allowed to proceed for 45 minutes. SWCNTs (5.23 mg) were then added to water (8.00 mL) and tip sonicated at 10 W for 5 minutes before adding to the reaction mixture. The tip sonicator was then added to one of neck on the round bottom flask and an airtight seal was created with rubber heat-shrink tubing. The reaction was sonicated at 5 W for 120 minutes before the sonicator was removed and the reaction vessel sealed. The reaction was stopped after 68 hours of functionalization, and after purification 17.7% of the tubes had been functionalized.

#### A.5. JCP-46D-111

In a dry 50 mL round bottom flask equipped with a Claisen adapter, under argon, vbTMAC (1.5028 g) was dissolved into water (16.1 mL). The resulting mixture was stirred until fully dissolved.  $\text{CuBr}_2$  (0.354  $\mu\text{mol}$ ) and TPMA (6.23 g) were added, followed by the addition of HEBiB (10.27  $\mu\text{L}$ ). The reaction flask was then placed into a 115  $^\circ\text{C}$  oil bath and allowed to reflux. A 23 mM AA solution was then fed into the reaction solution with a syringe pump at a rate of 2.11  $\mu\text{L}/\text{min}$  (48 nmol/min) to initiate polymerization while maintaining a low concentration of active radicals. Polymerization was allowed to proceed for 45 minutes. SWCNTs (5.28 mg) were then added to water (8.00 mL) and tip sonicated at 10 W for 5 minutes before adding to the reaction mixture. The reaction was stopped after 66 hours of functionalization, and after purification 14.4% of the tubes had been functionalized.

TABLE A.1: Summary of aqueous NanoResin synthesis results.

Reaction	Temperature (°C)	Polymer Length*	Functionalization Time (h)	Sonication Time (min)	AA Feed Rate (mmol/min)	Percent Functionalization
JCP-46D-88	90	<10 (est)	45	0	N/A	15.5
JCP-46D-96	98	81	24	183	11	15.1
JCP-46D-109 <sup>+</sup>	98	64	68	195	16	6.07
JCP-49D-26	94	9	68	120	48	17.7
JCP-46D-111	Reflux	23	66	0	48	14.2

\*Polymer length is based off of NMR measurements outlined in section 4.5.6

<sup>+</sup>All solvent evaporated during synthesis due to leak in the system